NEW ELECTRONIC-TRANSITION LASER SYSTEMS. PART I. ELECTRON PUMPED SYSTEMS. PART II. CHEMICALLY PUMPED SYSTEMS

STANFORD RESEARCH INSTITUTE
MENLO PARK, CALIFORNIA

DECEMBER 1976

Final Technical Report *December 1976*
Covering the Period 8 February 1974 to 15 December 1976
SRI No. MP 76-99

NEW ELECTRONIC-TRANSITION LASER SYSTEMS

Part I: Electron Pumped Systems

By: H. H. NAKANO, R. M. HILL, D. C. LORENTS,
D. L. HUESTIS, and M. V. McCUSKER

Part II: Chemically Pumped Systems

By: D. J. ECKSTROM

Prepared for:

DEFENSE ADVANCED RESEARCH PROJECTS AGENCY
WASHINGTON, D. C. 20301
AND
U. S. ARMY MISSILE COMMAND
REDSTONE ARSENAL, ALABAMA 35809

ARPA Order No. 1180
Contract DAAH01-74-C-0524 (8 February 1974 to 15 December 1976)
Contract Amount $852,268

SRI Project PYU-3190

STANFORD RESEARCH INSTITUTE
Menlo Park, California 94025 · U.S.A.

SECURITY CLASSIFICATION OF THIS PAGE (When Data Entered)

REPORT DOCUMENTATION PAGE

READ INSTRUCTIONS BEFORE COMPLETING FORM

1. REPORT NUMBER	2. GOVT ACCESSION NO. / 3. RECIPIENT'S CATALOG NUMBER
4. TITLE (and Subtitle) NEW ELECTRONIC TRANSITION LASER SYSTEMS Part I: Electron Pumped Systems Part II: Chemically Pumped Systems	5. TYPE OF REPORT & PERIOD COVERED Final Technical Report 8 Feb 1974-15 Dec 1975 6. PERFORMING ORG. REPORT NUMBER MP 76-99
7. AUTHOR(s) Part I: H. H. Nakano, R. M. Hill, D. C. Lorents, D. L. Huestis, and M. V. McCusker Part II: D. J. Eckstrom	8. CONTRACT OR GRANT NUMBER(s) DAAH01-74-C-0524
9. PERFORMING ORGANIZATION NAME AND ADDRESS Stanford Research Institute 333 Ravenswood Avenue Menlo Park, California 94025	10. PROGRAM ELEMENT, PROJECT, TASK AREA & WORK UNIT NUMBERS
11. CONTROLLING OFFICE NAME AND ADDRESS Defense Advanced Research Projects Agency 1400 Wilson Boulevard Arlington, Virginia 22209	12. REPORT DATE December 1976 13. NUMBER OF PAGES 114
14. MONITORING AGENCY NAME & ADDRESS(if different from Controlling Office) U.S. Army Missile Command Redstone Arsenal, Alabama 35809	15. SECURITY CLASS. (of this report) Unclassified 15a. DECLASSIFICATION/DOWNGRADING SCHEDULE

16. DISTRIBUTION STATEMENT (of this Report)

Distribution of this document is unlimited.

17. DISTRIBUTION STATEMENT (of the abstract entered in Block 20, if different from Report)

18. SUPPLEMENTARY NOTES

19. KEY WORDS (Continue on reverse side if necessary and identify by block number)

excimer lasers, e-beam pumping, rare gas-halide lasers, electronic transition, chemically pumped lasers

20. ABSTRACT (Continue on reverse side if necessary and identify by block number)

This report consists of two parts. Part I describes our program to develop a kinetic model for the energy flow in electron-beam pumped rare gas-halide lasers. Our experimental program involves observations of fluorescence from argon/krypton/fluorine mixtures pumped by a short pulse electron beam. In addition to the emissions at 193 nm (ArF^*) and 248 nm (KrF^*) we observe significant broad band emissions near 290 nm and 400 nm which we assign

DD FORM 1 JAN 73 1473 EDITION OF 1 NOV 65 IS OBSOLETE

Unclassified

SECURITY CLASSIFICATION OF THIS PAGE (When Data Entered)

20. Abstract (continued)

to Ar_2F^* and Kr_2F^*. The formation of these triatomics plays a significant role in the total KrF^* laser kinetics; in particular the dominant formation reaction chain of Kr_2F^* involves interception of the precursors of KrF^*. The important reactions that form ArF^* and KrF^* are also discussed in this report.

Part II summarizes the status of electronic-transition chemical laser development. There has not yet been a demonstration of gain in a visible chemical laser systems, and it appears unlikely that practical lasers of this type will be developed in the near future. Substantial progress has been made toward understanding the kinetics of highly exothermic reactions, but a complete knowledge of any one system is still to be achieved.

CONTENTS

LIST OF ILLUSTRATIONS

List of Illustrations (continued)

LIST OF TABLES

SUMMARY OF THE REPORT

Part I: Electron-Pumped Systems

During the last year, significant progress has been made in the development of efficient high-energy rare gas halide lasers. At the present time, efforts to scale KrF^* lasers to intermediate sizes are in progress. The introduction to this report presents a summary of the published results that characterize the rare gas halide lasers. Our program has been oriented toward the development of a kinetic model of the energy flow within gas mixtures that will produce laser action. To develop this kinetic model, we have made extensive studies of the intensity and time behavior of the optical emissions that arise from electron-pumped mixtures of argon and fluorine and mixtures of argon/krypton/fluorine. These data are compared in an iterative fashion with the computed predictions of a simple kinetic model that includes up to 30 molecular reactions relevant to these systems. The rate constants used in the model were adjusted until consistent and reasonable agreement between predictions and experiment were obtained. This modeling process and the details of the dominant energy flow pathways elucidated by this model are described in Sections 1-4 of this report.

One of our most significant observations was detection of intense fluorescence in broad bands at 290 nm and 400 nm, in addition to the well-known laser transitions at 193 nm (ArF^*) and 248 nm (KrF^*). These new bands were especially pronounced at higher total gas pressures. In Section 3 of Part I, we discuss our tentative assignments of these bands as arising from triatomic Ar_2F^* and Kr_2F^*. As described in Section 4, the kinetics that lead to these emissions are critical to the operation of large KrF^* laser systems because of our conclusion that their formation is due to an

interception of the precursors of the diatomic KrF^* laser molecules rather than a quenching. If the formation had been via a quenching reaction, efficient lasing on KrF^* could be recovered by raising the cavity flux. Thus, the results of our modeling efforts indicate a limited range of operating pressures over which KrF lasers will operate efficiently. It must be emphasized that our understanding of these processes is incomplete and it would be desirable to extend the range of experimental results in order to improve our knowledge of the complete reaction kinetics of this laser medium.

In cooperation with R. Hunter of Maxwell Laboratories in San Diego, California, we made an experimental gain measurement on the 400 nm transitions in e-beam pumped and e-beam sustained discharge excited $Ar/Kr/F_2$ mixtures. Using the 441.6 nm line from an He-Cd laser, we observed a small net absorption under the limited range of experimental conditions available in the apparatus. This effort and its impact on future efforts to develop a triatomic rare gas halide laser are described in the Appendix of Part I.

Part II: Chemically Pumped Systems

There has not yet been a demonstration of gain in a visible chemical laser system, and the development of practical lasers of this type appears unlikely in the near future. In view of that conclusion, studies of chemically pumped systems were de-emphasized during the last portion of the contract period. Our experimental efforts were confined to some intracavity dye laser spectroscopy studies of reactions of Ba, Ca, or Sr with $N_2O + CO$. These studies revealed absorption rather than gain on several candidate molecular transitions. We also carried out some laser-induced fluorescence studies in an attempt to measure the distributions among vibrational levels of $BaO(X\,^1\Sigma)$ in the $Ba + N_2O$ reaction. Analytical studies included an extension of our vibrational relaxation

modeling program and a completion of our numerical solution for the spherical diffusion flame with multiple reactions. All of these studies have been described in a series of preprints that have been submitted for publication.

OVERVIEW OF THE PROGRAM

Part I: Electron-Pumped Systems

Prior to June of 1975, studies of the kinetics of e-beam pumped molecular lasers at SRI were carried out under ARPA contract N00014-72-C-0478. The work under that contract was summarized in the final report [GHH75]. These studies were continued under the present contract that supported both the chemical laser studies and the studies of electron-pumped media.

These efforts were first oriented toward an understanding of the kinetic processes in electron-beam pumped molecular halogen lasers, particularly molecular iodine. This effort was particularly motivated by our observations that very large fluorescence efficiencies could be obtained in the near uv from electron-beam pumped chlorine, bromine, or iodine.

Our conclusions, described in a previous report [MLH76], were that the upper laser level of molecular iodine is efficiently populated through a two-step energy transfer mechanism. The excited noble gas atoms or molecules (argon) produced by the electron beam react with the halogen-bearing additive to form excited halogen atoms (I^*). These atoms subsequently collide with the additive to yield excited homonuclear halogen molecules (I_2^*). Vibrational and electronic relaxation to the upper laser level is rapid and efficient.

We concluded that these media showed excellent prospects for an efficient, scalable laser. Further, we noted that these media were suitable for pumping by e-beams, e-beam sustained discharges, or neutron-generated fission fragments.

Since the last technical report for this contract [MLH76], we have concentrated our efforts on determining the kinetic processes important to e-beam and discharge pumped rare gas halide lasers, especially KrF^*. The results of this effort are presented in detail in this report.

Part II: Chemically Pumped Systems

Our attempts to develop a visible chemical laser began in 1973. At that time, there was virtually no quantitative data base for assessing the prospects of this attempt, and so early studies concentrated on determination of visible photon yields in exothermic reactions and on spectral characterization of the emissions. Our efforts have involved reactions of metal atoms with oxygen or halogen donors, with metal atoms generated in electrically heated ovens, by thermal decomposition of volatile metal compounds in shock tubes, or by stripping of volatile polyhalides in an excess of alkali atoms. Most of our studies have been carried out in diffusion flames, using both excess oxidizer and excess metal.

The photon yield measurement program indicated a number of reactions with large yields, including:

Reaction	Yield	Pressure at Maximum Yield (Torr)
$Ba + N_2O$	0.25	4
$Ba + O_3$	0.36	1.7
$Ba + NF_3$	0.50	2
$Sm + N_2O$	0.38	3
$Sm + F_2$	0.64	0.8
$Sm + NF_3$	0.70	2.3
$Eu + N_2O$	0.20	1.1

We carried out unsuccesful lasing attempts and resonant cavity spectroscopy studies of the Ba + N_2O and Sm + NF_3 reactions. We also searched unsuccessfully for gain in Ba, Ca, or Sr + N_2O + CO flames using sensitive intracavity dye laser spectroscopy. We concentrated more detailed study on the Ba + N_2O reaction, including studies of quenching by Ba carried out in a heat-pipe-oven reactor and laser-induced fluorescence studies of $BaO(X\,^1\Sigma, v'')$ distributions.

In spite of the studies carried out at SRI and elswhere, no one candidate reaction is yet completely understood. In addition, many of the straightforward approaches toward achieving a visible chemical laser have been tried. The status of several approaches is described in Part II of this report. It seems likely that an extended period of fundamental research will be required before a successful visible chemical laser is developed.

PART I: ELECTRON-PUMPED SYSTEMS

1. INTRODUCTION

During the last two years, remarkable progress has been achieved in the development of large, efficient noble gas halide lasers. Such developments have been carried out primarily, but not entirely, in laboratories supported by ARPA. In addition to the DoD requirements, the wavelengths available in lasers and lamps that operate on transitions in these molecules also appear to have applicability to isotope separation schemes of interest to ERDA. This report details the results of our ARPA-funded program that seeks to provide the kinetic information vital to the full exploitation and scaling of these systems.

The first suggestion of the possibility of lasing on these molecules was presented by Setser in June of 1974 [KS74] at the Fourth Conference on Chemical and Molecular Lasers. This work was subsequently published in expanded form in March of 1975 [VS75]. That paper described the emission spectra of XeF^*, $XeCl^*$, $XeBr^*$, and XeI^* and emphasized the similarity between the physical and electronic properties of alkali atoms with the corresponding metastable rare gases. Independently, Golde and Thrush used this resemblance to discuss emissions they observed from $ArCl^*$ [GT74]. Ewing and Brau used this model to predict the structure and emission spectra in most of the diatomic rare gas halogen molecules [EB75c]. They illustrated the success of the prescription by comparing their predictions with spectra observed from XeI^*. They placed particular emphasis on the impact of these molecules on future laser development. In a subsequent paper, they further confirmed the model by comparing predicted and experimental results of emission from $XeBr^*$, $XeCl^*$, XeF^* and KrF^* [Be75a].

The first noble gas halide excimer laser was demonstrated at NRL by Searles and Hart [SH75] who used $XeBr^*$. Groups at AVCO, Northrop, and

Sandia all demonstrated laser action on a variety of noble gas halogen pairs. Since these initial demonstrations, several other laboratories have also demonstrated lasers based on these systems (see Table 1) using electron beams for excitation. The use of an e-beam sustained discharge to pump noble gas halide lasers was first demonstrated at AVCO [MJ75].

These systems can be pumped by other methods as well; in September of 1975, Burnam et al. reported lasing on XeF^* by avalanche discharge pumping [BHD75]. While such pumping methods appear to offer no promise of the efficiencies and scalability required by ARPA at the present time, the high repetition rate available with this pumping method is particularly attractive for other uses. This activity has proceeded so rapidly that at least two commercial companies offer electrical drives that can be used to pump XeF^*, KrF^*, and ArF^* (Tachisto and NRG) [BHD76, BB76, SSG76, BD76]. In addition, a scheme was recently described whereby energy from a pulsed nuclear reactor could be used to pump these molecules [LMR76].

The potential scalability and high efficiency of these systems has motivated the present DoD interest. Table 1 presents a summary of some of the values of energy and efficiency that have been published or reported. This table is incomplete; several efforts described at conferences reported values that exceed those in the tables but have been omitted because complete information is lacking. Direct comparisons of laser systems operated in different laboratories should be made cautiously. However, a clear record of progress can be seen.

Whether rare gas halide lasers are pumped by pure electron beams or by discharges, a kinetic model must depict the energy transfer from the source (in this case Ar^*) to the laser molecule (KrF^* or XeF^*). Several processes can reduce the selectivity of this transfer, and others can act to quench the laser molecule once it is formed. These processes are schematically illustrated in Figure 1. The optimum energy flow path proceeds from the pump to Ar^* and subsequently, through possible

Table 1

SUMMARY OF RECENT RARE GAS HALIDE LASER DEMONSTRATIONS

Molecule	Citation	Laboratory	PUMP			LASER CAVITY		GAS		P_{out} (MW)	E_{out} (J)	Quoted Efficiency (%)
			$I(a/cm^2)$	V(kV)	t(ns)	Dimensions	Mirrors	Total Pressure torr	Typical Ratio			
XeBr*	SH75	NRL		433	50	15 x 1	99.5% (external)	764	995:5	-	-	-
XeCl*	EB75a	AVCO	150	350	100	15 x 1 cm	1% total output (external)	> 1500	9000:100:1	3×10^{-3}	5×10^{-5}	-
KrF*	EB75a	AVCO						760 → 3000	9900:10:1	-	8×10^{-3}	0.4
XeF*	BE75b	AVCO	200	300	100	15 x 1 cm	99.97% + 97.5%		996:3:1	6×10^{-3}		0.01%
XeF*	MJD76	AVCO	12 (Discharge: 4.9J)	150		15 x 10 cm	30% output	3000	995:4:1 ($Ar:Xe:NF_3$)		10^{-2}	0.3% *
XeF*	ABB75	Northrop	1000 (Transverse)	1000	20	30 cm^3	95% + 95%	1300	250:25:1 ($Ar:Xe:NF_3$)	0.5	5×10^{-3}	0.5%
			260J (input) (Coaxial)		100	100 cm^3						
KrF*	BAA76	Northrop	(Transverse)				75% + 75%	1500 → 2650	1300:130:1 ($Ar:Kr:NF_3$)		0.1	5%
			(Coaxial)				75% + 75%	1500 → 2650	1300:130:1 ($Ar:Kr:NF_3$)		1.5	15%
ArF*	HHT76	Sandia	55,000 (Axial pump)	200	55	180 cm x 15 cm dia	aluminum flat + quartz output	1400	1400:4 ($Ar:F_2$)		92	3%
KrF*	HHT76	Sandia	55,000 (Axial pump)	200	55	180 cm x 15 cm dia	aluminum flat + quartz output	1400	1300:100:4 ($Ar:Kr:F_2$)		108	3%
KrCl*	MP76	LLL		600keV (760 Joules)	50	2 x 10 cm	42% + 99%	3300	970:3:.15 ($Ar:Kr:Cl_2$)		.05	
KrF*	MP76	LLL		600keV (760 Joules)	50	2 x 10 cm	54% 90%	3300	970:3:.15 ($Ar:Kr:NF_3$)		0.6	
KrF*	HH076	Maxwell	6	300	1000	2000 x 20 x 20 cm	max refl, aperture output	760	710:50:1 ($Ar:Kr:F_2$)		150	6%

* These authors stated that Ewing had demonstrated 6% efficiency from a pure e-beam but did not describe conditions. Earlier discharge studies at AVCO are reported in Reference MJ75.

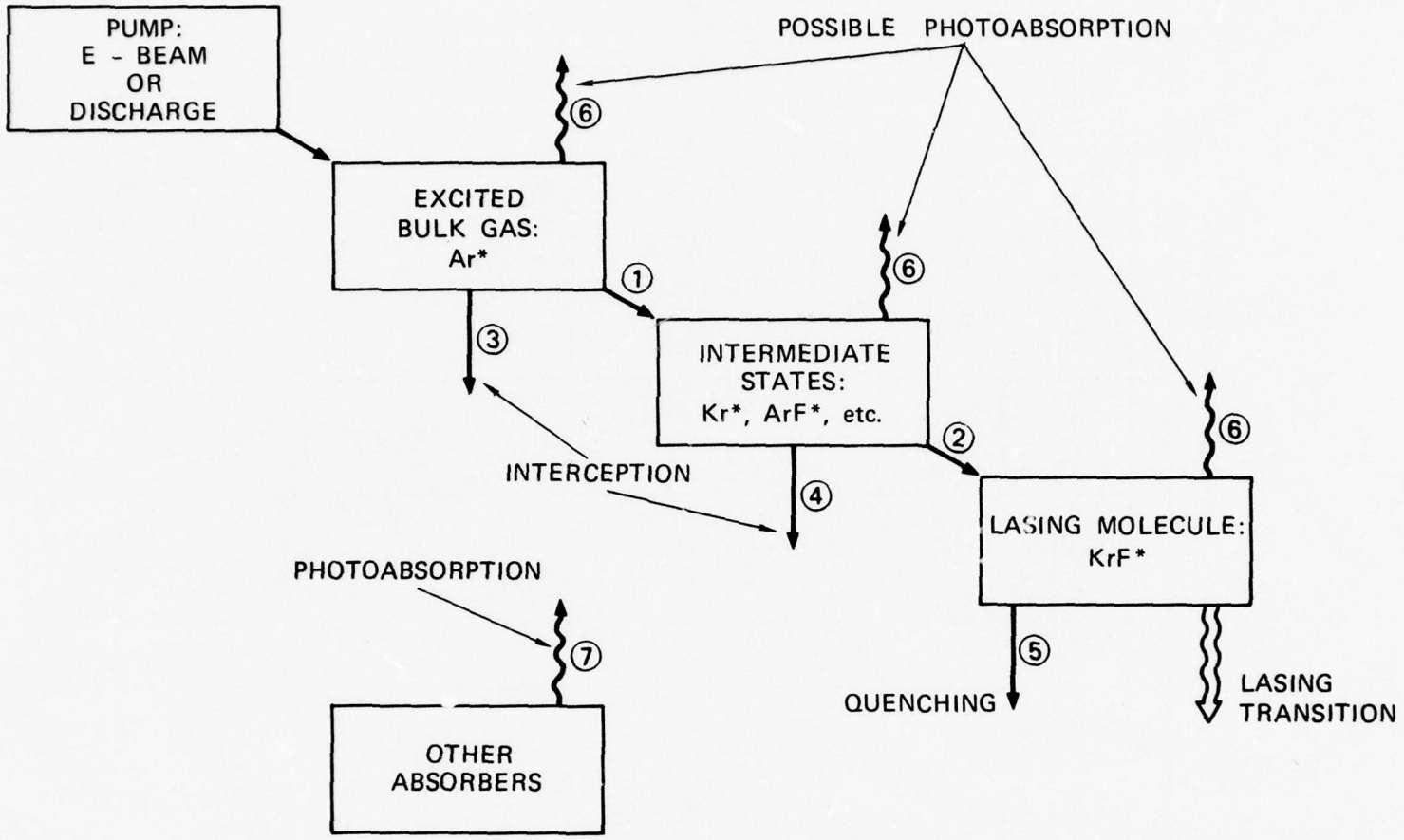

FIGURE 1 SCHEMATIC DIAGRAM OF THE ENERGY FLOW PATHWAYS APPLICABLE TO THE RARE GAS HALIDES

intermediates, to the laser molecule (Steps 1 and 2). At every intermediate point, however, reactions may exist that quench or remove energy from this preferred path (Steps 3 and 4). This energy is generally not recoverable; the function of the kinetic model is to determine those operating conditions that minimize the contributions of these deleterious effects. Processes for quenching of the laser molecule by atoms or electrons (see, for example, MJD76) are similar; however, the negative effect here may be offset by increasing the cavity flux to stimulate the laser molecule to radiate more rapidly than it is quenched. This option is not available if the quenching process intercepts the precursors. Thus, the determination of the relative rates of Process 5 to Processes 3 and 4 is of key importance in future laser-scaling efforts.

Once the laser radiation is produced, photoabsorption processes (Steps 6 and 7) may severely reduce the extraction and efficiency. Such absorptions have been studied recently in pure rare gases [ZHL76] and in rare gas oxygen mixtures [MP75]. We have recently noted their importance in halogen-containing mixtures [HOH76, see the appendix of this report]. Such absorptions may occur in the precursors (ionization, detachment or dissociation by the laser photon) or possibly in the laser molecule. Photoabsorption may also occur in species that are not direct intermediates in the energy flow chain (ground states such as F_2) or fragments such as NF_2. The nature and magnitude of these effects should be the subject of considerable future research.

One of our most significant interests in the initiation of this work was to determine the kinetics of the energy flow chain and particularly to emphasize the quenching processes that deactivate KrF^* and XeF^*. During these studies, we discovered that some of the eventual products of these interception and quenching reactions were triatomic molecules that under appropriate conditions were capable of radiating a considerable fraction of the pump energy. Since these radiators could

be efficiently created, we considered the possibility that laser action could be produced on them in preference to the diatomics. This led to a collaborative effort with R. O. Hunter and his colleagues at Maxwell Laboratories to measure gain on these molecules. A preprint describing this effort is being submitted for publication and is included as the appendix in this report.

2. EXPERIMENTAL PROCEDURE

The experimental technique has been discussed in many of our previous reports [MLH76, GHH75, HGH75, HGH74] and will be outlined only briefly here. Those aspects of particular interest to the studies of the rare gas halogen system will be given in more detail. The excitation source is a high-power electron beam from a Hewlett-Packard Febetron 706 (500 kV, 2000 A/cm^2, 3 ns). The beam is turned on for a time short compared with that of the kinetic steps under study. The excitation occurs in the dominant rare gas, usually Ar. Because of the rare gas pressure and excitation density, the rate of production of Ar-excited states is also fast in comparison with that in the other kinetic processes being studied [L76]. The emissions of the rare gas excimers, the diatomic rare gas halides, and the triatomic rare gas halides are then studied as a function of time and wavelength. The photon detection system, including lenses, spectrometer, and photomultiplier tube, is calibrated so that the absolute intensity of the emission as a function of time can be determined.

For all of these measurements, the photomultiplier output was recorded by a Tektronix Transient Digitizer System (WP2222), in digital form. These data can be analyzed to yield decay times and integrated intensities, and the data can be graphically recorded by the display unit.

We used a mixture of Ar + 5% N_2 to determine the energy deposition by measuring the absolute intensity of the second positive, 2+, radiation in the same experimental setup used for the rare gas halides. In addition, we used an Optical Multichannel Analyzer (Princeton Applied Research) that provides a time-integrated spectrum over a broad wavelength range as a check on both the reproducibility and the absolute value of the energy deposition.

Figure 2 is a block diagram of the experimental apparatus. The electron beam source is a Febetron 706, providing a pulse of electrons at approximately 500 kV for 3×10^{-9} sec and about 2000 amps/cm^2 through the foil in the gas cell. The gas cell is similar to those previously used; it has a cylindrical stainless-steel chamber with two MgF_2 windows, a thin metal foil mounted on a perforated stainless-steel grid connected to the electron-beam source, and a magnetically activated stirring rod enclosed off the optical axis to permit dynamical mixing of the gases. The optical radiations are observed with a ½-meter McPherson vacuum uv spectromter using a 1P28 photomultiplier. For measurements in the vuv region, the photomultiplier tube is coated with sodium salicylate. This optical detection system was calibrated over the range from 120 nm to 700 nm using a combination of standard lamp and molecular branching ratio techniques. This method is discussed in an earlier report [GHH75]. It has been possible to determine the transmission characteristics of the spectrometer independent of the photomultiplier tube by making an absolute calibration of the sensitivity of the photomultiplier tube at one wavelength using a calibrated optical filter. This greatly speeds up the calibration procedures since it is no longer necessary to remeasure the entire wavelength spectrum where the photomultiplier has to be changed. The optical multichannel analyzer is connected to the second exit window as shown in Figure 2 and has been used to measure the relative integrated intensity from 200-600 nm.

We have encountered several experimental problems with the rare gas halogen systems. In particular, the diatomic rare gas halide emissions occur very rapidly; in order to get accurate temporal information, a change in our photomultiplier structure was required. Some signal reproducibility problems were traced to difficulty in determining the partial pressures of each gas. Getting accurate measurements of fluorescence yields for the various observed emissions required considerable

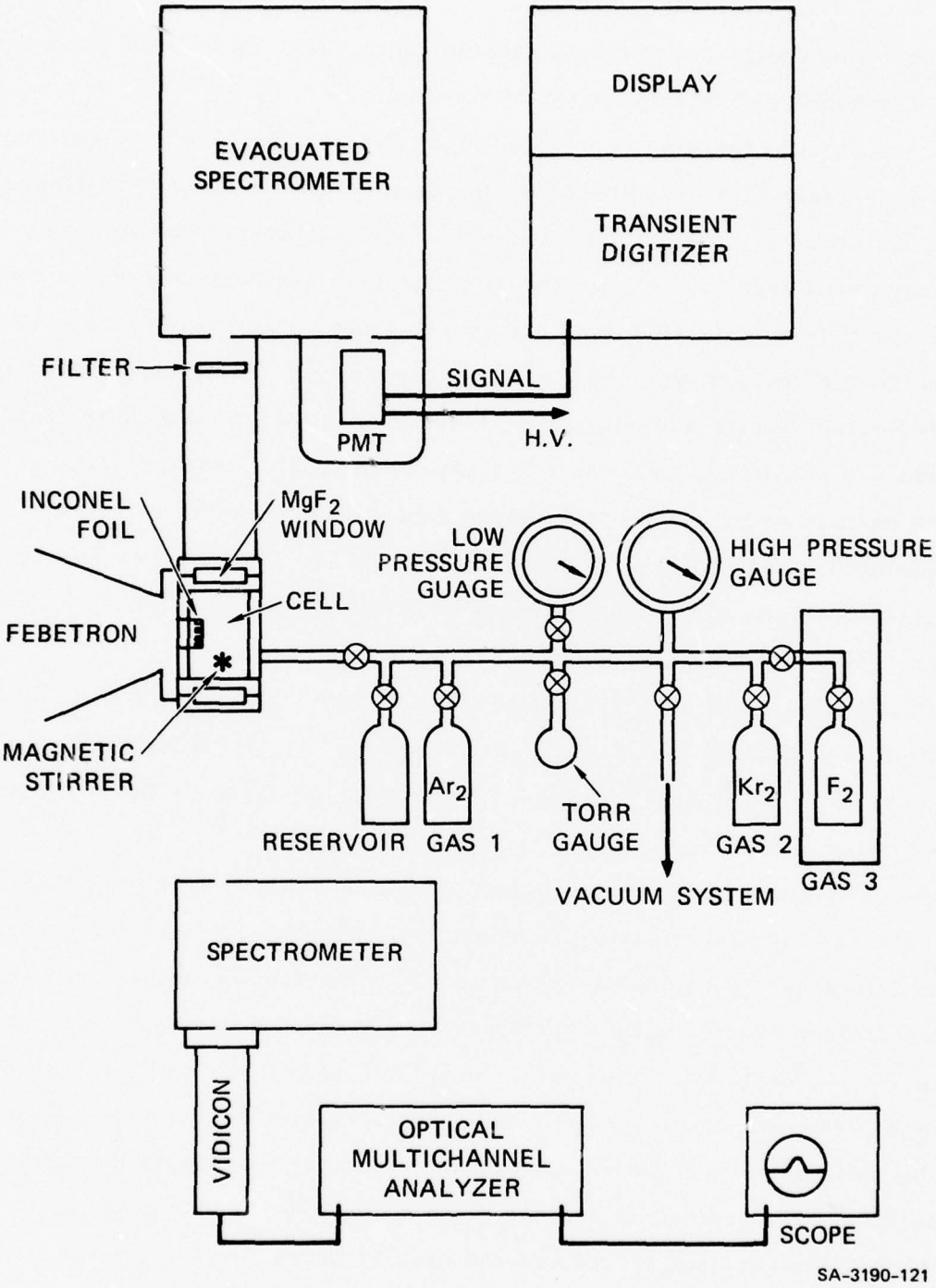

FIGURE 2 SCHEMATIC DIAGRAM OF APPARATUS

effort. Although the absolute accuracy with which these were determined is not high, the relative accuracy is good.

Both ArF^* radiation at 193.0 nm and KrF^* at 248.4 nm were observed to have rapid rise and decay when the Kr partial pressures were in excess of 50 torr. As noted in the discussions of the kinetic model, these decay rates were 150 MHz or more. Our initial attempts to measure these decays gave results that were very noisy, both in intensity versus time and in the derived value of the decay frequency. We believe that this difficulty results from operating the photomultiplier tube under maximum gain conditions for such short but intense signals. Under maximum gain, the maximum number of photoelectrons that can be accepted per resolution time without saturating the PMP output is small. To keep the photomultiplier from saturating or being nonlinear, the number of photoelectrons that may enter the first dynode within the resolution time ($\sim$ 3 nsec) is probably less than 10. For example, a 1P28 with a gain of 2×10^6 and a resolution time of 3 nsec would have a current at the final anode of $I = 10/3 \times 10^{-9} \times 2 \times 10^6 \approx 6 \times 10^{15}$ e/sec, which is close to the saturation value for this tube.

Collecting such a small number of photoelectrons will produce signals that have large statistical fluctuations. Since the saturation condition is determined by the space charge at the collection anode, we operated the photomultiplier with fewer stages and increased the optical signal on the photocathode. This was done by picking off the current at the 7th rather than the 10th dynode in the photomultiplier chain, thus decreasing the overall gain of the system without achieving a saturation current density. This technique did not degrade the time resolution of the photomultiplier, but it reduced the overall noise level by approximately a factor of 10.

We experienced severe difficulty in obtaining reproducible data. This problem was traceable to the difficulty in getting known partial

pressures of the various gases. The method that finally led to reproducible results involved filling the cell from 3 separate bottles, F_2, Kr, and Ar, in that order and measuring the pressure of each constituent separately. The cell was first evacuated to a pressure of 10^{-5} torr. Fluorine was first admitted to the cell, and the pressure was measured by a Tru-Torr capacitance manometer pressure gauge. The Tru-Torr gauge was then valved off and Kr was admitted to the cell. The total pressure was measured with a diaphragm manometer. The Ar was then admitted and the pressure measured by a second diaphragm manometer. With this technique, signal amplitude values could be measured that were reproducible within the variability of the deposition from the Febetron. Only the first data point per gas fill was used. We found significant decreases in light output for subsequent Febetron shots apparently due to a decrease in available F_2. This rather elaborate procedure was adapted after concluding that long-term storage of prepared argon/fluorine mixtures in passivated storage cells led to poor reproducibility.

We have calibrated the fluorescence yield measurements in much the same way as was reported earlier [MLH76, GHH75, HGH74]. The energy deposition from the e-beam is measured by determining the N_2 second positive (2+) band emission from Ar + 5% N_2 mixtures excited in the same experimental apparatus. The fluorescence yield for this system has been determined in our previous studies to be 17.6%/P, where P is the argon pressure in atmospheres. Therefore, by measuring the total photon emission in the band under study and comparing it with that observed from the $N_2(2+)$ at the same argon pressure, the fluorescence yield can be determined. We found that small quantities of residual F_2 or Kr had a strong influence on the observed $N_2(2+)$ emission. These calibration measurements were reliable when the experimental cell was evacuated properly.

The OMA allowed us to make a cross-check on the broad 400-nm band of Kr_2F^*. This instrument can be used to measure the integrated band

intensity directly. The $N_2(2+)$ 0-3 band at 405.9 nm which contains 4.2% of the total band emission can be used to calibrate the 400 nm Kr_2F emissions. The number of counts in the 405.9-nm band $N_2(2+)$ taken with an Ar + 5% gas fill could be compared directly with the number of signal counts observed in the much broader 410-nm band from Kr_2F.

3. IDENTIFICATION OF OPTICAL EMISSIONS: EMISSIONS FROM EXCITED $Ar/Kr/F_2$ MIXTURES

We have been studying e-beam excited $Ar/Kr/F_2$ mixtures in order to establish the important energy flow pathways and to determine the essential reaction rate constants. As described in Section 2, a Febetron 706 has been used to excite the gas mixtures with a 3-ns pulse of 500-keV electrons. To establish and monitor the important reactions and energy flow channels, we have observed the available radiative emissions and measured their intensities and time evolution as a function of the densities of the mixture components. Spectra have been obtained on film with a calibrated photomultiplier-spectrometer combination and with an optical multichannel analyzer that permits the measurements of time-integrated, single-shot spectra.

In the $Ar/Kr/F_2$ mixture, the known observable emitters, Ar_2^* (126 nm), Kr_2^* (147 nm), ArF (193 nm) and KrF^* (248 nm), were monitored with the primary objective of improving the understanding of the formation and decay kinetics of KrF^*. In the course of these studies, we have observed two additional emissions indicative of two additional radiating species that must be included in the energy flow scheme. These emissions are structureless, broadband, and peaked at 290 and 400 nm. Our initial observations of these emissions were described at a recent conference [LHH76]. The band shapes and widths are independent of pressure. In Ar/F_2 mixtures without Kr, only the 126-nm (Ar_2^*), 193-nm (ArF), and 290-nm emissions are observed. A scan of the 290-nm band is shown in Figure 3. Neither the broad bandwidth nor the energy of this transition can be explained by the accepted energy level structure of ArF [MH76, HD76]. Evidently, the emitter is an excited molecule consisting of only Ar and F atoms, $Ar_mF_n^*$, but is not ArF^*.

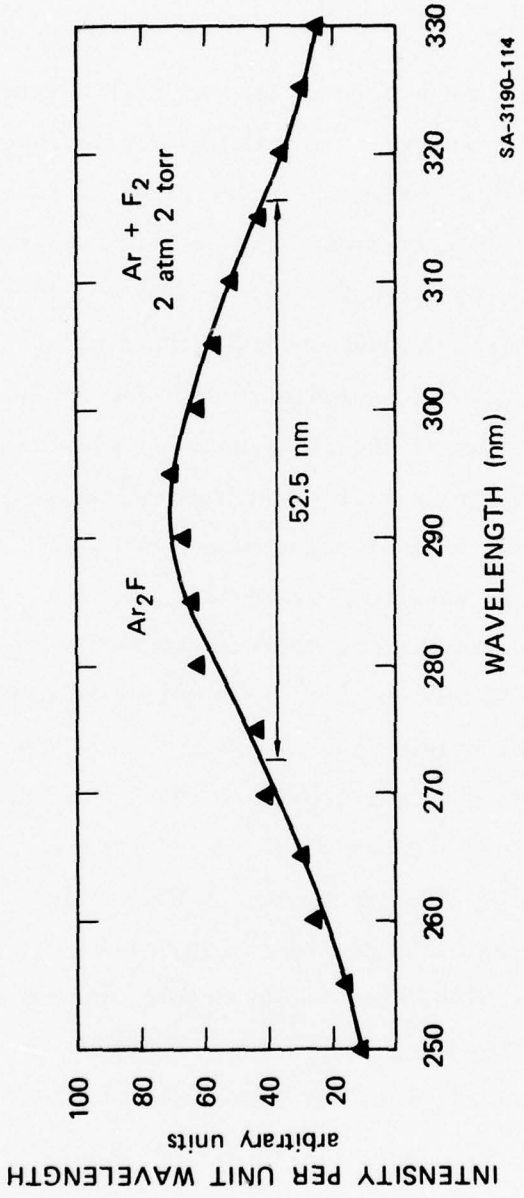

FIGURE 3 Ar_2F EMISSION BAND NEAR 290 nm

The pressure dependence of the fluorescence yield of the 193-nm and 290-nm bands is shown in Figure 4. The fluorescence yield is defined as the ratio of the total number of photons emitted in a band to the total number of excited states produced initially in the host gas (as described in the previous section). That the total fluorescence yield does not add up to 100% suggests that some nonradiative processes are also significant. These data taken from the time and wavelength integrated emission profiles show that the dominant emission at higher argon pressures and lower fluorine pressures is at 290 nm rather than 193 nm. The decrease of the ArF emission and the much slower decrease of 290-nm emission as the Ar pressure is increased suggests that the 290-nm emission is not from the same upper level as the 193-nm radiation and that it lies lower than the ArF level. The general downward flow of electronic energy to the lowest stable emitter under high-density, collision-dominated conditions supports this suggestion. In addition, we have observed the decay time of the 290-nm emission to be considerably longer ($\tau_{290} \approx 10\tau_{193}$) than the ArF^* decay time indicating again that the 290-nm emitter is not the same as the 193-nm emitter and that it is either formed later in the kinetic chain or has a longer radiative lifetime.

A similar set of observations has been conducted on the 400-nm band. This band is observed together with the 248-nm band of KrF^* in Kr/F_2 mixtures containing no Ar and therefore is identified as a $Kr_mF_n^*$ molecule. Observation of this band has also been reported by Lawrence Livermore Laboratory [RW76]. The emission profile of the 400-nm band is shown in Figure 5. The Kr pressure dependence of the fluorescence yields of each of the radiators in an $Ar/Kr/F_2$ mixture is shown in Figure 6. In this case, we observe that the 400-nm band becomes the dominant emitter as the Kr pressure is increased above about 20 torr in a mixture of 5-atm Ar and 1-torr F_2. As in the case of 290-nm emission from Ar/F_2 mixtures, the decay time of the 400-nm emission in the $Ar/Kr/F_2$ mixtures is much

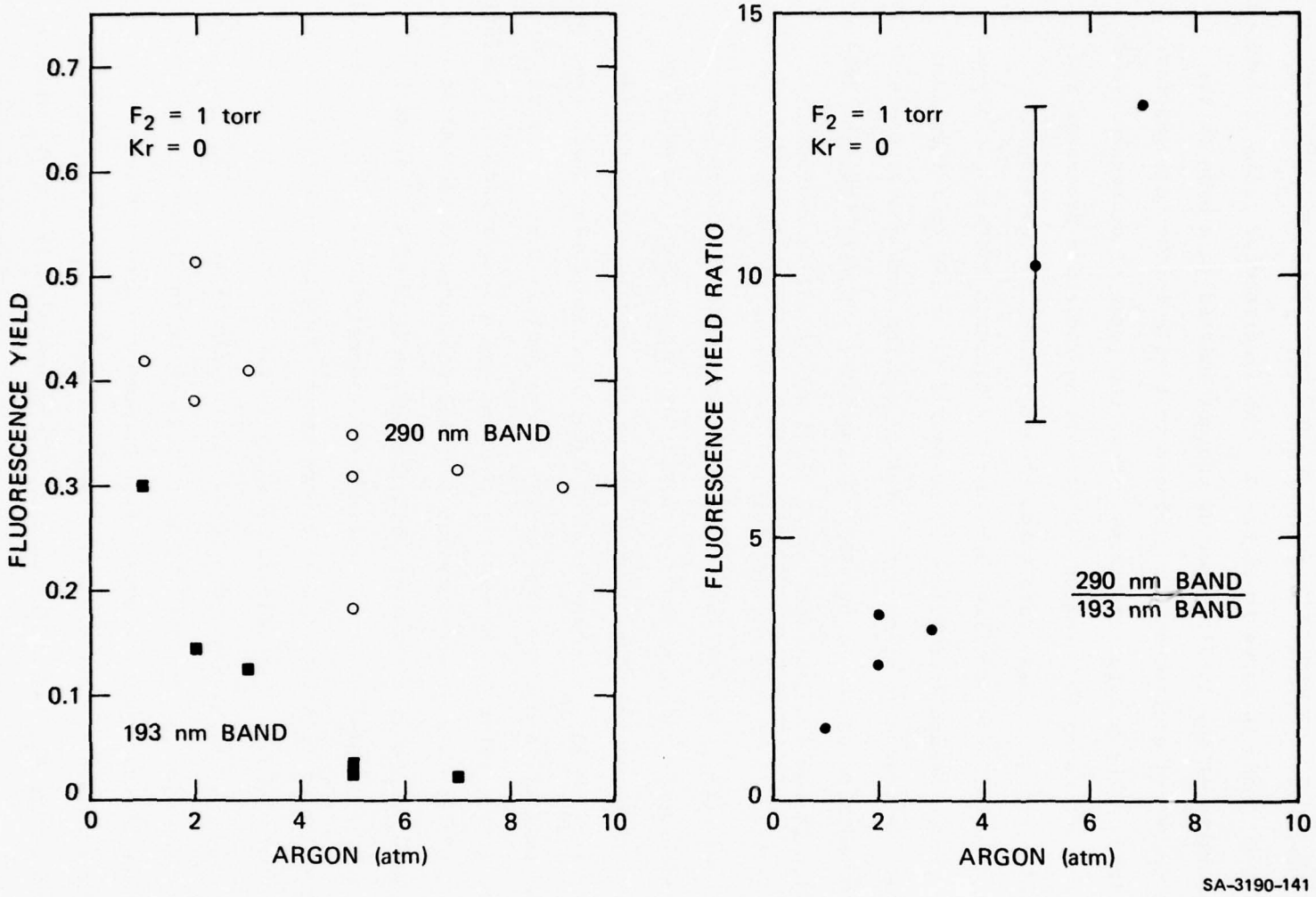

FIGURE 4 ARGON PRESSURE DEPENDENCE OF 193 nm BAND AND 290 nm BAND FLUORESCENCE YIELDS

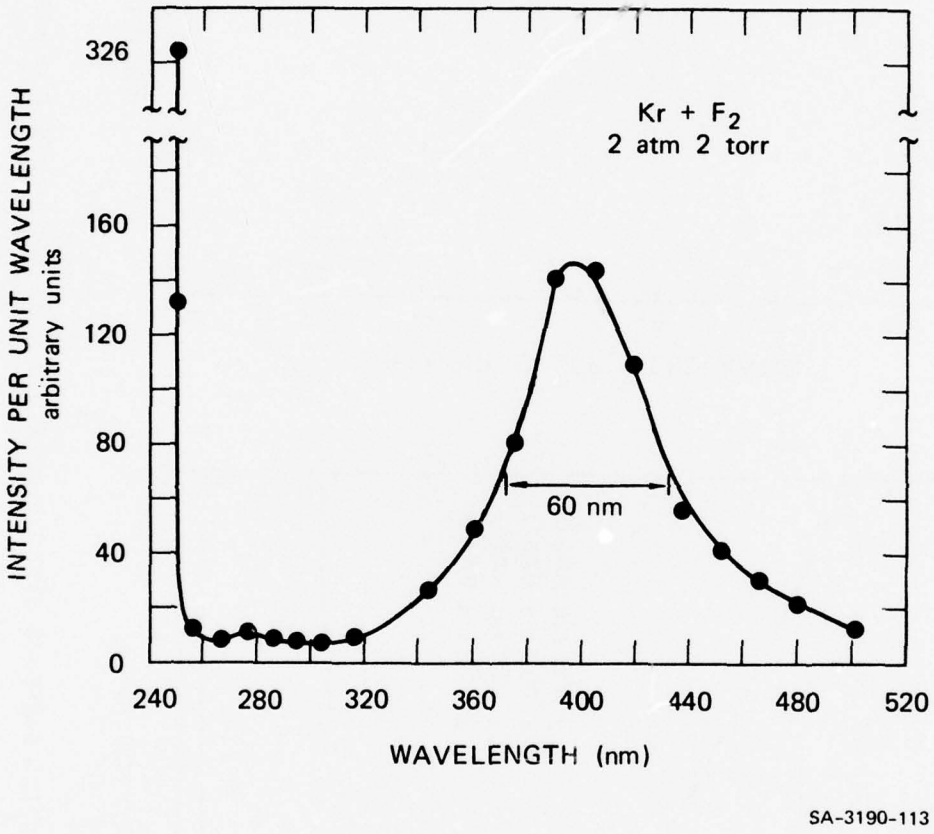

FIGURE 5 Kr_2F EMISSION BAND NEAR 400 nm

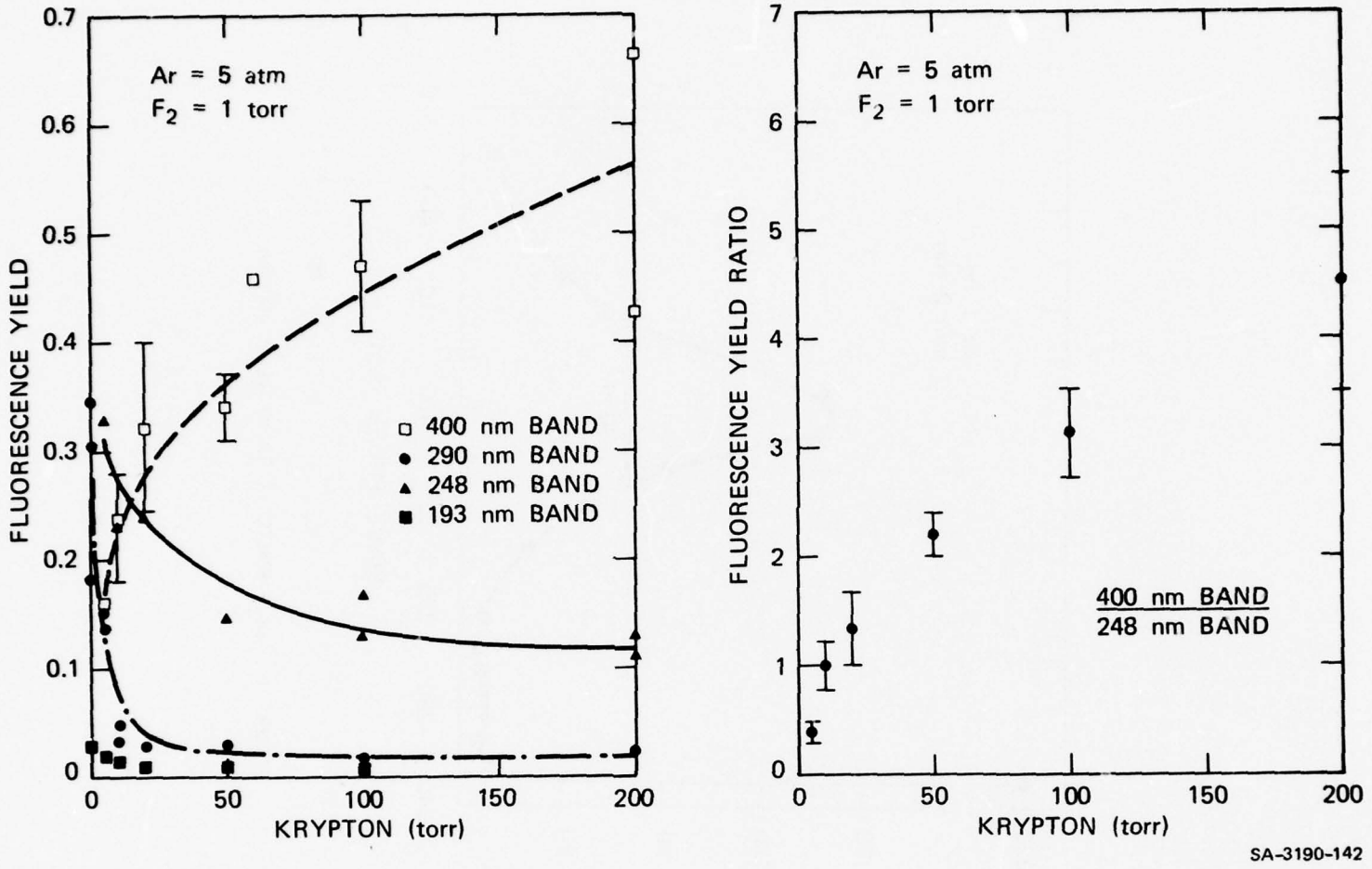

FIGURE 6 KRYPTON PRESSURE DEPENDENCE OF THE RARE GAS HALIDE FLUORESCENCE YIELDS

longer than that of any of the other emissions. Thus, we conclude that in this case the 400-nm emitter is the lower-lying electronic level to which most of the energy is flowing. Since the total fluorescence yield is not 100%, some of the emission is being quenched, probably by F_2. There is also some radiation at 126 nm (Ar_2^*) and 147 nm (Kr_2^*).

We have also observed the same 400-nm band in $Ar/Kr/NF_3$ mixtures, as has Northrop [B76]. In this mixture, the fluorescence yield is higher and the decay time slower than they are in $Ar/Kr/F_2$ mixtures. The same general characteristics are observed for the 290-nm band in Ar/NF_3 mixtures.

In $Ar/Xe/F_2$ mixtures, we have observed a broadband emission peaked at about 460 nm. This band, which was also seen by Brau and Ewing [BE75a], but identified as a Σ-Π transition in diatomic XeF, behaves differently from the broadband emissions described above. Its decay rate is fast and identical to that of the 351-nm XeF^* emission. However, the ratio of the intensities of the 460- and 351-nm emissions is found to increase with increasing Ar density. For this reason, the 460 nm emission cannot arise from the same state as the XeF 351 nm emission. Further, the fluorescence yield of the 460-nm radiation increases with decreasing Xe. We conclude that the 460-nm emitter requires both an Ar and Xe atom and therefore is of the form $ArXeF_n$. The simplest case requires $n = 1$. We have not as yet been able to observe an emission in Xe/F_2 mixtures that behaves like the 400-nm emission in Kr/F_2.

The 400-nm band cannot be explained in terms of the well-established electronic structure of the KrF molecule [BE75a, DH76, THH76]. Nor is it possible to explain the 290-nm band in terms of the structure of ArF [HD76, MH76]. We conclude that these bands are not emitted by a diatomic, and the next simplest species to consider are triatomics. In analogy with the Ar^+F^- and Kr^+F^- ionic bonds, two possible ionically bonded triatomics, $Ar_2^+F^-$ and $Ar^+F_2^-$, (similarly for Kr) can be suggested.

Either of these excited states should lie lower in energy than the corresponding diatomic because of the energy of the additional bond; this is the diatomic rare gas ion bond in one case ($\sim$ 1.2 eV) and the F_2^- bond ($\sim$ 1.4 eV) in the other case. In contrast, the ground state of Ar_2F will certainly be repulsive due to the repulsive interaction between the Ar atoms (the Ar-F interaction is probably very weak at the expected internuclear separations). However, ArF_2 in the ground state may have some binding (with respect to ArF + F) due to the strong F_2 bond, but in any case should not be repulsive. These arguments are dependent upon the geometry assumed for the ionic upper state at its minimum. However, it is difficult to imagine any geometry of ArF_2 that will be sufficiently repulsive in the ground state to explain both the energy and bandwidth of the observed transitions. Hence, we are led to suggest that the 290-nm emitter is Ar_2F^* and that the 400-nm emitter is Kr_2F^*. This conclusion is substantiated further by the observation of the same bands in mixtures in which the F_2 is replaced by NF_3. If, in analogy with the alkali halides, these species are formed by charge transfer interactions, it is most likely that only F is abstracted from the fluorine donor.

These assignments are given further support by studies of the analogous dialkali-halide molecules. Ewing and Brau [BE75a,EB75] had considerable success in predicting the bond energies of RgX^* ionic states using the known bond energies of corresponding alkali halides, AX. The utility of this method of estimating bond strengths is due to the strongly ionic nature of both the AX and RgX^* bonds together with the similarity in sizes of adjacent A^+ and Rg^+ ions.

Since the Rg_2^+ and A_2^+ diatomic ions are stable and bound with energies of 0.5 to 1.0 eV, an analog to the Rg_2X^* excited state should be the corresponding A_2X ground-state molecule. Unfortunately, because of the lack of spectroscopic studies of A_2X molecules, the ground-state surfaces of these molecules are not well understood. However, the

existence of bound A_2X molecules has been established from beam-scattering studies of A_2 with X where A_2X is observed as a long-lived intermediate complex that decays into the products AX + X [FKG72, SKM75, WHG73]. It is generally established that the intermediate complex is formed by the crossing from a covalent to a bonding ionic surface (also known as the harpoon or electron jump model). In the single-collision case in which the total energy remains positive, the collision complex usually decays via an intersection with a second covalent surface. For example, the reaction $K_2 + Cl \rightarrow K_2^+Cl \rightarrow K + KCl$ is observed with a cross section of 50-100 Å; the reaction also branches to $K^* + KCl$ about equally. The $A_2 + X_2$ collisions are also observed to proceed through an intermediate ionic complex that usually decays to A + AX + X.

Stimulated by these measurements, several groups have theoretically investigated the structure of the A_2X surfaces using pseudo-potential techniques [LWG73, RC68, S73]. It was found that these molecules are bound ionically, with the most stable geometry being triangular. The potential energy well depths with respect to A + AX dissociation are in the range from 0.5 to 1 eV. Although the triatomic analogy to Rg_2X is not as obvious as the diatomic case, the suggestion that the Rg_2X^* will have stable ionic states ($Rg_2^+X^-$) that are formed by a harpooning reaction of Rg_2^* with X_2 is strongly supported by the observations on the A_2X molecules. Further, we expect the stable geometry of Rg_2X^* to be triangular. In contrast to the beam case, the strongly exoergic $Rg_2^* + X_2$ reactions are occurring in a high-density environment where multiple collisions during the lifetime of the complex can relax it to the stable potential minimum before it radiates or dissociates. We can also expect that bound Rg_2X^* molecules will be formed by the reaction

$$RgX^* + 2Rg \rightarrow Rg_2X^* + Rg \quad .$$

The relevant energy levels for the ArF molecules and the postulated Ar_2F molecule are shown in Figure 7. Here we have assumed a triangular geometry for the excited ionic state with the Ar^+-Ar spacing equal to the Ar_2^+ equilibrium separation. A vertical transition to the ground state ends on a repulsive state having an energy of about 1 eV due to the Ar_2 repulsion at that internuclear separation (the Ar-F ground-state interaction is assumed to be negligible). The upper level is then determined by the 290-nm transition wavelength and lies about 1.1 eV below ArF^*. If we now assume that the slope of the ground state Ar_2F potential at R_e is equal to that of Ar_2 at the equilibrium separation of Ar_2^* and the shape of the upper states is similar, then the bandwidth of the 400-nm band is easily scaled from the bandwidth of Ar_2^* emission at 125 nm. This scaling gives a value of 41 nm-full width at half maximum as compared with the observed value of 52.5 nm. In the Kr_2F case, the bandwidth scaling gives 53 nm as compared with 60 nm observed.

The pseudo-potential calculations referred to above have indicated that heteronuclear dialkali-halides may also have stable ionic ground states. This suggests the possibility of stable heteronuclear excited rare gas halide triatomics and supports the suggested identification of emission from $ArXeF^*$ in $Ar/Xe/F_2$ mixtures. Although no optical emission has been clearly identified with $ArKrF^*$, the suggestion that this species plays a role in the reaction kinetics is certainly plausible.

Evidence in the kinetic data also supports the conclusions that the broadband emissions are due to Rg_2X^* molecules. In the following section, data are presented showing that the temporal decay rate of Ar_2F^* exactly follows that of Ar_2^* under conditions where the ArF^* is disappearing much faster. The same behavior is observed in the decay of Kr_2F^* and Kr_2^* as demonstrated in Section 4 (see Figure 15). It is concluded that these decay rates reflect the formation rates of Ar_2F and Kr_2F from the reactions

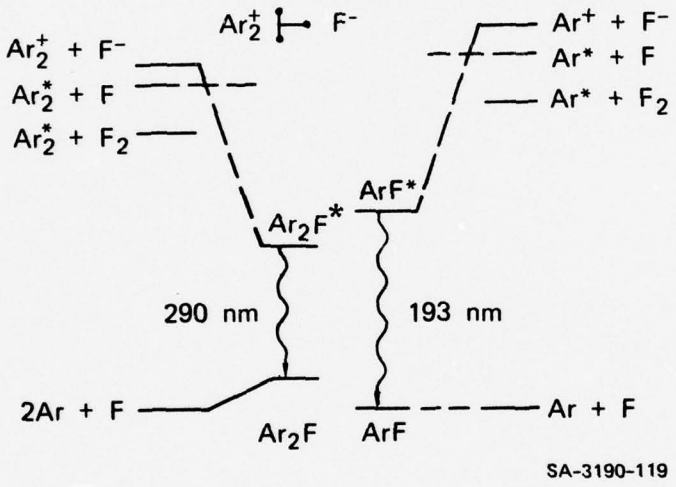

FIGURE 7 RELEVANT ArF AND Ar_2F ENERGY LEVELS

$$Ar_2^* + F_2 \rightarrow Ar_2F^* + F \qquad (5)$$

$$Kr_2^* + F_2 \rightarrow Kr_2F^* + F \quad . \qquad (21)$$

Reaction (5) is obviously consistent with the predominance of Ar_2F^* emission at high densities of Ar where Ar_2^* is formed rapidly by the three-body process. It is significant to note from Figure 7 that ArF^* could energetically be formed from the reaction of $Ar_2^* + F_2$. However, it is clear from the very different decay times and fluorescence yields of the two species that the contribution from this channel is not very significant.

4. ArF/KrF KINETICS

Overview of Energy Flow Concepts

In the following sections we will describe in some detail our experimental observations of the fluorescence yield and time decay of each of the various emissions arising from electron-beam excited argon/krypton/fluorine mixtures. A kinetic model will be presented that explains most of the observations. Many of the rate coefficients have been estimated by numerical comparison of the kinetic model with the experimental data. The gas pressures chosen and the excitation conditions used are not necessarily typical of those chosen for laser operation. Rather, the pressures have been chosen to isolate or emphasize one or another of the kinetic processes under investigation. The fast, high-intensity, small-volume excitation source is used because of its convenience in making time-decay measurements.

One might argue that the excitation conditions we have chosen will not be representative of the slow, low-current, large-volume e-beam/discharge devices now under development. While a number of differences exist between the kinetic processes operating under the two types of excitation conditions, all of the kinetic processes that are important under e-beam excitation are also important under e-beam/discharge excitation, as we will show below.

The details of the rare gas energy flow kinetics have been discussed at some length previously [L76, LEH73, LO72] and need only brief review here. The primary electrons deposit their energy through ionization

$$e + X \rightarrow X^+ + 2e \quad .$$

The resulting secondary electrons cool through successive ionization steps and atomic excitation

$$e + X \rightarrow X^{*} + e$$

until their energy drops below the excitation threshold. Subsequent elastic collisions rapidly cool the electrons to a few tenths of an eV where continued cooling is retarded by the Ramsauer minimum in the cross section.

The electron-ion recombination in the pure rare gases occurs mainly through the dissociative mechanism involving the molecular ion

$$X^{+} + 2X \rightarrow X_2^{+} + X$$

$$X_2^{+} + e \rightarrow X^{**} + X$$

populating predominately the second group of atomic excited states, $X(np^5(n+1)p)$. These p levels relax via the reactions

$$X^{**} + 2X \rightarrow X_2^{**} + X$$

$$X_2^{**} + (X) \rightarrow X^{*} + X + (X)$$

to the s levels that finally populate the excimer levels

$$X^{*} + 2X \rightarrow X_2^{*}(^{1,3}\Sigma_u^{+}) + X \quad .$$

The interpretation of the fluorescence from the singlet and triplet excimers is complicated [under the normal high excitation density conditions] by the near coincidence of the two levels (less than 1000-cm^{-1} separation), the greatly differing radiative lifetimes [e.g., 4 nsec for $Ar_2^{*}(^{1}\Sigma_u^{+})$ and 3 μsec for $Ar_2^{*}(^{3}\Sigma_u^{+})$], and by the rapid mixing of the two levels by the secondary plasma electrons.

Subsequent reactions of the excited rare gas species with additive gases have been under investigation for several years. Lasers have been demonstrated based on energy transfer from the excited atoms [Ar/N_2 (HGH74)]

or from the excimers [XeO (HGH75)]. As will be shown below, reactions of excited atoms and excimers both give rise to important emissions in $Ar/Kr/F_2$ mixtures.

One of the complicated features which arises with the use of fluorine (or halogen-containing molecules generally) is dissociative electron attachment. Under the Febetron 706 excitation conditions used here, the competition between the reactions

$$e + Ar_2^+ \rightarrow Ar^* + Ar$$

and

$$e + F_2 \rightarrow F^- + F$$

appears to be decided in favor of electron recombination under most pressure conditions. Further, about one-fourth of the electron beam energy is deposited directly into Ar^*. The rate coefficient for electron recombination varies from 10^{-7} cm^3/sec at 1 eV to 10^{-6} cm^3/sec [BB70] at thermal energies. Taking the electron attachment rate coefficient to be 10^{-9} [H76, JM76] and the charge density 10^{15}[Ar(atm)]cm^{-3}, we see at 3-atm Ar and 1-torr F_2 that the electron-recombination proceeds at a frequency of 3×10^8 to 3×10^9 sec^{-1} while the attachment, at about 3×10^7 sec^{-1}, cannot compete. Of course, under lower-excitation density conditions in which the electron density is low and electron-ion recombination slowed, electron attachment may become more important.

Under e-beam controlled discharge excitation, it is expected that most of the energy deposition is to be accomplished through excitation by the discharge electron reactions:

$$e + Ar \rightarrow Ar^* + e$$

$$e + Kr \rightarrow Kr^* + e \quad ,$$

and that the subsequent energy flow will be through neutral reaction channels.

Thus, under the conditions reported here, we may consider that the energy deposited by the electron beam rapidly finds its way to the lowest few excited states of the argon atom. The dominant energy pathways to the important emitting species (ArF^*, Ar_2F^*, KrF^*, and Kr_2F^*) are

$$
\begin{array}{l}
Ar^* \rightarrow ArF^* \rightarrow KrF^* \\
\quad \downarrow \\
\quad Ar_2^* \rightarrow Ar_2F^* \\
\quad\quad \downarrow \\
\quad\quad Kr^* \rightarrow KrF^* \\
\quad\quad\quad \downarrow \\
\quad\quad\quad ArKr^* \rightarrow Kr_2^* \rightarrow Kr_2F^*
\end{array}
\quad .
$$

The multitude of kinetic steps are illustrated in Figure 8.

Overview of the Kinetic Data

In this subsection we present a brief summary of the experimental observations and the preliminary qualitative conclusions. A detailed comparison of the data with the kinetic model is in the following subsection.

We have followed the four major emitting species ArF^*, Ar_2F^*, KrF^*, and Kr_2F^*, which vary in decay time and relative intensity as a function of the three gas pressures (Ar, Kr, F_2). The most reliable technique for measuring rate coefficients depends on the linear relationship between the reaction frequency and a product of the appropriate reactant pressures. For a multireaction process one does not always know which reaction in the kinetic chain is the rate-determining step. In particular, a common problem which is present for each of the rare gas halide species, is that the formation kinetics are always slower than the sum of radiation and quenching. Since the observed decay always represents the slowest important kinetic step, the radiative lifetimes and quenching coefficients cannot be determined from a simple decay-frequency plot.

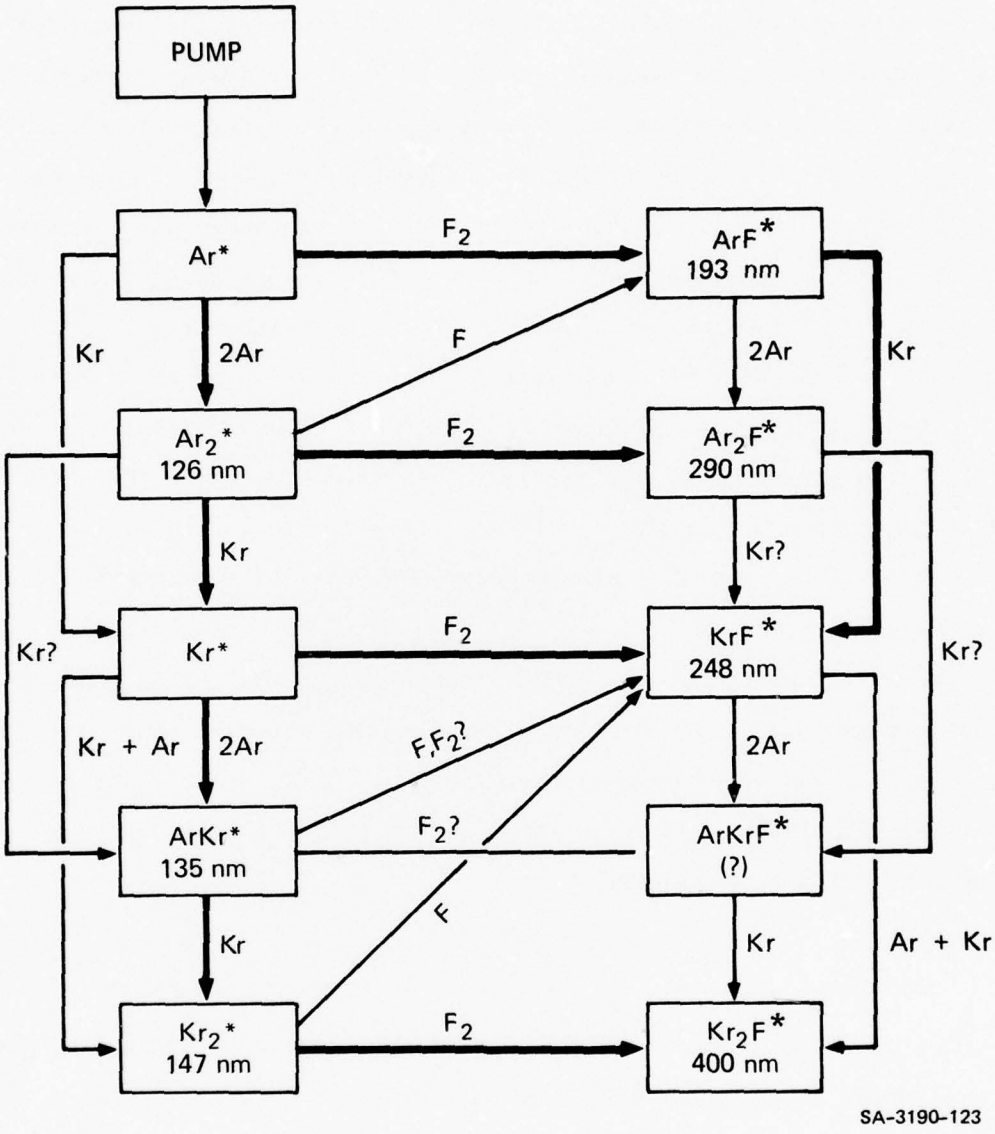

FIGURE 8 ENERGY FLOW DIAGRAM FOR $Ar/Kr/F_2$. MAJOR PATHWAYS SHOWN AS BOLD ARROWS. ALL RARE GAS HALIDES SUBJECT TO RAPID QUENCHING BY FLUORINE.

Emissions of ArF^*

The time-dependent population of ArF^* was monitored through its emission near 193 nm. The signal was observed to decay very rapidly (40-250 MHz)--so rapidly that due to the limitations of the detection instrumentation and the pulse length of the Febetron itself, irreproducibility of the time-decay data prevented direct determinations of the relevant reaction rate coefficients. Generally, the decay became more rapid if any of the argon, krypton, or fluorine pressures were increased. Such behavior is consistent with known rapid reactions of Ar^*, the precursor of ArF^*, with $F_2 \rightarrow ArF^*$ [Reaction (1)]† and with $2Ar \rightarrow Ar_2^*$ [Reaction (3)], as well as the presumed rapid radiation of ArF^*, quenching by F_2 [Reaction (8)] and exchange with $Kr \rightarrow KrF$ [Reaction (9)]. At very low fluorine pressures (< 0.2 torr) or high argon pressures (> 5 atm) a long-lived component appears. This is evidently due to reaction $Ar_2^* + F \rightarrow ArF^* + Ar$ with a slower decay-time that is characteristic of the decay of Ar_2^*.

The ArF fluorescence yields were surprisingly small (30% being the greatest observed). They decreased rapidly with added krypton [exchange Reaction (9)] and added argon [interception of Ar^* to Ar_2^*, Reaction (3)]. They were relatively independent of fluorine pressure [evidence for quenching by F_2, Reaction (8)].

Emissions of Ar_2F^*

The broadband emission in the region from 260 nm to 320 nm has been characterized above as arising from the triatomic rare gas halide Ar_2F^*. The decay of emissions in this wavelength region are typically much slower than those of ArF^*, specifically from (4-160 MHz), although at the higher krypton pressures they became similar. This indicates that

---

† Reaction numbers refer to the reactions listed in the next subsection (Table 2).

ArF cannot be the dominant source [Reaction (10)] of Ar_2F^* (for $F_2 \leq 7$ torr, Kr ≤ 50 torr, Ar ≤ 9 atm). Generally the decay frequencies were independent of the argon pressure and increased linearly with added fluorine or krypton. All of this is consistent with rate-determining steps being that at which the precursor Ar_2^* either reacts with F_2 to give Ar_2F^* [Reaction (5)], reacts with Kr to give Kr^* [Reaction (4)], or radiates to give 126 nm photons [Reaction (6)].

The fluorescence yields were surprisingly high (40-50%) even at low argon pressures. As expected, the fluorescence yields decreased rapidly with added krypton [Reaction (4)], as more and more of the Ar_2^* precursor was consumed by energy transfer to krypton (some direct quenching of Ar_2F^* by krypton is also probable [Reaction (13)]). The decrease of the fluorescence yield with added fluorine is attributed to the interception of Ar^* (the precursor of Ar_2^* which itself is the precursor of Ar_2F^*) to make ArF [Reaction (1)]. Surprisingly, the Ar_2F^* also decreased slightly with increasing argon pressure. This is in contrast to the expected rise from low values at low argon pressures to a plateau at higher pressures. This apparent contradiction may be due in part to reaction of Ar_2^* with fluorine atoms to produce ArF^* instead of Ar_2F^*.

Emissions of KrF^*

The time-dependent population of KrF^* was monitored through its emission near 248 nm. The time scale of the fluorescence decay was observed to be quite similar to that of Ar_2F^* (20-200 MHz) under the same conditions, and again, for Kr < 50 torr, was much slower than the decay of ArF^*. The time-decay of KrF^* was dominated under most conditions by the time dependence of its slowest precursor, Kr^*. At low krypton pressures (≤ 50 torr), the KrF^* decay frequency increased linearly as a function of added krypton, following the reaction $Ar_2^* + Kr \rightarrow Kr^*$ as described above for the decay of Ar_2F^*. Above 50 torr of krypton, both KrF^* and Ar_2F^* decayed immeasurably fast (> 150 MHz).

The decay frequency also increased with added argon pressure. Under most conditions, KrF^* decayed much more rapidly than we would expect from the two straightforward loss processes for Kr^*:

$$Kr^* + F_2 \rightarrow KrF^* + F$$

$$Kr^* + Kr + Ar \rightarrow Kr_2^* + Ar \quad .$$

Since the decay of a species cannot proceed faster than the decay of the slowest of its important sources, we must conclude that Kr^* has some more rapid means of decay. The most plausible suggestion is

$$Kr^* + Ar + Ar \rightarrow ArKr^* + Ar \quad .$$

While this reaction is not well characterized (the postulated product has been observed in emission [CGR73, VOF75]), it is needed to explain the observed KrF^* decay frequencies.

The dependence of the decay frequency on fluorine pressure was less thoroughly investigated, but as expected, it generally increased as the fluorine pressure was increased. We also note that at all F_2 pressures, there was a very slow component to the KrF^* decay. At very low F_2, most of the signal intensity is in the slow component. The interpretation is that this component results from the reaction $Kr_2^* + F \rightarrow KrF^* + Kr$ and that the decay of Kr_2^* is quite slow, as we see below.

The fluorescence yield of KrF^* was observed to be very high, approaching 100% at low argon pressures. The fluorescence yield decreased rapidly as the argon pressure was increased. This may be explained as a combination interception {less ArF^* to exchange with [Reactions (1), (3), (9), (10)], conversion of $Kr^* \rightarrow ArKr^* \rightarrow Kr_2^*$ [Reactions (14), (16), (19)]} and quenching to the as yet unobserved $ArKrF^*$ [Reaction (25)]. The fluorescence yield was observed to decrease slowly as the krypton pressure was increased. This is interpreted as a decrease in the

importance of $ArKr^*$ as a source of KrF^* [Reaction (18)], as Reaction (19), $ArKr^* + Kr \rightarrow Kr_2^* + Ar$ becomes more rapid.

Emissions of Kr_2F^*

Kr_2F^* has been assigned above as the radiator of the 400 ± 30-nm band observed in e-beam excited $Ar/Kr/F_2$ mixtures. The time evolution of this species was monitored as a function of argon, krypton, and fluorine pressures. It was the observation of no dependence of the decay frequency on the argon and krypton pressures and the linear dependence on fluorine pressure which led to the identification of the reaction

$$Kr_2^* + F_2 \rightarrow Kr_2F^* + F \qquad (21)$$

as the rate-determining kinetic step and helped identify Kr_2F as the radiating molecule. However, as we will discuss below, Kr_2^* may not be the only source of Kr_2F^*. An additional source is probably

$$ArKrF^* + Kr \rightarrow Kr_2F^* + Ar \quad . \qquad (28)$$

The Kr_2F^* fluorescence yield increased and reached a plateau as the argon or krypton pressure was increased. The increased argon pressure facilitated the three body reactions leading from $Ar^* \rightarrow Ar_2^* \rightarrow Kr^* \rightarrow ArKr^* \rightarrow Kr_2^* \rightarrow Kr_2F^*$ and $KrF^* \rightarrow ArKrF^* \rightarrow Kr_2F^*$. An increase in the krypton pressure accomplishes an interception of the formation of KrF^* by $ArKr^* + Kr \rightarrow Kr_2^*$ [Reaction (19)] and rapidly converts $ArKrF^*$ into Kr_2F^* [Reaction (28)]. An increase in the F_2 pressure reduced the Kr_2F^* fluorescence yield. This is explained by interception of Kr^* or $ArKr^*$ to make KrF^* [Reactions (14),(18)] and by quenching of Kr_2F^* by F_2 [Reaction (30)].

Details of the Kinetic Model

In this subsection, we present a preliminary kinetic model for the energy flow in electron-beam excited $Ar/Kr/F_2$ mixtures. The model is based on the assumption (discussed above) that the energy deposited by the electron-beam is rapidly collected in the lower excited states of atomic argon. We postulate a collection of 30 reactions listed in Table 2, and use these reactions to explain the observed time decay and fluorescence yield of each of the emitting species. The data are used to establish consistent values of the rate coefficients (few of which are available in the literature).

The model and the values of the rate coefficients must be considered preliminary for three basic reasons:

- The data are incomplete. A variety of other combinations of gas pressures are yet to be investigated and many of the experiments must be repeated before they can be considered sufficiently accurate.
- The model does not yet accurately predict the data that have been taken. Only the first iteration has been completed in the determination of the rate coefficients.
- An important class of reactions has not yet been included; namely, reactions of Ar_2^* and Kr_2^* with F atoms produced by previous dissociation of the F_2. This makes the calculation of the various fluorescence yields inaccurate above 5 atm of total pressure since under those conditions as much as one-third of the F_2 can be dissociated.

Nevertheless, the progress that has been made is very encouraging. It appears that most of the important energy pathways have been identified, and the important rate coefficients appear to be determined to within at least a factor of two.

Table 2

REACTIONS AND RATE CONSTANTS RELEVANT TO THE RARE GAS HALIDE KINETIC MODELING

Reaction	Rate[a]	Uncertainty[b]	Ref.	Remarks
(1) $Ar^* + F_2 \rightarrow ArF^* + F$	7.5×10^{-10}	0.1	VKS76	
(2) $Ar^* + Kr \rightarrow Kr^* + Ar$	6×10^{-12}	0.1	PSC75	
(3) $Ar^* + 2Ar \rightarrow Ar_2^* + Ar$	1×10^{-32}	0.3	HGH74	
(4) $Ar_2^* \rightarrow h\nu(126nm) + 2Ar$	3.8×10^{6}	0.5	TW[c]	Effective value in the presence of F_2, 1-9 atm Ar
(5) $Ar_2^* + F_2 \rightarrow Ar_2F^* + F$	2.5×10^{-10}	0.2	TW	From decay of Ar_2^* and Ar_2F^* vs F_2
(6) $Ar_2^* + Kr \rightarrow Kr^* + 2Ar$	8×10^{-11}	0.2	TW, Z76	From decay of Ar_2F^* and KrF^* vs Kr [Zamir Ar_2^* vs Kr]
(7) $ArF^* \rightarrow h\nu(193nm) + Ar + F$	3.3×10^{7}	1.0	TW	From ArF^* fluorescence yield, relative to $ArF^* + F_2$
(8) $ArF^* + F_2 \rightarrow$ products	10^{-9}	1.0	TW	Guessed
(9) $ArF^* + Kr \rightarrow KrF^* + Ar$	1.5×10^{-10}	1.0	TW	From ArF^* fluorescence yield vs Kr, relative to $ArF^* + F_2$
(10) $ArF^* + 2Ar \rightarrow Ar_2F^* + Ar$	2×10^{-33}	2.0	TW	From ArF^* fluorescence yield, relative to $ArF^* + F_2$ (minor reaction)
(11) $Ar_2F^* \rightarrow h\nu(290nm) + 2Ar + F$	2×10^{8}	2.0	TW	From Ar_2F^* fluorescence yield, relative to $Ar_2F^* + F_2$
(12) $Ar_2F^* + F_2 \rightarrow$ products	10^{-9}	1.0	TW	Guessed
(13) $Ar_2F^* + Kr \rightarrow ArKrF^* + Ar$	10^{-10}	2.0	TW	From Ar_2F^* fluorescence yield vs Kr, relative to $Ar_2F^* + F_2$ (minor reaction)
(14) $Kr^* + F_2 \rightarrow KrF^* + F$	7.2×10^{-10}	0.1	VKS76	
(15) $Kr^* + Kr + Ar \rightarrow Kr_2^* + Ar$	5×10^{-32}	1.0	KVC73	(minor reaction)
(16) $Kr^* + 2Ar \rightarrow ArKr^* + Ar$	1×10^{-32}	1.0	TW	From decay and fluorescence yield of KrF^* vs Ar
(17) $ArKr^* \rightarrow h\nu(135nm) + Ar + Kr$	3×10^{6}	2.0	TW	Guessed in analogy with Ar_2^* and Kr_2^*
(18) $ArKr^* + F_2 \rightarrow KrF^* + Ar + F$	6×10^{-10}	2.0	TW	From KrF^* and Kr_2F^* fluorescence yields vs F_2
(19) $ArKr^* + Kr \rightarrow Kr_2^* + Ar$	1×10^{-10}	1.0	TW	From decay and fluorescence yield of KrF^* vs Kr relative to $ArKr^* + F_2$

Reaction	Rate[a]	Uncer-tainty[b]	Ref.	Remarks
(20) $Kr_2^* \rightarrow h\nu(147nm)+2Kr$	3.3×10^{6}	0.5	TW	Effective value in the presence of F_2, 1-9 atm argon, and 5-500 torr Kr
(21) $Kr_2^* + F_2 \rightarrow Kr_2F^* + F$	3×10^{-10}	0.3	TW	From decay of Kr_2^* and Kr_2F^* vs F_2
(22) $KrF^* \rightarrow h\nu(248\ nm) + Kr + F$	1.5×10^{8}	1.0	HD76	Constant with KrF^* fluorescence yield
(23) $KrF^* + F_2 \rightarrow$ products	1×10^{-9}	1.0	TW	Guessed
(24) $KrF^* + Kr + Ar \rightarrow Kr_2F^* + Ar$	2×10^{-33}	2.0	TW	Guessed by analogy to $ArF^* + 2Ar$ (minor reaction)
(25) $KrF^* + 2Ar \rightarrow ArKrF^* + Ar$	4×10^{-33}	2.0	TW	Estimated from KrF^* fluorescence yield vs Ar relative to $KrF^* + F_2$
(26) $ArKrF^* \rightarrow h\nu + Ar + Kr + F$	5×10^{7}	2.0	TW	Guessed in analogy to other lifetimes
(27) $ArKrF^* + F_2 \rightarrow$ products	10^{-9}	2.0	TW	Guessed
(28) $ArKrF^* + Kr \rightarrow Kr_2F^* + Ar$	10^{-10}	2.0	TW	Guessed in analogy with other exchange reactions consistent with Kr_2F fluorescence yields
(29) $Kr_2F^* \rightarrow h\nu(400nm) + 2Kr + F$	6.7×10^{7}	1.0	TW	From Kr_2F fluorescence yield vs F_2 relative to $Kr_2F^* + F_2$
(30) $Kr_2F^* + F_2 \rightarrow$ products	10^{-9}	1.0	TW	Guessed

a. (cm^3/sec, etc.)

b. as a fraction of the value of the rate coefficient. An uncertainty of 0.2 means 20%; an uncertainty of 1.0 means a factor of two.

c. TW = This Work

Reactions of Ar^* and ArF

The reactions of Ar^* have received considerable study in recent years. Three reactions of importance in the current instance are

$$Ar^* + F_2 \rightarrow ArF^* + F \qquad k_1 = 7.5 \times 10^{-10}\ cm^3/sec \qquad (1)$$

$$Ar^* + Kr \rightarrow Kr^* + Ar \qquad k_2 = 6 \times 10^{-12}\ cm^3/sec \qquad (2)$$

$$Ar^* + 2Ar \rightarrow Ar_2^* + Ar \qquad k_3 = 10^{-32}\ cm^6/sec \qquad (3)$$

Flowing afterglow studies by Setser and colleagues [PSC75, VKS76] and others [HGH74, L76] have characterized the reactions of $Ar(^3P_2)$ well and to a less extent $Ar(^3P_0)$. Under the e-beam excitation conditions of the work reported here, the contribution of $Ar(^1P_1)$ and $Ar(^3P_1)$ will be expected to be important. Lacking other information, we chose the reaction rate coefficients to be the same for all four low-lying argon excited states.

The reactions of ArF^* have only recently come under investigation. Four of these are considered here:

$$ArF^* \rightarrow Ar + F + h\nu \qquad k_7 \sim 3.3 \times 10^7\ sec^{-1} \qquad (7)$$

$$ArF^* + F_2 \rightarrow \text{products} \qquad k_8 \sim 10^{-9}\ cm^3/sec \qquad (8)$$

$$ArF^* + Kr \rightarrow KrF^* + Ar \qquad k_9 \sim 1.5 \times 10^{-10}\ cm^3/sec \qquad (9)$$

$$ArF^* + 2Ar \rightarrow Ar_2F^* + Ar \qquad k_{10} \leq 2 \times 10^{-33} \qquad (10)$$

As mentioned, the observed decay of ArF^* was so rapid that its dependence on the gas pressures was an unreliable approach for determining the various rate coefficients. Instead, we examined the pressure dependence of the fluorescence yield (determined experimentally as explained above).

The kinetic model suggests that the ArF^* fluorescence yield at 193 nm may be represented by

$$FY_{193} = \frac{k_1F_2}{k_1F_2 + k_2Kr + k_3Ar^2} \cdot \frac{k_7}{k_7 + k_8F_2 + k_9Kr + k_{10}Ar^2}$$

The first of these factors gives the probability that Ar^* reacts with F_2 to give ArF^* instead of reacting with Kr or 2Ar to give Kr^* or Ar_2^*. The second factor gives the probability that the ArF^*, once made, succeeds in radiating instead of reacting with F_2, Kr, or 2Ar. We immediately see that the fluorescence yield should drop rapidly as the Kr or Ar pressure is increased. The dependence upon the F_2 pressure will be slightly more complicated; namely, rising from zero at zero F_2, reaching a peak when most of the Ar^* has been converted to ArF^*, and finally decreasing again as F_2 quenching dominates. These trends can be seen in Figures 9-11. The lines drawn near the data are calculated through the kinetic model equation given above. As further illustrated in Figure 12, the agreement between the kinetic model and the experimental values may be considered adequate (factor of 2) although not complete. The model overestimates the low experimental values observed.

Since investigation of the fluorescence yields can only give relative values of the rate coefficients, we have chosen the quenching of all of the rare gas halides (ArF^*, Ar_2F^*, KrF^*, $ArKrF^*$, and Kr_2F^*) to occur with the same rate coefficient of 10^{-9} cm^3/sec. The low fluorescence yields observed at Ar = 1 atm and F_2 = 1-6 torr indicate that fluorine quenching must compete effectively with ArF^* radiation at all of these fluorine pressures. This suggests a rather long radiative lifetime. The preliminary value is 30 nsec [Reaction (7)].

We may examine the Kr and Ar pressure dependence more simply through the reciprocal of the fluorescence yield

$$\frac{1}{FY_{193}} = \frac{k_1F_2 + k_2Kr + k_3Ar^2}{k_1F_2} \cdot \frac{k_7 + k_8F_2 + k_9Kr + k_{10}Ar^2}{k_7}$$

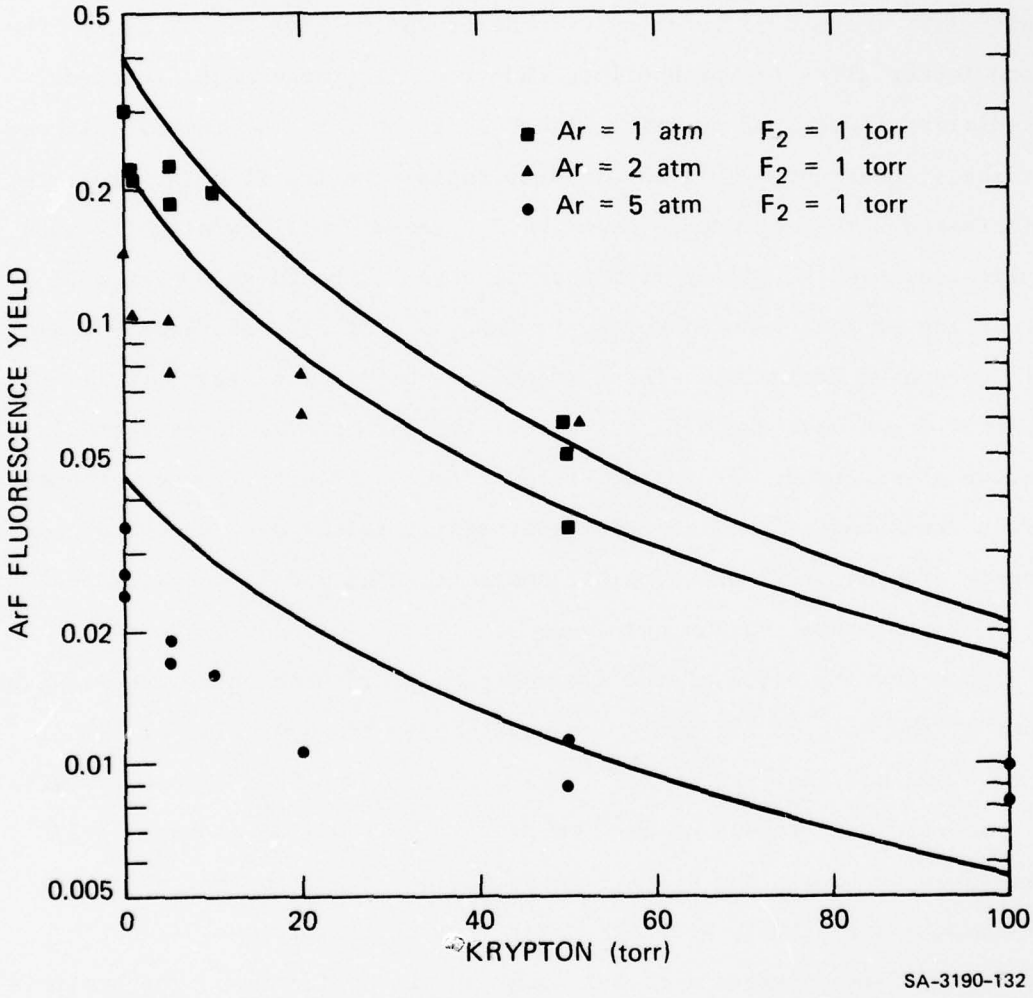

FIGURE 9 KRYPTON PRESSURE DEPENDENCE OF ArF FLUORESCENCE YIELD

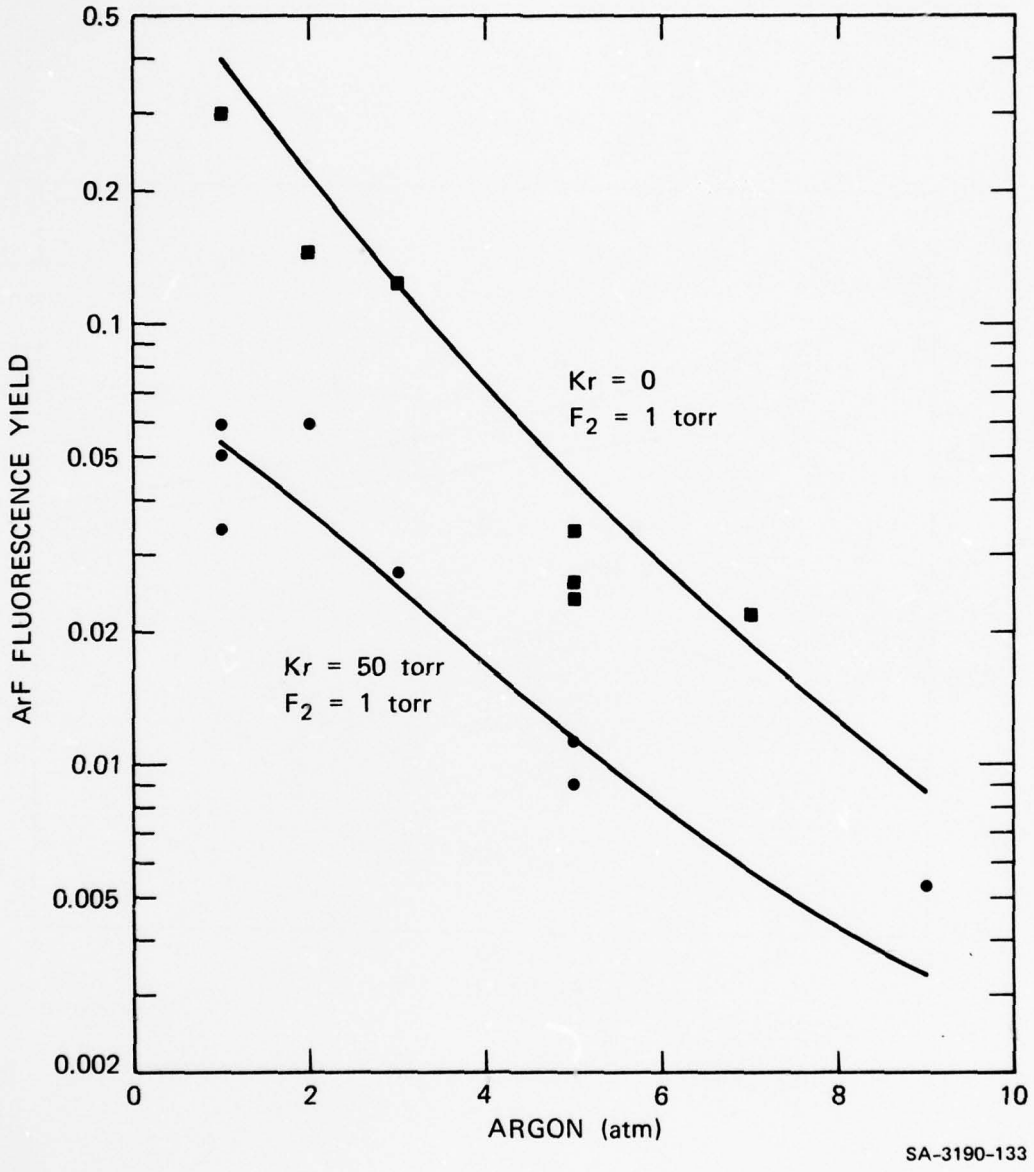

FIGURE 10 ARGON PRESSURE DEPENDENCE OF ArF FLUORESCENCE YIELD

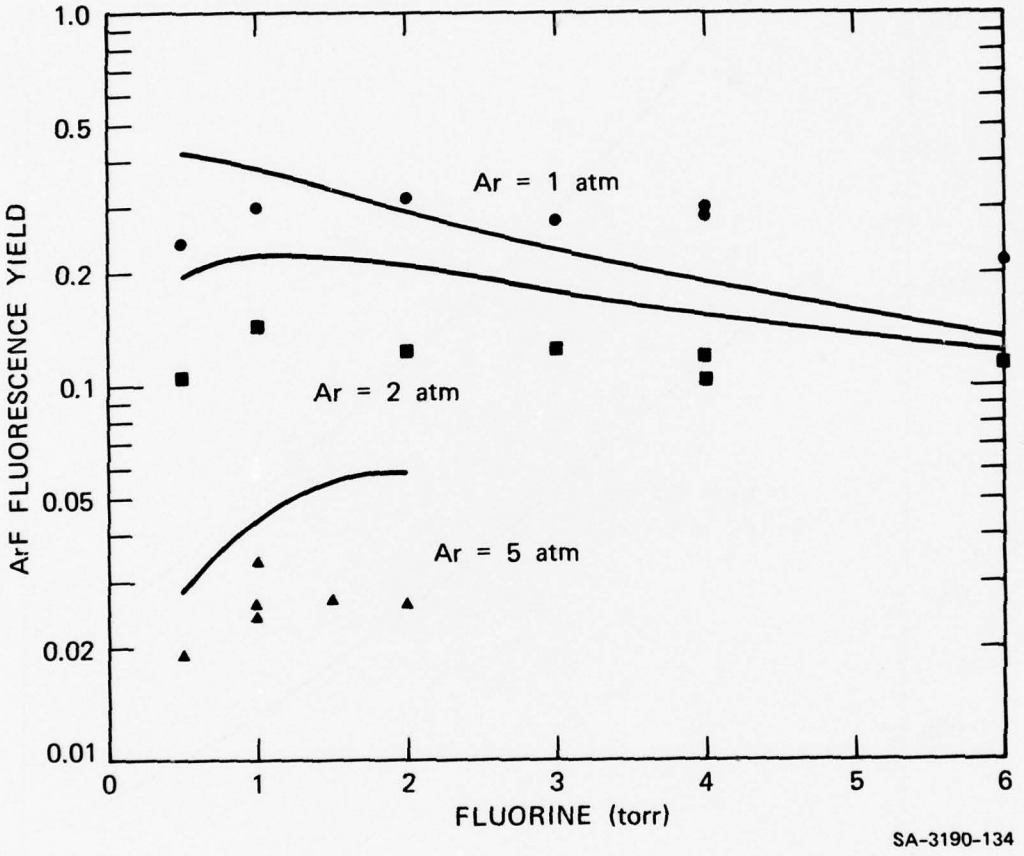

FIGURE 11 FLUORINE PRESSURE DEPENDENCE OF ArF FLUORESCENCE YIELD (Kr = 0)

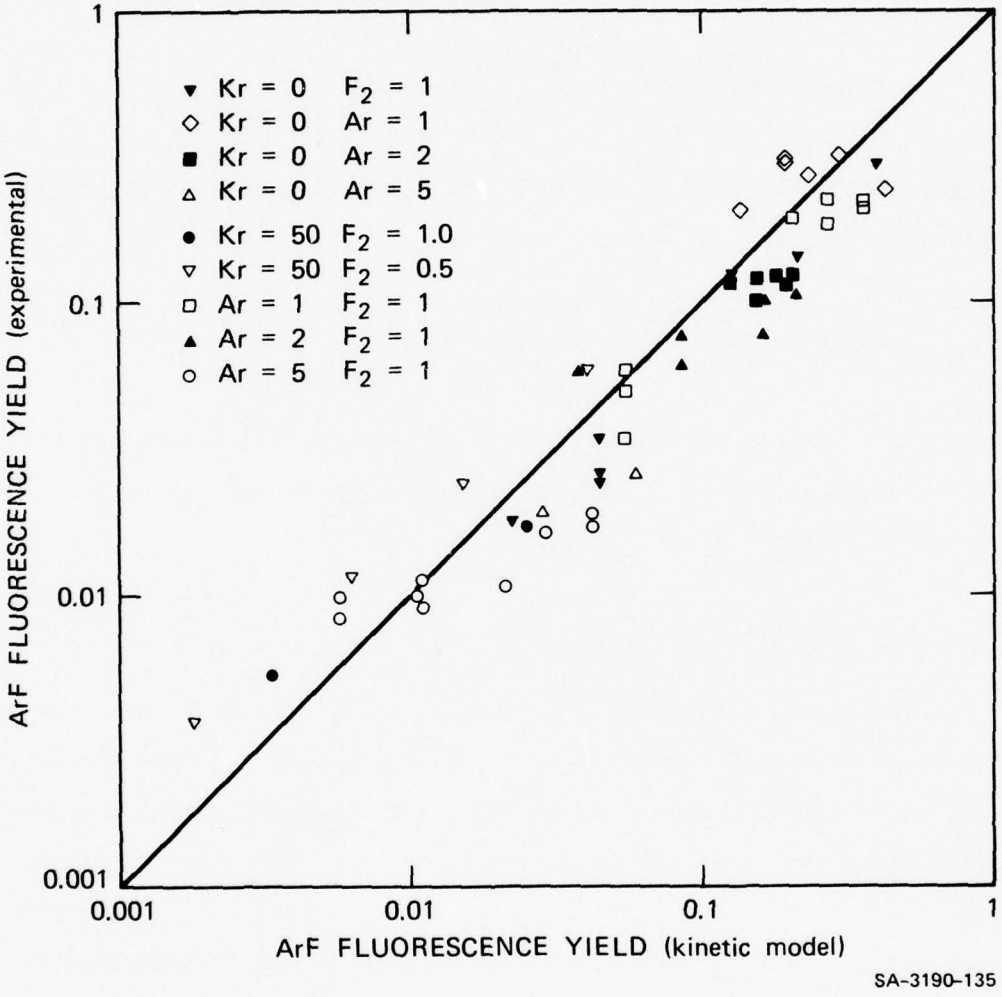

FIGURE 12 COMPARISON OF EXPERIMENTAL ArF FLUORESCENCE YIELDS WITH KINETIC MODEL

Since, as we will find, $k_9 \gg k_2$ and $k_3 \gg k_{10}$, a graph of $\frac{1}{FY_{193}}$ versus Kr or Ar^2 will be dominated by k_9 and k_3 respectively. This is illustrated in Figures 13 and 14. In Figure 13, for example, we can see that the slope near Kr = 0 should give

$$\text{Slope} \approx \frac{k_1F_2 + k_3Ar^2}{k_1F_2} \frac{k_9}{k_7} \quad ,$$

which provides a value of k_9 (relative to k_7). Similarly in Figure 14, the slope (versus Ar^2) near Ar = 0 gives

$$\text{Slope} \approx \frac{k_3}{k_1F_2} \frac{k_7 + k_8F_2 + k_9Kr}{k_7} \quad .$$

The ratio of k_3/k_1 so determined is consistent with the literature values. Further, the small (or nonexistent) curvature versus Ar^2 can be used to set an upper limit on k_{10} (of 2×10^{-33} cm^6/sec).

Reactions of Ar_2^* and Ar_2F^*

In the current context, the reactions of Ar_2^* and Ar_2F^* are important because Ar_2^* is the dominant source of Kr^* which leads to KrF^* and Ar_2F^* is a potential laser molecule in its own right. Over the last few years, considerable effort has been dedicated toward the understanding of the rare gas excimer kinetics [L76] leading to the development of rare gas excimer lasers, fluorescence light sources, and energy transfer lasers. The observed time decay of the excimer fluorescence is affected by a number of rather subtle factors, not the least of which is the effect of collisions with the 0.1 to 0.5-eV secondary electrons. The energy distribution of the secondary electrons is expected to be strongly influenced by inelastic collisions with added molecular gases--in this case fluorine.

Under the conditions investigated here, the Ar_2^* is rapidly formed by the three-body reaction (3) discussed above ($Ar^* + 2Ar \rightarrow Ar_2^* + Ar$).

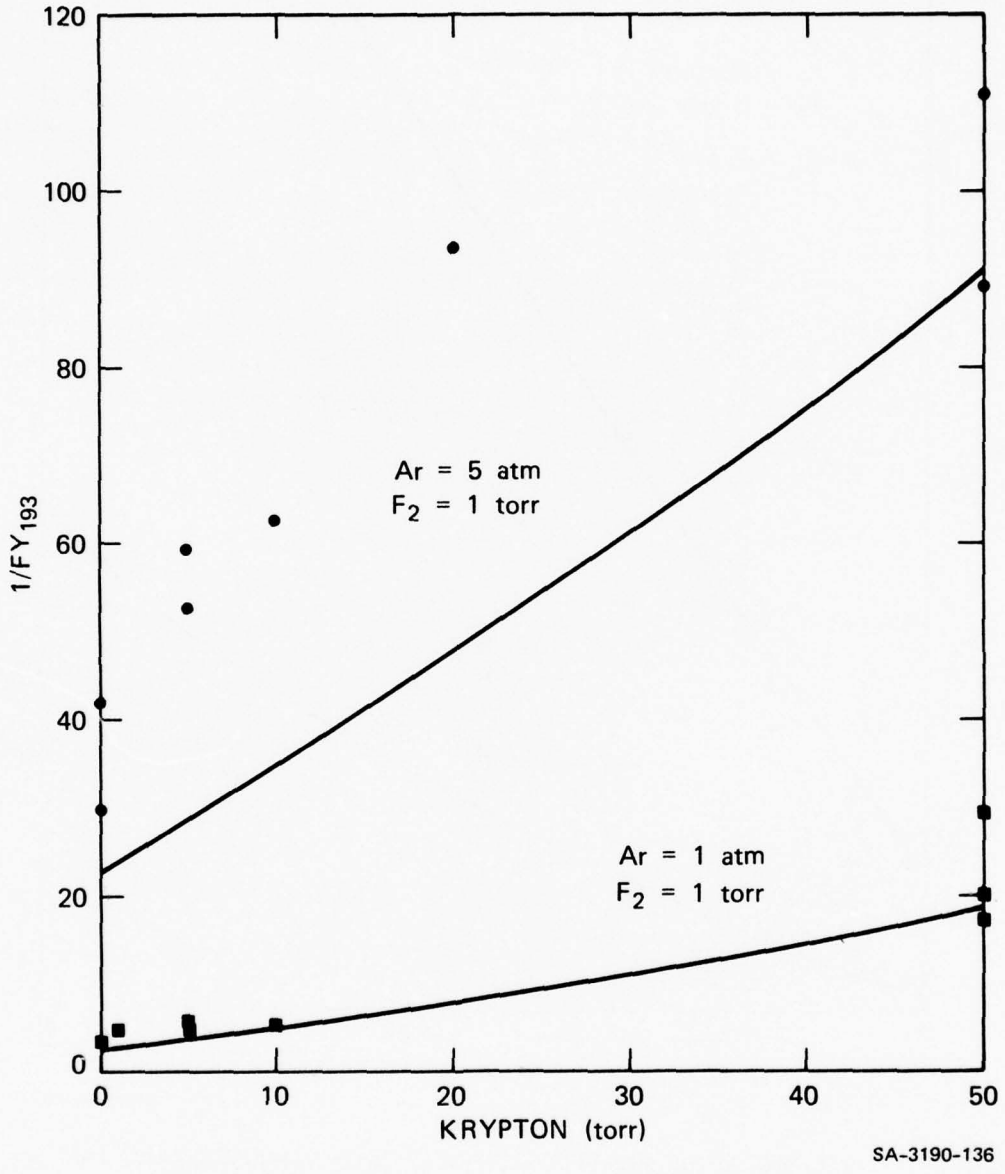

FIGURE 13 RECIPROCAL OF ArF FLUORESCENCE YIELD VERSUS KRYPTON PRESSURE

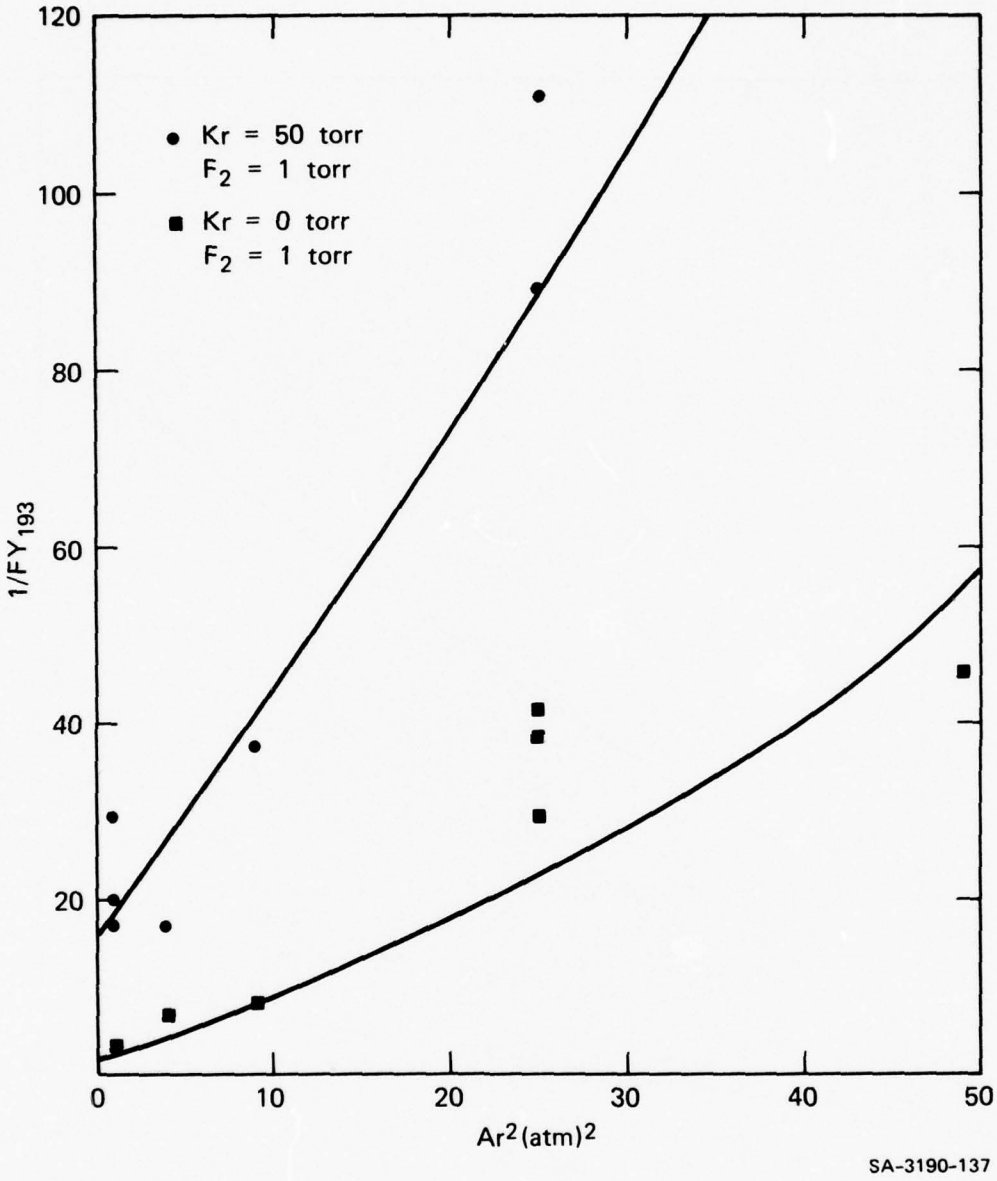

FIGURE 14 RECIPROCAL OF ArF FLUORESCENCE YIELD VERSUS THE SQUARE OF THE ARGON PRESSURE

The subsequent decay is dominated by the reactions listed below.

$$Ar_2^* \rightarrow 2Ar + h\nu \ (126 \text{ nm}) \qquad k_4 = 3.8 \times 10^6 \text{ sec}^{-1} \qquad (4)$$

$$Ar_2^* + F_2 \rightarrow Ar_2F + F \qquad k_5 = 2.5 \times 10^{-10} \text{ cm}^3/\text{sec} \qquad (5)$$

$$Ar_2^* + Kr \rightarrow Kr^* + 2Ar \qquad k_6 = 8 \times 10^{-11} \text{ cm}^3/\text{sec} \qquad (6)$$

Only with some difficulty can the Ar_2^* fluorescence be observed directly at 126 nm in $Ar/Kr/F_2$ mixtures. Quenching by F_2 and Kr is rather rapid, and the fluorescence presumably is further attenuated by F_2 photoabsorption. As we will conclude below, Ar_2F^* radiates much more rapidly than it is produced and hence serves as a monitor of the time decay of its source, i.e. Ar_2^*.

Figure 15 shows the observed decay frequency of Ar_2F^* versus fluorine pressure. As we can see, the argon pressure dependence is negligible and the fluorine pressure dependence is linear. We interpret the slope of the line drawn through the data as representing Reaction (15), $Ar_2^* + F_2 \rightarrow Ar_2F^* + F$, with the rate coefficient stated above. A few decay measurements were made with NF_3 as the source of fluorine atoms, yielding the data points shown in Figure 15. The value obtained for the rate coefficient is

$$Ar_2^* + NF_3 \rightarrow Ar_2F^* + NF_2 \qquad k_{5a} = 9 \pm 2 \times 10^{-11} \text{ cm}^3/\text{sec}. \qquad (5a)$$

The common intercept observed with F_2 and NF_3 suggests that we choose an argon pressure-independent value of 3.8×10^6 sec^{-1} for the radiative decay frequency of Ar_2^*.

Figure 16 shows the observed decay frequency of Ar_2F^* (as well as KrF^* and Kr_2F^* to be discussed subsequently) versus krypton pressure. Once again we interpret the slope of the line drawn through the data as representing Reaction (6), $Ar_2^* + Kr \rightarrow Kr^* + 2Ar$. The rate coefficient

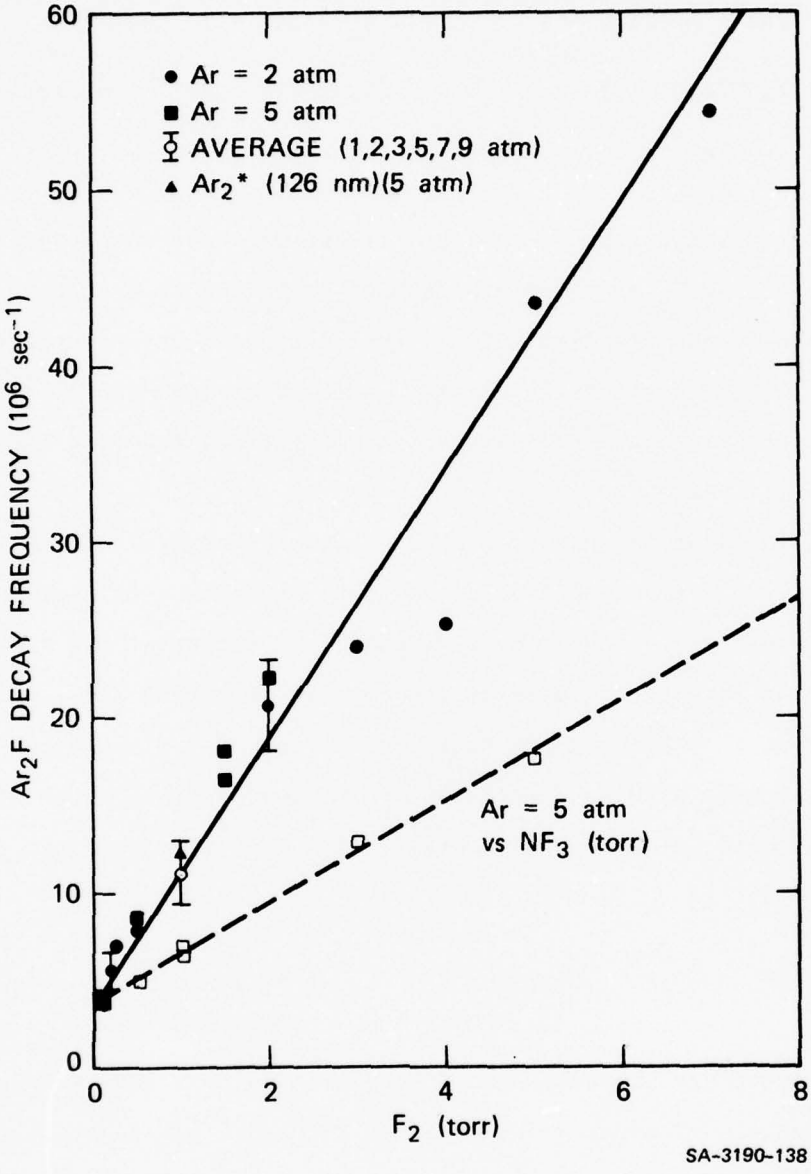

FIGURE 15 Ar_2F AND Ar_2^* DECAY FREQUENCIES VERSUS F_2 AND NF_3 PRESSURES (Kr = 0)

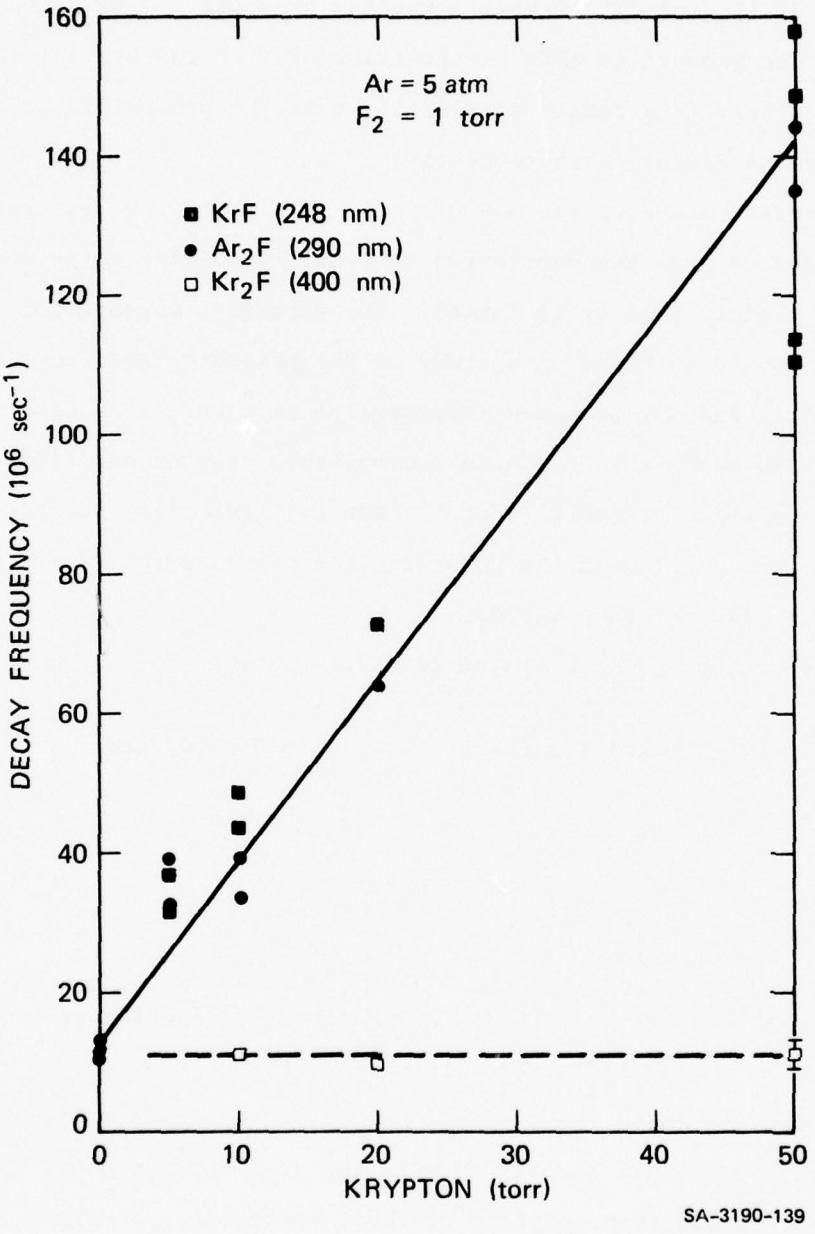

FIGURE 16 Ar_2F, KrF, AND Kr_2F DECAY FREQUENCIES VERSUS KRYPTON PRESSURE

obtained ($8 \pm 2 \times 10^{-11}$ cm^3/sec) is in excellent agreement with the value of $7 \pm 2 \times 10^{-11}$ obtained independently by Zamir [Z76] by monitoring the decay of Ar_2^* at 126 nm versus krypton pressure. Conclusive identification of the product of this energy-transfer reaction has not yet been obtained. There is a remote possibility that the product is $ArKr^*$, a molecule to be discussed subsequently.

As mentioned above, the use of Ar_2F^* as a monitor of the reactions of Ar_2^* depends upon the conclusion that Ar_2F^* radiates or is quenched much more rapidly than it is formed. The strongest support for this conclusion would be based on a study of the pressure dependence of the decay of Ar_2^* and the presumed agreement of Ar_2^* and Ar_2F^* decay frequencies. To date, this has been accomplished only at one fluorine (1 torr) and argon pressure (5 atm) shown in Figure 15. Further evidence will be provided below in the consideration of the pressure dependence of the Ar_2F^* fluorescence yields.

The reactions of Ar_2F^* to be considered are:

$$Ar_2F^* \rightarrow h\nu\ (290\ nm) + 2Ar + F \qquad k_{11} \sim 2 \times 10^8\ sec^{-1} \qquad (11)$$

$$Ar_2F^* + F_2 \rightarrow \text{quenched} \qquad k_{12} \sim 10^{-9}\ cm^3/sec \qquad (12)$$

$$Ar_2F^* + Kr \rightarrow ArKrF + Ar \qquad k_{13} \sim 10^{-10}\ cm^3/sec \qquad (13)$$

To study Reactions (11) and (12), we examine the fluorine pressure dependence of the Ar_2F^* fluorescence yield. Examination of the reactions of ArF discussed above leads to the conclusion that $ArF^* + 2Ar \rightarrow Ar_2F^* + Ar$ can make only a negligible contribution to the Ar_2F^* fluorescence. The Ar_2F^* fluorescence yield then consists of three factors (or branching ratios):

$$f_1 = \frac{k_3 Ar^2}{k_1 F_2 + k_3 Ar^2} \; ; \quad \text{the probability that } Ar^* \text{ makes } Ar_2^*,$$

$$f_2 = \frac{k_5 F_2}{k_4 + k_5 F_2} \; ; \quad \text{the probability that } Ar_2^* \text{ makes } Ar_2F^*,$$

$$f_3 = \frac{k_{11}}{k_{11} + k_{12} F_2} \; ; \quad \text{the probability that } Ar_2F^* \text{ radiates.}$$

Figure 17 shows the observed Ar_2F^* fluorescence yields for Ar = 2 atm and Kr = 0 versus fluorine pressure. Also shown are graphs of the fluorescence yield computed from the full kinetic model ($f_1 \cdot f_2 \cdot f_3$ + contributions from ArF^* and 2Ar) and the formation branching ratios (f_1 and $f_1 \cdot f_2$). We can see that the probability of forming Ar_2F^* (i.e., $f_1 \cdot f_2$) is very close to the observed fluorescence yields. We conclude that Ar_2F^* is not strongly quenched by F_2. As explained above, all of the rate coefficients for quenching of the rare gas halides by F_2 have been chosen to have the common value of 10^{-9} cm^3/sec. The observation of rather high fluorescence yields would then require a short radiative lifetime for Ar_2F^* (t nsec).

The alternative interpretation of the decay frequencies shown in Figure 15 is that the observed decay represents the quenching of Ar_2F^* which is somehow rapidly formed, from Ar_2^*, presumably. An upper gound to the expected fluorescence yield can then be computed from two factors:

$$f_1 = \frac{k_3 Ar^2}{k_1 F_2 + k_3 Ar^2} \; ; \quad \text{the probability that } Ar^* \text{ makes } Ar_2^* \text{ (as above)}$$

and

$$f_4 = \frac{3.8 \times 10^6}{3.8 \times 10^6 + 2.5 \times 10^{-10} F_2} \; ; \quad \text{the probability that } Ar_2F^* \text{ radiates.}$$

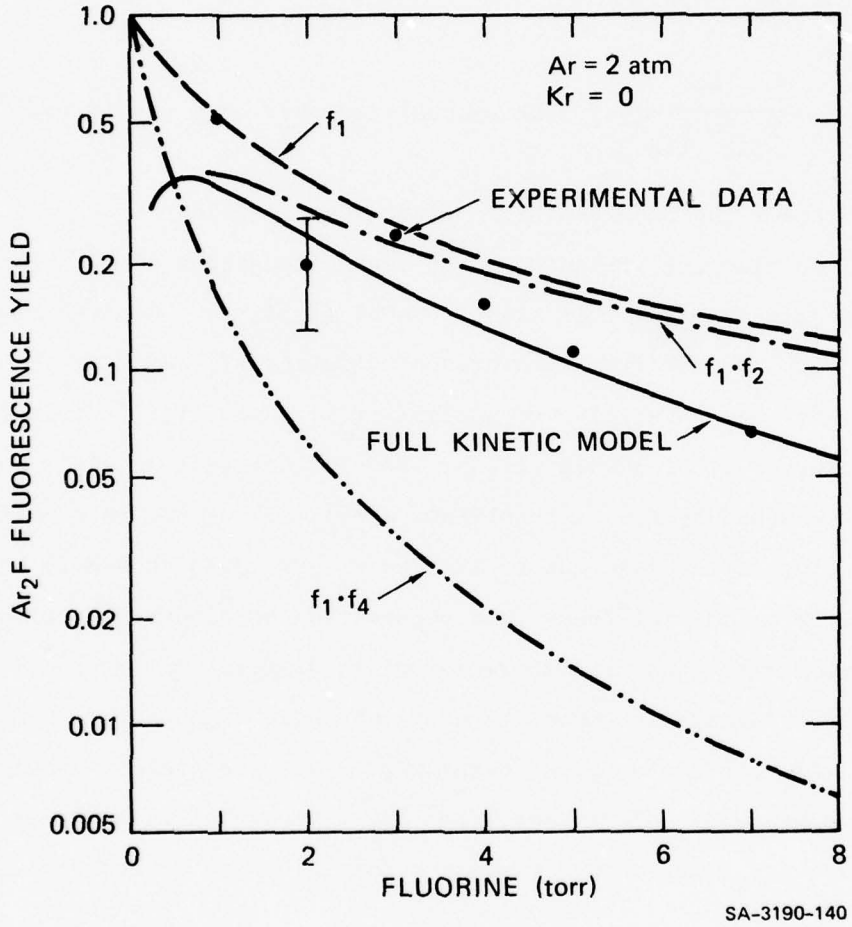

FIGURE 17 Ar_2F FLUORESCENCE YIELD VERSUS FLUORINE PRESSURE. COMPARISON BETWEEN KINETIC MODEL AND EXPERIMENT.

A plot of the product $(f_1 \cdot f_4)$ of these two is shown in Figure 17. It is apparent that this procedure predicts far too small a fluorescence yield and supports the conclusion that the observed decay of Ar_2F^* is indicative of the decay of its source (Ar_2^*) rather than the radiation and quenching of Ar_2F^* itself.

The Reaction (13) of krypton with Ar_2F^* is rather difficult to monitor directly since Reaction (6) with Ar_2^*, the precursor of Ar_2F^*, is relatively rapid. The situation is further complicated by a secondary KrF^* emission feature near 270 nm that would interfere with observation of Ar_2F^* at high krypton pressures. Finally, the nature of the product resulting from $Ar_2F^* + Kr$ [Reaction (13)] is not well established. We have arbitrarily chosen the product resulting from replacement of one argon atom ($ArKrF^*$), although one may argue plausibly that KrF^* could be preferred. In any case, this is not an important energy pathway.

Having decided that the decay frequency of Ar_2F^* is representative of the decay of Ar_2^*, we must again turn to the Ar_2F^* fluorescence yield to follow the reaction $Ar_2F^* + Kr$. Following the procedure used above, we write the Ar_2F^* fluorescence yield as a product of the factors

$$f_1 = \frac{k_3 Ar^2}{k_1 F_2 k_2 Kr + k_3 Ar^2} \quad ; \quad \text{probability of making } Ar_2^* \ ,$$

$$f_2 = \frac{k_5 F_2}{k_4 + k_5 F_2 + k_6 Kr} \quad ; \quad \text{probability of making } Ar_2F^* \ ,$$

and

$$f_3 = \frac{k_{11}}{k_{11} + k_{12} F_2 + k_{13} Kr} \quad ; \quad \text{probability that } Ar_2F^* \text{ radiates.}$$

Figure 18 shows the krypton pressure dependence of observed Ar_2F^* fluorescence yield. As we can see from the plot of $f_1 \cdot f_2$, the probability

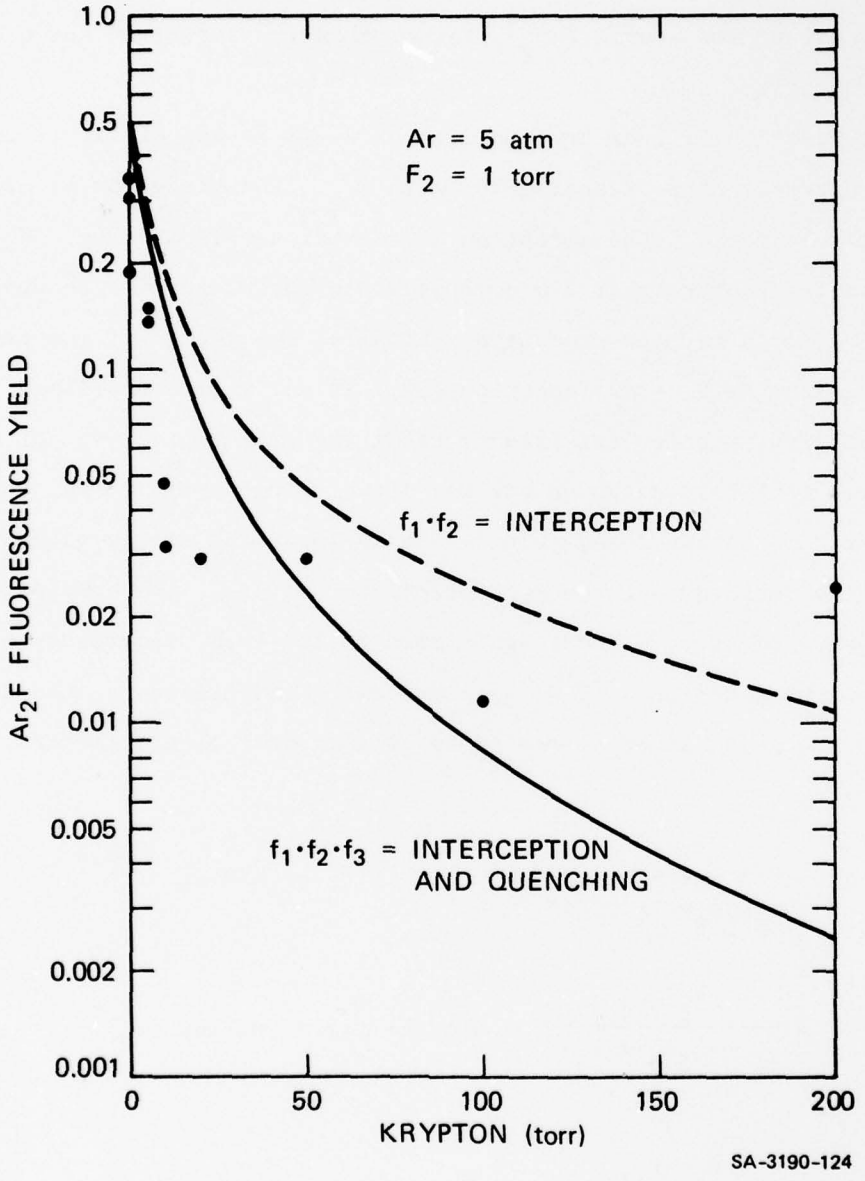

FIGURE 18 Ar_2F FLUORESCENCE YIELD VERSUS KRYPTON PRESSURE

of Ar_2F^* formation, the effect of interception of Ar_2^* by Kr is rather pronounced. Choosing a krypton quenching rate coefficient of $k_{13} = 10^{-10}$ cm^3/sec gives the lower curve shown in Figure 18 (labeled $f_1 \cdot f_2 \cdot f_3$) in reasonable agreement with the observations. As mentioned above, this determination is rendered imprecise by the contribution of the 270-nm band of KrF^*. Further, the model predicts a fluorescence yield that is much too high at zero krypton pressure, so that an absolute comparison of the computed and observed fluorescence yields is unreliable.

The argon pressure dependence of the Ar_2F^* fluorescence yield is shown in Figure 19. As is obvious from the figure, the data and the kinetic model disagree on the trend. The data show a gradual decrease with increasing argon pressure while the model predicts an increase. The only plausible explanation which has surfaced to date is that at the higher argon pressures a significant fraction of the fluorine is dissociated by energy transfer (about 1/3 torr at 10 atmospheres) and that if the reaction $Ar_2^* + F \rightarrow ArF^* + Ar$ is sufficiently rapid ($3\text{-}10 \times 10^{-10}$) a significant fraction of the Ar_2^* population will be redirected toward ArF^* instead of Ar_2F^*. This subject obviously requires further work to understand the data we have obtained, and because reactions with F atoms are certain to be important in laser media with long pumping pulses.

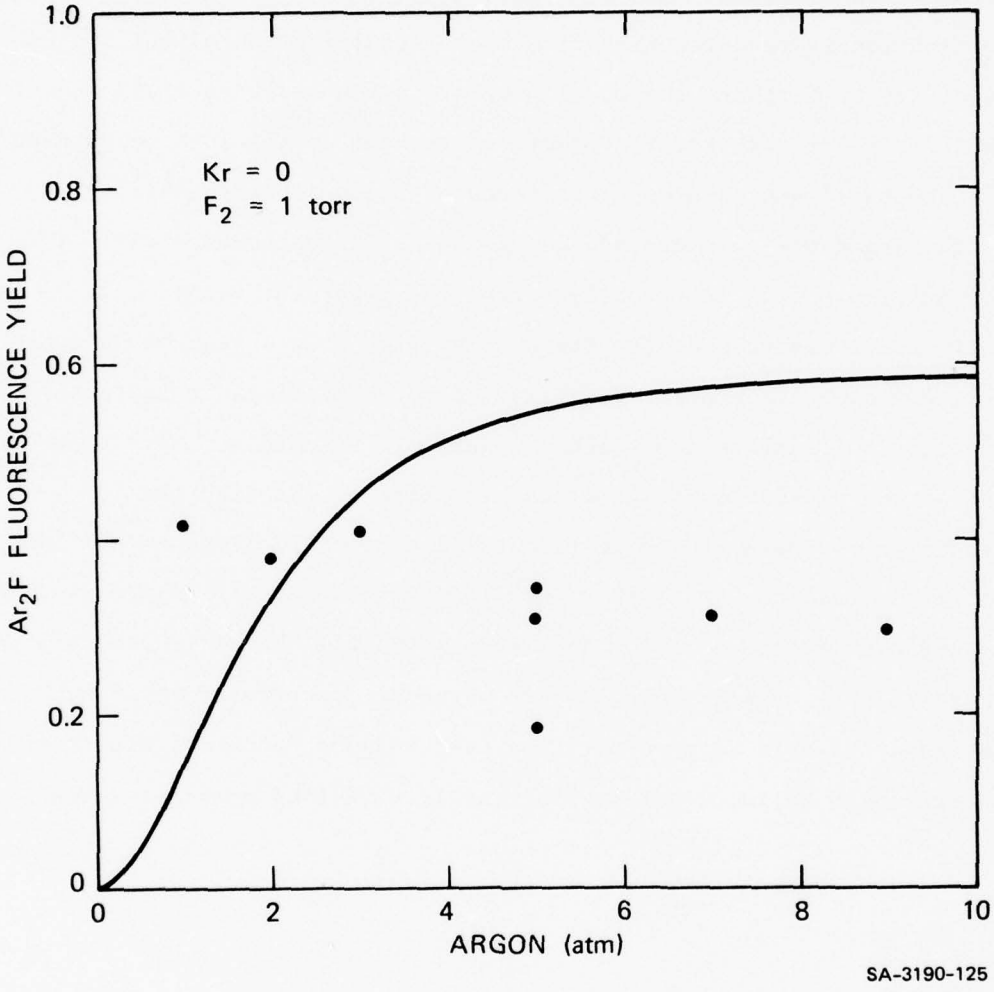

FIGURE 19 Ar_2F FLUORESCENCE YIELD VERSUS ARGON PRESSURE

Reactions of Kr^*, $ArKr^*$, and KrF

The reactions to be considered in this section are:

$$Kr^* + F_2 \rightarrow KrF^* + F \qquad k_{14} = 7.2 \times 10^{-10}\ cm^3/sec \qquad (14)$$

$$Kr^* + Kr + Ar \rightarrow Kr_2^* + Ar \qquad k_{15} \sim 5 \times 10^{-32}\ cm^6/sec \qquad (15)$$

$$Kr^* + 2Ar \rightarrow ArKr^* + Ar \qquad k_{16} \sim 10^{-32}\ cm^6/sec \qquad (16)$$

$$ArKr^* \rightarrow h\nu(135nm) + Ar + Kr \qquad k_{17} \sim 3 \times 10^{6}\ sec^{-1} \qquad (17)$$

$$ArKr^* + F_2 \rightarrow KrF^* + Ar + F \qquad k_{18} \sim 6 \times 10^{-10}\ cm^3/sec \qquad (18)$$

$$ArKr^* + Kr \rightarrow Kr_2^* + Ar \qquad k_{19} \sim 10^{-10}\ cm^3/sec \qquad (19)$$

$$KrF^* \rightarrow h\nu(248nm) + Kr + F \qquad k_{22} = 1.5 \times 10^{8}\ sec^{-1} \qquad (22)$$

$$KrF^* + F_2 \rightarrow \text{quenched} \qquad k_{23} \sim 10^{-9}\ cm^3/sec \qquad (23)$$

$$KrF^* + Kr + Ar \rightarrow Kr_2F^* + Ar \qquad k_{24} \sim 2 \times 10^{-33}\ cm^6/sec \qquad (24)$$

$$KrF^* + 2Ar \rightarrow ArKrF^* + Ar \qquad k_{25} \sim 4 \times 10^{-33}\ cm^6/sec \qquad (25)$$

The reaction of Kr^* with fluorine has been studied by Setser and colleagues [VKS76]. They found the value listed above [Reaction (14)], and that this reaction has essentially a 100% branching ratio to yield excited KrF^*. The formation of Kr_2^* in pure krypton is also well characterized [KVC73]. The rate coefficient with argon as the third body has apparently not been determined. We have chosen the value found in pure krypton. Due to the low density of krypton (compared with that of argon), this reaction is of little importance in the present study.

Before discussing the remaining reactions, it will be useful to remember that the fluorescence day of KrF^* serves as a monitor for its sources rather than for the time scale of its own radiation and quenching.

Perhaps the most important single number we wished to obtain was the KrF^* radiative lifetime. Unfortunately, under all the conditions we have examined, the KrF^* radiative decay frequency is camouflaged by its production kinetics. We are reduced to the statement that the value of 7 nsec reported by Hay and Dunning [DH76, HD76] is consistent with our observations, having chosen the fluorine quenching to proceed with a rate coefficient of 10^{-9} cm^3/sec.

In Figure 20, the KrF^* decay frequency is shown as a function of the argon pressure. The dashed line near the bottom of the figure shows the decay frequency expected for Kr^* if Reaction (16) were not operative. Clearly, if Kr^* is an important source of KrF^*, which we will demonstrate to be the case at the higher argon pressures, Kr^* must be disappearing much more rapidly than predicted by Reactions (14) and (15) above. Further, if we choose the quite plausible Reaction (16) as suggested, a value of the rate coefficient nearly as large as 10^{-32} cm^6/sec must be used to explain the rapid disappearance of KrF^* and hence Kr^*. Despite the likelihood that the $ArKr^*$ well depth is less than that for the homonuclear rare gas excimers, the suggested formation rate coefficient is reasonable.

Since the existence of the mixed excimer $ArKr^*$ is necessary to explain the KrF^* decay frequencies, we are faced with the difficult task of identifying the reactions in which it participates and determining or at least estimating the rate coefficients. On the basis of the identification of Cheshnovsky et al. [CGR73] and Verkhovtseva et al. [VOF75], we expect $ArKr^*$ to radiate near 135 nm. We have arbitrarily chosen a radiative transition rate of $k_{19} = 3 \times 10^6$ sec^{-1} in analogy with the effective value in the presence of F_2 used above for Ar_2^* and the value obtained below for Kr_2^*. The reaction of $ArKr^*$ with F_2 is difficult to monitor directly since neither $ArKr^*$ nor one possible product, $ArKrF^*$, has been observed in our laboratory. We will argue that in order to explain the observed KrF^* fluorescence yields, the

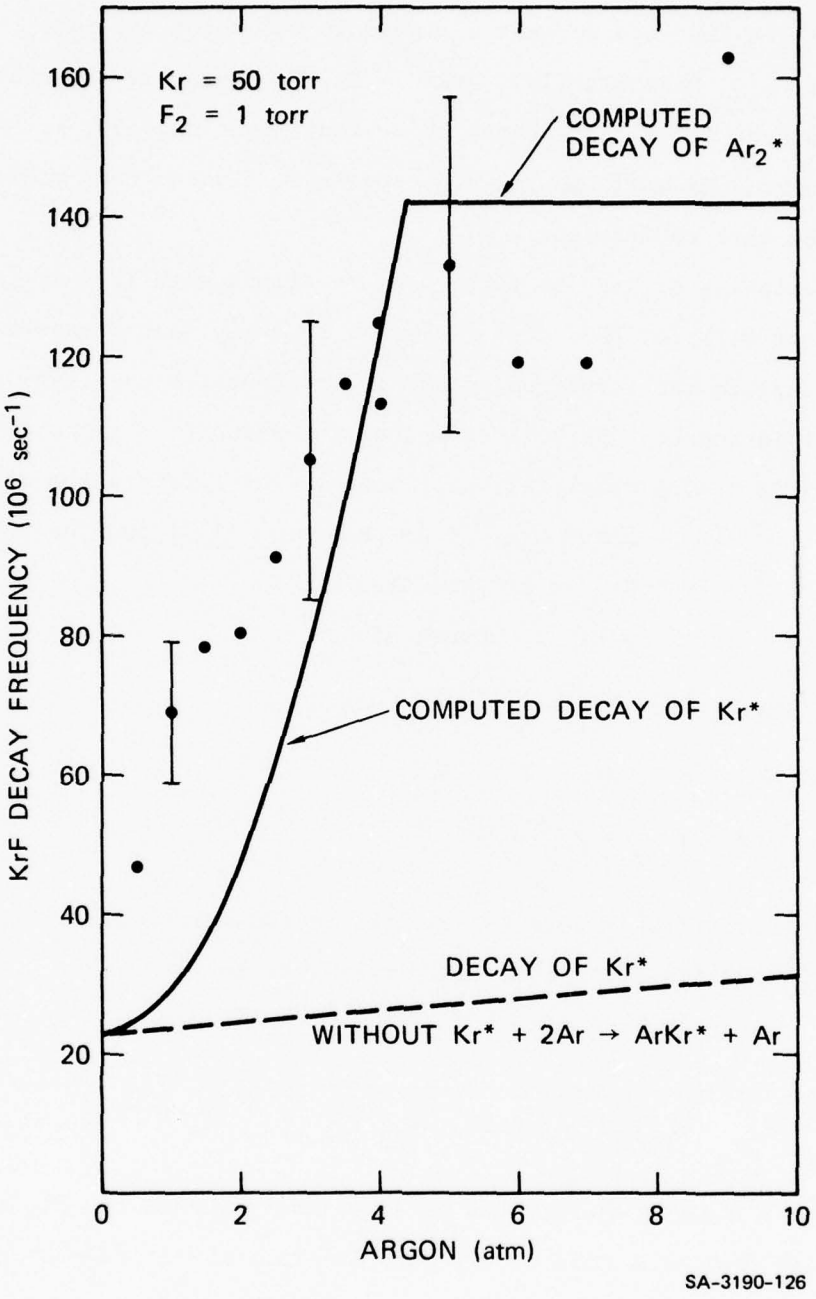

FIGURE 20 KrF DECAY FREQUENCY VERSUS ARGON PRESSURE

product must be KrF^* and suggest a plausible value for the rate coefficient k_{18}. Reaction (19), $ArKr^* + Kr$, is obviously the most important source of Kr_2^* since the three-body Reaction (15), $Kr^* + Kr + Ar$, is much slower. We will use the KrF^* and Kr_2F^* fluorescence yields to estimate the rate coefficient k_{19}.

The quenching of KrF^* by three-body reactions with Kr + Ar [Reaction (19)] or with 2Ar [Reaction (20)] has recently been proposed [MJ76, JMS76] to explain the reduction in KrF^* fluorescence as the argon or krypton pressure is increased. We will show that the reduction in the fluorescence yield is almost completely explained by the interception of the KrF^* precursor, $Kr^* + 2Ar \rightarrow ArKr^* + Ar$ [Reaction (16)] and the subsequent reaction $ArKr^* + Kr \rightarrow Kr_2^* + Ar$ [Reaction (19)].

The three most important sources of KrF^*:

$$ArF^* + Kr \rightarrow KrF^* + Ar \qquad (9)$$

$$Kr^* + F_2 \rightarrow KrF^* + F \qquad (14)$$

$$ArKr^* + F_2 \rightarrow KrF^* + Ar + F \qquad (18)$$

contribute to the KrF^* fluorescence yield as shown in Table 3. The probability that the KrF^*, once made, will radiate is

$$\frac{k_{22}}{k_{22} + k_{23}F_2 + k_{24}KrAr + k_{25}Ar^2} \quad .$$

This suggests that as the krypton pressure is increased the fluorescence that results from reactions of ArF^* and Kr^* can only increase. Figure 21 illustrates the observed gradual decrease of the KrF^* fluorescence yield as the krypton pressure is increased. This is interpreted to indicate the importance (at low krypton pressure) of $ArKr^*$ as a source of KrF^*; this source is rapidly consumed by added krypton through the reaction $ArKr^* + Kr \rightarrow Kr_2^* + Ar$ [Reaction (19)].

Table 3

SOURCES OF KrF^*

Source	Chance of Being Made	Chance of Giving KrF^*
ArF^*	$\dfrac{k_1F_2}{k_1F_2 + k_2Kr + k_3Ar^2}$	$\dfrac{k_9Kr}{k_7 + k_8F_2 + k_9Kr + k_{10}Ar^2}$
Kr^*	$\dfrac{k_2Kr + \dfrac{k_3Ar^2\, k_6Kr}{k_4 + k_5F_2 + k_6Kr}}{k_1F_2 + k_2Kr + k_3Ar^2}$	$\dfrac{k_{14}F_2}{k_{14}F_2 + k_{15}KrAr + k_{16}Ar^2}$
$ArKr^*$	$Kr^* \cdot \dfrac{k_{16}Ar^2}{k_{14}F_2 + k_{15}KrAr + k_{16}Ar^2}$	$\dfrac{k_{18}F_2}{k_{17} + k_{18}F_2 + k_{19}Kr}$

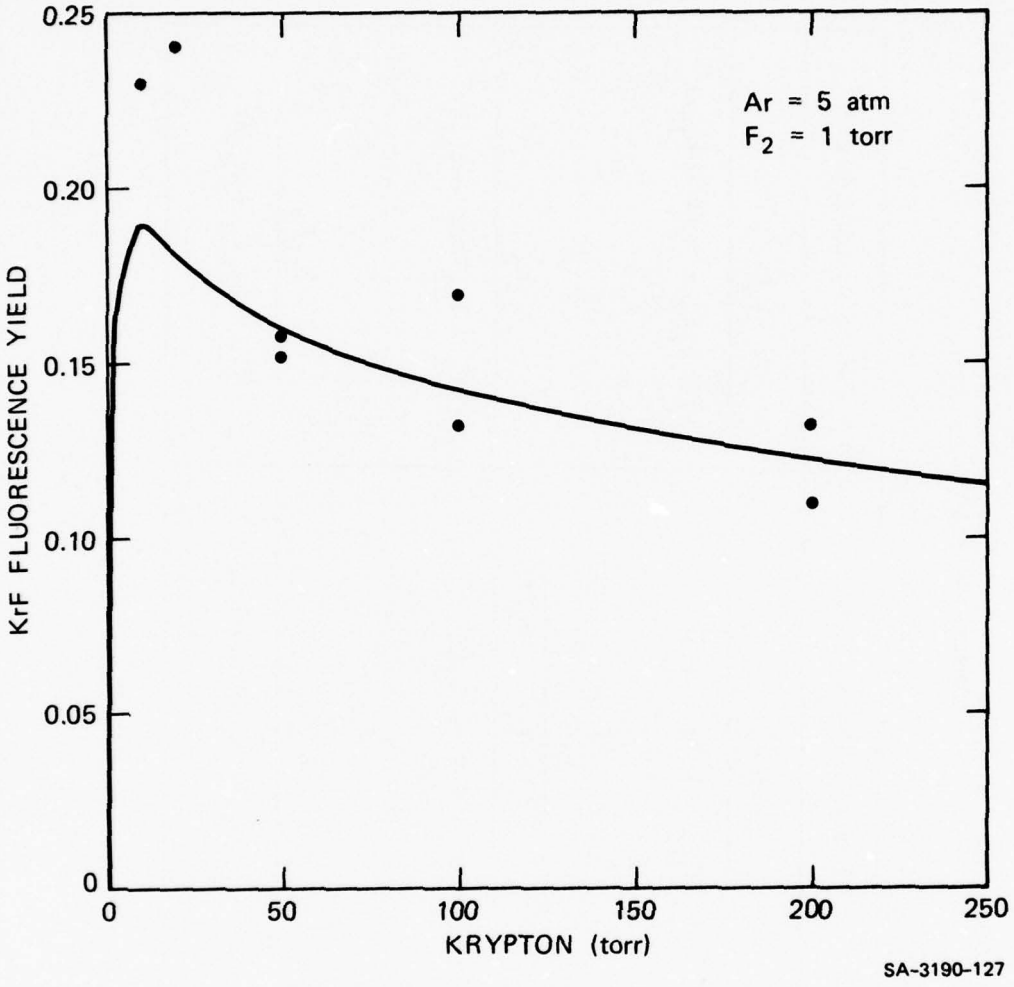

FIGURE 21 KrF FLUORESCENCE YIELD VERSUS KRYPTON PRESSURE

Finally, the argon pressure dependence of the KrF fluorescence yield is shown in Figure 22. Inspection of the formulas in Table 3 of the contributions of the various sources of KrF^* shows that ArF^* and Kr^* are both strongly intercepted by added argon [Reactions (10) and (16)]. Their contribution to the KrF^* fluorescence yield should decrease sharply with increased argon pressure. This leaves only $ArKr^*$ as a source of KrF^* [Reaction (18)], but it reacts very rapidly with Kr to give Kr_2^* [Reaction (19)] so Kr^* once converted to $ArKr^*$ is essentialy lost (for Kr ≥ 50 torr) as a source of KrF^*. This strong interception by argon of the sources of KrF^* is nearly enough to explain the argon pressure dependence shown in Figure 22. The value specified ($k_{25} \sim 4 \times 10^{-33}$ cm^6/sec) for the reaction

$$KrF^* + 2Ar \rightarrow ArKrF^* + Ar \qquad (25)$$

can be taken as an upper bound. This is to be compared with the value suggested by Jacobs et al. [JMS76] of 1.2×10^{-31} cm^6/sec in the absence of interception. Under the highest pressure conditions that we have investigated (9 atm), Reaction (25) reduces the fluorescence by about a factor of two, in addition to the much larger decreased caused by the interception Reaction (16).

Reactions of Kr_2^*, $ArKrF^*$, and Kr_2F^*

The relevant reactions are:

$$Kr_2^* \rightarrow h\nu(147nm) + 2Kr \qquad k_{20} = 3.3 \times 10^6 \text{ sec}^{-1} \qquad (20)$$

$$Kr_2^* + F_2 \rightarrow Kr_2F^* + F \qquad k_{21} = 3 \times 10^{-10} \text{ cm}^3/\text{sec} \qquad (21)$$

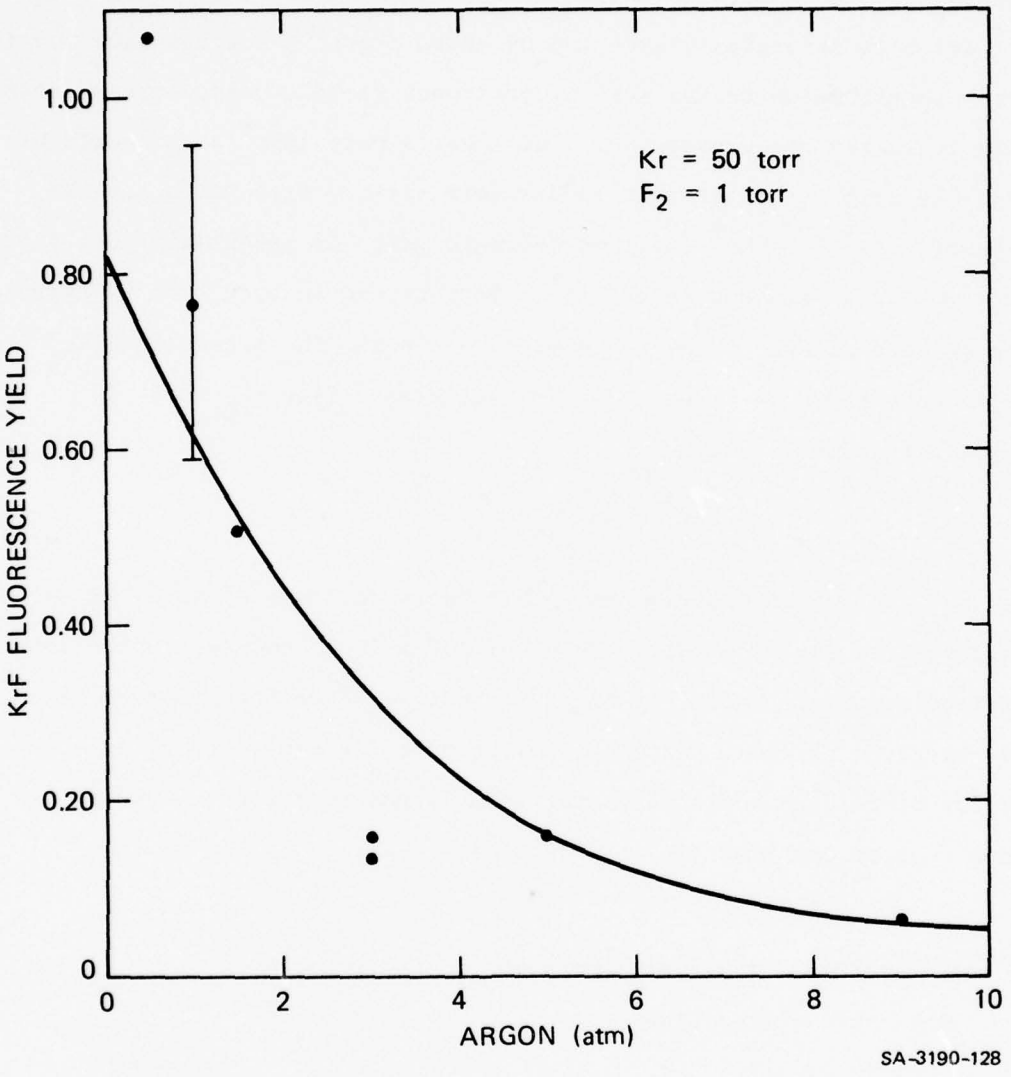

FIGURE 22 KrF FLUORESCENCE YIELD VERSUS ARGON PRESSURE

$$ArKrF^* \rightarrow h\nu(?) + Ar + Kr + F \qquad k_{26} \sim 5 \times 10^{7}\ sec^{-1} \qquad (26)$$

$$ArKrF^* + F_2 \rightarrow \text{quenched} \qquad k_{27} \sim 10^{-9}\ cm^3/sec \qquad (27)$$

$$ArKrF^* + Kr \rightarrow Kr_2F^* + Ar \qquad k_{28} \sim 10^{-10}\ cm^3/sec \qquad (28)$$

$$Kr_2F^* \rightarrow h\nu(400nm) + 2Kr + F \qquad K_{29} \sim 6.7 \times 10^{7}\ sec^{-1} \qquad (29)$$

$$Kr_2F^* + F_2 \rightarrow \text{quenched} \qquad k_{30} \sim 10^{-9}\ cm^3/sec \qquad (30)$$

The same arguments apply here to justify the use of the time decay of Kr_2F^* to follow its precursor Kr_2^*, as were used in the case of Ar_2F^*/Ar_2^* and KrF^*/Kr^*.

Figure 23 shows the Kr_2F^* decay frequency as a function of fluorine pressure. Two data points given also show the decay of Kr_2^* at 1 and 2 torr of fluorine. A few data points taken with NF_3 as the source of fluorine are shown as well. The slopes give

$$k_{21}(F_2) = 3 \pm 1 \times 10^{-10}\ cm^3/sec,\ k_{21a}(NF_3) = 2.5 \pm 0.5 \times 10^{-11}\ cm^3/sec\ .$$

The intercept with respect to fluorine ($3.3 \times 10^{6}\ sec^{-1}$) is taken to be the effective Kr_2^* radiative decay frequency. (The NF_3 data taken while this report was being written suggest that $5 \pm 2 \times 10^{6}\ sec^{-1}$ is more reasonable).

The rate coefficients for the reactions of $ArKrF^*$ are essentially subject to arbitrary specification. Indeed, the species has not been identified experimentally and apparently could be eliminated from the kinetic model with only minor consequences. Under the current version of the kinetic model, relatively little $ArKrF^*$ is produced. At the higher krypton pressure (> 20 torr) normally used, the $ArKrF^*$ is rapidly converted into Kr_2F^* in any case. The values given have been guessed in analogy with the other reactions of the same general types discussed above.

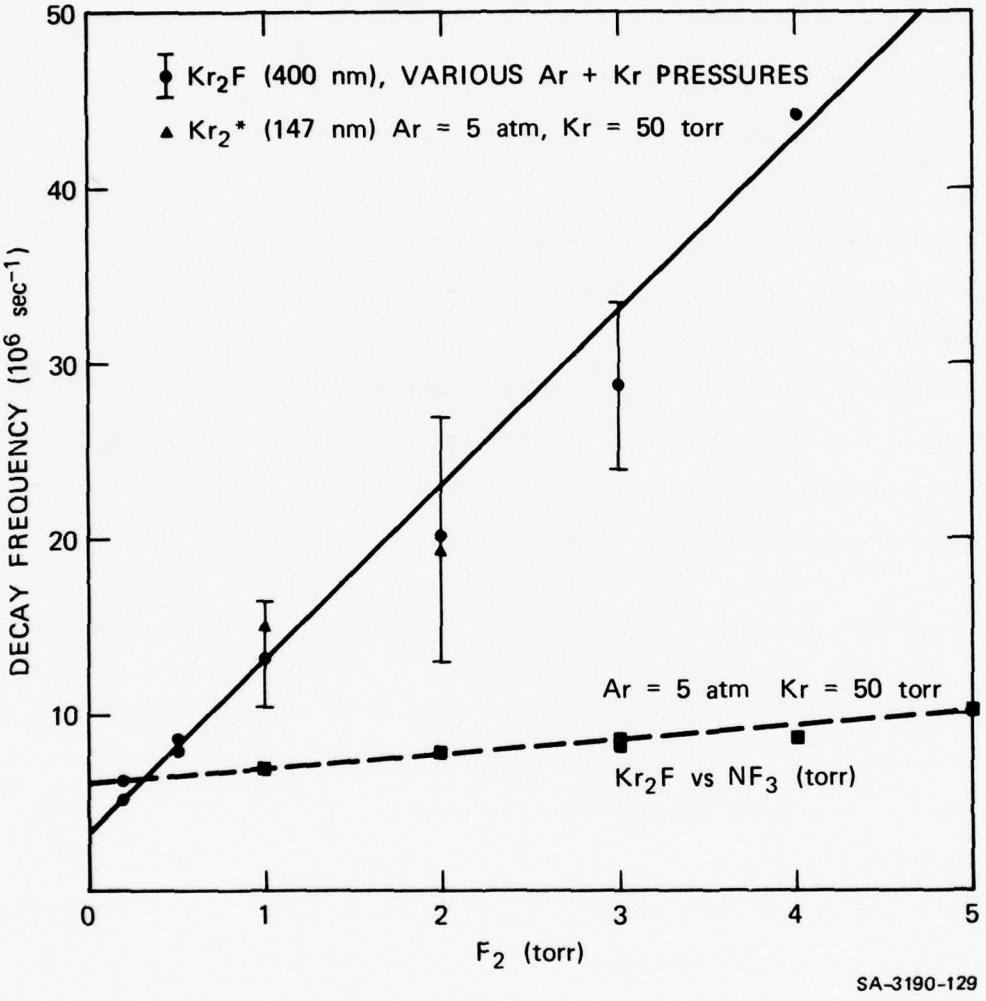

FIGURE 23 Kr_2F DECAY FREQUENCY VERSUS FLUORINE PRESSURE

Figure 24 shows the Kr_2F^* fluorescence yield as a function of the argon pressure and Figure 25 for the krypton pressure. In both cases, the kinetic model does a reasonable job of describing the observations. The only rate coefficient yet to be determined is the radiative decay frequency of Kr_2F^* [Reaction (29)]. Relative to the stipulated F_2 quenching rate coefficient [Reaction (30)], this may be estimated from the reduction in the Kr_2F^* fluorescence yield shown in Figure 25 as the F_2 pressure is raised from 1 to 3 torr. Part of the reduction is due to interception of Kr^* (the precursor of $ArKr^*$, of Kr_2^*, and of Kr_2F^*) by F_2 [Reaction (14)]. The remainder may be attributed to quenching of Kr_2F^* by F_2 [Reaction (30)], which we have used to estimate the radiative decay frequency [Reaction (29)].

Kinetic Conclusions

An experimental and modeling study of the energy transfer kinetics in e-beam pumped argon-krypton-fluorine mixtures has been carried out. For the high excitation density conditions of a fast e-beam pump, the kinetics are dominated by the multistep neutral reaction scheme.

$$\begin{array}{l} Ar^* \rightarrow ArF^* \rightarrow KrF^* \\ \quad \downarrow \\ \quad Ar_2^* \rightarrow Ar_2F^* \\ \quad\quad \downarrow \\ \quad\quad Kr^* \rightarrow KrF^* \\ \quad\quad\quad \downarrow \\ \quad\quad\quad ArKr^* \rightarrow Kr_2^* \rightarrow Kr_2F^* \end{array} \quad .$$

Under appropriate conditions, a high (30-100%) fluorescence yield can be obtained on each of the rare gas fluorides (ArF^*, Ar_2F^*, KrF^*, Kr_2F^*).

Assuming that all of the rare gas fluorides are quenched by fluorine with the same rate coefficient (10^{-9} cm^3/sec), estimates are provided for the radiative lifetimes.

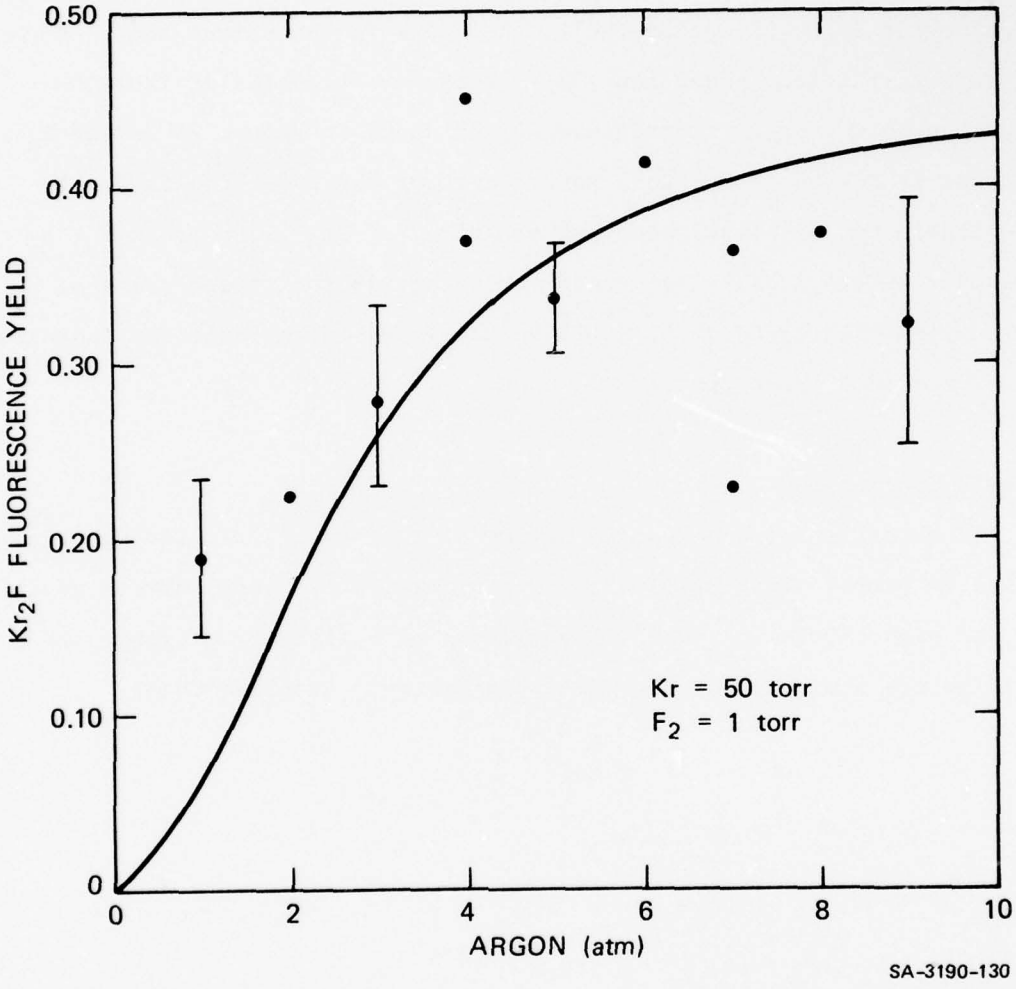

FIGURE 24 Kr_2F FLUORESCENCE YIELD VERSUS ARGON PRESSURE

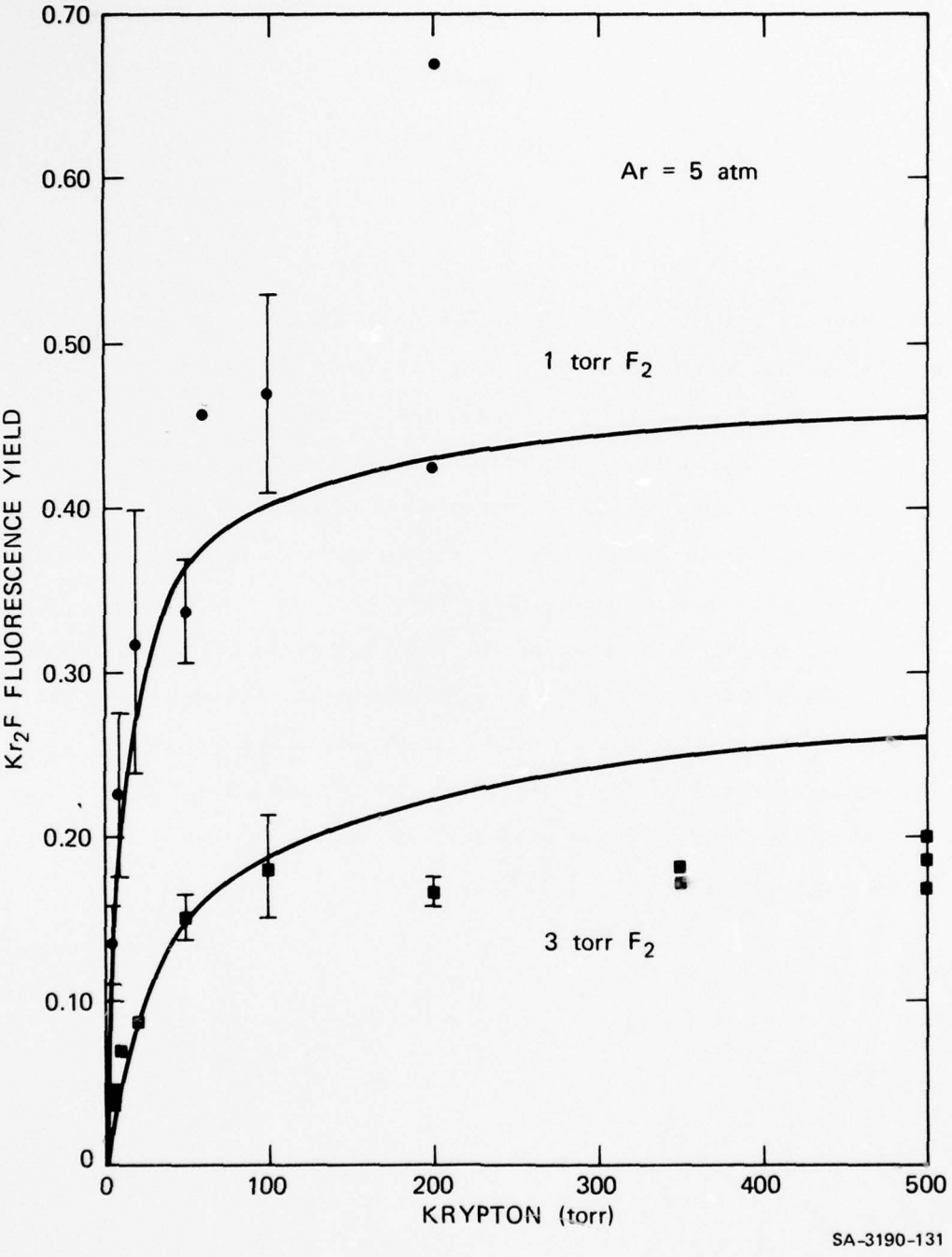

FIGURE 25 Kr_2F FLUORESCENCE YIELD VERSUS KRYPTON PRESSURE

ArF^*: 30 ± 15 nsec

Ar_2F^*: 5 to 10 nsec

KrF^*: 5 to 10 nsec

Kr_2F^*: 15 ± 5 nsec

We suggest that KrF^* is more weakly quenched by argon (which would give $ArKrF^*$) than was indicated by Mangano et al. [MJ76,JMS76]. Rather, its precursors are intercepted by argon ($Ar^* \rightarrow Ar_2^* \rightarrow ArKr^* \rightarrow Kr_2^*$). This makes the choice of laser operating pressures more critical. Quenching of the laser molecule can be overcome by an increase in the intracavity flux, but interception can be avoided only by optimal choice of the argon, krypton, and fluorine pressures.

Approximate values of most of the important rate coefficients are provided. It is expected that this contribution to the understanding of the dominant energy flow pathways in $Ar/Kr/F_2$ mixtures can assist the optimization of the existing ArF^* and KrF^* lasers, and it may lead to new lasers operating on the transitions near 290 nm and 400 nm in Ar_2F^* and Kr_2F^* respectively.

REFERENCES
Part I

ABB75 E. R. Ault, R. S. Bradford, Jr., and M. L. Bhaumik, Appl. Phys. Lett. 27, 413 (1975).

B76 M. L. Bhaumik, private communication.

BB70 J. N. Bardsley and M. A. Biondi in Advances in Atomic and Molecular Physics, Academic Press, New York, 1970, Chap. I.

BB76 I. J. Bigio and R. F. Begley, Appl. Phys. Lett. 28, 263 (1976).

BBA76 M. L. Bhaumik, R. S. Bradford, Jr., and E. R. Ault, Appl. Phys. Lett. 28, 23 (1976).

BD76 R. Burnham and N. Djeu, Appl. Phys. Lett. 29, 707 (1976).

BE75a C. A. Brau and J. J. Ewing, J. Chem. Phys. 63, 4640 (1975).

BE75b C. A. Brau and J. J. Ewing, Appl. Phys. Lett. 27, 435 (1975).

BHD75 R. Burnham, D. Harris, and N. Djeu, Postdeadline paper at the Second Summer Colloquium on Electronic Transition Lasers, Woods Hole, Mass., September 1975.

BHD76 R. Burnham, D. Harris and N. Djeu, Appl. Phys. Lett. 28, 86 (1976).

CGR73 O. Cheshnovsky, A. Gedanken, B. Raz, and J. Jortner, Chem. Phys. Lett. 22, 23 (1973).

DH76 T. H. Dunning and P. J. Hay, Appl. Phys. Lett. 28, 649 (1976).

EB75a J. J. Ewing and C. A. Brau, Appl. Phys. Lett. 27, 350 (1975).

EB75c J. J. Ewing and C. A. Brau, Phys. Rev. A12, 129 (1975).

FKG72 P. B. Foreman, G. M. Kendall, and R. Grice, Mol. Phys. 23, 127 (1972).

GHH75 R. A. Gutcheck, R. M. Hill, D. L. Huestis, D. C. Lorents, and M. V. McCusker, "Studies of E-Beam Pumped Molecular Lasers," Final Report, Contract N00014-72-C-0478, SRI MP75-43, Stanford Research Institute, August 1975.

GT74 M. F. Golde and B. A. Thrush, Chem. Phys. Lett. 29, 486 (1974).

H76 R. L. Hunter, private communication.

HD76 P. J. Hay and T. H. Dunning, Jr., Third Summer Colloquium on Electronic Transition Lasers, Snowmass-at-Aspen, Colorado, September 1976.

HGH74 R. M. Hill, R. A. Gutcheck, D. L. Huestis, D. Mukherjee, and D. C. Lorents, "Studies of E-beam Pumped Molecular Lasers," Tech. Report No. 3, Contract N00014-72-C-0478, SRI MP74-39, Stanford Research Institute, 1974.

HGH75 D. L. Huestis, R. A. Gutcheck, R. M. Hill, M. V. McCusker, and D. C. Lorents, "Studies of E-Beam Pumped Molecular Lasers," Tech. Report No. 4, Contract N00014-72-C-0478, SRI MP75-43, Stanford Research Institute, January 1975.

HHO76 R. Hunter, C. Howton, J. Oldnettel, Postdeadline paper at the Third Summer Colloquium on Electronic Transition Lasers, Snowmass-at-Aspen, Colorado, September 1976. Machine parameters were provided to us by private communication from R. Hunter.

HHT76 J. M. Hoffman, A. K. Hayes, and G. C. Tisone, Appl. Phys. Lett. 28, 538 (1976).

HOH76 R. O. Hunter, J. Oldnettel, C. Howton, and M. V. McCusker, "Gain Measurements at 4416 Å on ArXeF and Kr_2F", (to be published).

JM76 J. H. Jacob and J. A. Mangano, private communication.

JMS76 J. H. Jacob, J. A. Mangano, and E. T. Salesky, 29th Gaseous Electronics Conference, Cleveland, Ohio, Paper A1, October 1976.

KS74 D. L. King and D. W. Setser, Fourth Conference on Chemical and Molecular Lasers, St. Louis, Missouri, October 1974, IEEE J. Quant. Elect. QE-11, 708 (1975).

KVC73 R. T. Ku, J. T. Verdeyen, B. E. Cherrington, and J. C. Eden, Phys. Rev. A8, 3123 (1973).

L76 D. C. Lorents, Physica 82C, 19 (1976).

LEH73 D. C. Lorents, D. J. Eckstrom and D. L. Huestis, "Excimer Formation and Decay Processes in Rare Gases," Final Report MP73-2, Contract N00014-72-C-0457, SRI Project 2018, Stanford Research Institute, Menlo Park, Ca., September 1973.

LHH76 D. C. Lorents, R. M. Hill, D. L. Huestis, M. V. McCusker, and H. H. Nakano, Third Summer Colloquium on Electronic Transition Lasers, Snowmass-at-Aspen, Colorado, September 1976.

LMR76 D. C. Lorents, M. V. McCusker, and C. K. Rhodes, "Nuclear Fission Fragment Excitation of Electronic Transition Laser Media", in "Partially Ionized Plasmas including the Third Symposium on Uranium Plasmas," Princeton University Conference, Meeting 133, Princeton, New Jersey, June 10-12, 1976.

LO72 D. C. Lorents and R. E. Olson, "Excimer Formation and Decay Processes in Rare Gases," Semiannual Tech. Report No. 1, Contract N00014-72-C-0457, SRI Project 2018, Stanford Research Institute, Menlo Park, Ca., December 1972.

LWG73 S. M. Lin, J. G. Wharton, and R. Grice, Mol. Phys. 26, 317 (1973).

MH76 H. H. Michels and R. H. Hobbs, Third Summer Colloquium on Electronic Transition Lasers, Snowmass-at-Aspen, Colorado, September 1976.

MJ75 J. A. Mangano and J. H. Jacob, Appl. Phys. Lett. 27, 495 (1975).

MJ76 J. A. Mangano and J. H. Jacob, Third Summer Colloquium on Electronic Transition Lasers, Snowmass-at-Aspen, Colorado, September 1976.

MJD76 J. A. Mangano, J. H. Jacob, and J. B. Dodge, Appl. Phys. Lett. 29, 426 (1976).

MLH76 M. V. McCusker, D. C. Lorents, D. L. Huestis, R. M. Hill, H. H. Nakano, and J. A. Margevicius, "New Electronic Transition Laser Systems," Technical Report No. 4A, Contract DAAH01-74-C-0624, SRI MP76-46, Stanford Research Institute, May 1976.

MP76 J. R. Murray and H. T. Powell, Appl. Phys. Lett. 29, 252 (1976).

PM75 H. T. Powell and J. R. Murray, LLL Laser Program Annual Report 1974 (March 1975, unpublished).

PCS75 L. G. Piper, D. W. Setser, and M. A. A. Clyne, J. Chem. Phys. 63, 4018 (1975).

RC68 A. C. Roach and M. S. Child, Mol. Phys. 14, 1 (1968).

RW76 T. N. Rescigno and N. W. Winter, Third Summer Colloquium on Electronic Transition Lasers, Snowmass-in-Aspen, Colorado, September 1976.

S73 W. S. Struve, Mol. Phys. 25, 777 (1973).

SH75 S. K. Searles and G. A. Hart, Appl. Phys. Lett. 27, 243 (1975).

SKM75 W. S. Struve, J. R. Krenos, D. L. McFadden, and D. R. Herschbach, J. Chem. Phys. 62, 404 (1975).

SSG76 D. G. Sutton, S. N. Suchard, O. L. Gibb, and C. P. Wang, Appl. Phys. Lett. 28, 522 (1976).

THH76 J. Tellinghuisen, A. K. Hays, J. M. Hoffman, and G. C. Tisone, J. Chem. Phys., (to be published).

VKS76 J. E. Velazco, J. H. Kolts, and D. W. Setser, J. Chem. Phys. 65, 3469 (1976).

VOF75 E. T. Verkhovtseva, A. E. Ovechkin, Ya. M. Fagel, Chem. Phys. Lett. 30, 120 (1975).

VS75 J. E. Velazco and D. W. Setser, J. Chem. Phys. 62, 1990 (1975).

WHG73 J. C. Whitehead, D. R. Hardin and R. Grice, Mol. Phys. 25, 515 (1973).

Z76 E. Zamir, private communication.

ZHL76 E. Zamir, D. L. Huestis, D. C. Lorents, and H. H. Nakano, "Visible Absorptions by Electron Beam Pumped Rare Gases," Third Summer Colloquium on Electronic Transition Lasers, Snowmass-in-Aspen, Colorado, September 1976.

Appendix

GAIN MEASUREMENTS AT 4416 Å ON $ArXeF^*$ and Kr_2F^*

R. O. Hunter, J. Oldenettel and C. Howton
Maxwell Laboratories, Inc.
9244 Balboa Avenue
San Diego, California 92123

and

M. V. McCusker
Stanford Research Institute
333 Ravenswood Avenue
Menlo Park, California 94025

ABSTRACT

Recent measurements of radiation from certain rare gas-halogen mixtures have indicated the efficient production of broad band emitters in the visible.[1] This paper reports a gain measurement at 4416 Å of two emitters tentatively identified as Kr_2F^* (λ_{max} = 4000 Å, FWHM = 900 Å) and $ArXeF^*$ (λ_{max} = 4600 Å, FWHM = 900 Å). Attenuation of the 4416 Å probe laser during electron-beam and electron-beam-sustained discharge excitation of 2-3 atmosphere pressure mixtures of argon-krypton-fluorine and argon-xenon-fluorine indicates absorption only. The fluorescence signals from $ArXeF^*$ and XeF^* ($Ar/Xe/F_2$ mixture), and KrF^* and Kr_2F^* ($Ar/Kr/F_2$ mixtures) were monitored simultaneously with the absorption of the probe laser. Since the absorption was not proportional to the fluorescence of these species, it is tentatively concluded that it is due to another transient

[1] Spectroscopy and Kinetics of the 248 and 414 nm Bands from Electron Beam Pumped Argon-Krypton-Fluorine Mixtures, D. C. Lorents, R. M. Hill, D. L. Huestis, M. V. McCusker, and H. H. Nakano, Presented at the 3rd Conference on Electronic Transition Lasers.

species. Typical absorptions of 10^{-3} cm^{-1} were observed at pump levels of 10^{5} watts cm^{-3}. A knowledge of the absorption mechanism will be required to assess the efficiency with which such lasers can be made to operate, if at all.

INTRODUCTION

Recently,[1] efficient visible radiation production from electron beam pumped mixtures of rare gases and fluorine has been reported. These broad band emission continua have been ascribed to transitions in triatomic species from a bound excited state to an unbound lower state. In mixtures of $Ar/Kr/F_2$, the continuum centered at 4000 Å has been assigned to Kr_2F^*; in $Ar/Xe/F_2$ mixtures, the 4500 Å continuum has been assigned to $ArXeF^*$. A ratio of stimulated emission cross sections on the order of 1/5 is anticipated for such triatomic species to that of the corresponding diatomic (KrF^* or XeF^*) under ideal conditions (assuming no absorption from other species or the excited state). As candidates for visible lasers, then, these species are extremely attractive, offering high potential efficiencies in the visible, tunability, and ready scalability to large energies.

The work reported in this paper consists of gain measurements made at a single wavelength (4416 Å) at moderate pressures (2-3 atmospheres) in electron-beam and electron-beam-sustained discharge configurations at pump levels of 10^{5} watts cm^{-3}. This probe wavelength falls near the center of the transition ascribed to $ArXeF^*$ and corresponds to about 1/3 the peak of the Kr_2F^* emission on the red side of the line center. Figure 1 shows the shape of the emission spectrum for Kr_2F^*. Also, an attempt was made to achieve lasing in a broadband cavity that had an equivalent optical loss of 2.5×10^{-3} cm^{-1}. No lasing was observed, and under all conditions tested the probe indicated net absorption in the medium on the order of 10^{-3} cm^{-1}. However, the tests were not conducted under conditions optimum

for achieving net gains, i.e., higher pressure. In any case, even if net gain is observed, the presence of absorption of this magnitude would seriously limit the performance of the transition in a laser device. In conjunction with the gain measurements the fluorescence from both the diatomic counterpart (XeF^* and KrF^*) and the triatomic species were monitored. It did not correlate with the temporal behavior of the absorption, indicating that the absorption is not due primarily to the diatomic or triatomic species, but rather to other unidentified species.

EXPERIMENTAL

The experimental apparatus includes three main types of equipment: (1) the means of generating and delivering into the active region the electron beam and the electrical pulse to drive the discharge, (2) the high pressure container and the associated gas handling system, and (3) the optical train, including the probe laser and optical detectors for monitoring the various emissions. Figure 2 shows the basic layout.

ELECTRON BEAM AND DISCHARGE PARAMETERS

The electron beam is generated in a vacuum region and injected into the high pressure region through a 0.001 in. Ti foil. The voltage is nominally 400 kV, the pulse lengths is 10^{-6} sec, and the transmitted current density is 10 amperes/cm^2 for the direct pumped cases. The energy deposition is estimated from one-dimensional deposition curves scaled from data in Ar and from earlier pressure rise measurements.

The discharge, when it is utilized, is driven by a fast capacitor bank (10 microfarads, up to 60 kV charge voltage, $\sim 5.0 \times 10^{-8}$ Henry inductance). Voltage and current monitors for both systems are calibrated with reference injected pulses. The voltage probes are resistive dividers, and the current probes two arrays of B loops, the signals of which are integrated in the screen room.

PUMPING CHAMBER AND GAS HANDLING SYSTEM

The active region is 8 cm x 20 cm x 200 cm and is contained within a 300 liter pressure vessel constructed of aluminum and high density polyethylene. Seals are made with Viton O-rings and Buna-N flat gaskets. The chamber is pumped through a gate valve by a 260 liter/sec turbomolecular pump and is evacuated to a pressure less than 10^{-4} torr prior to a passivation or fill procedure. The maximum pressure for this experiment was set by the structural characteristics of the chamber. The long axis of the active region is terminated by two end bells that contain mirrors. Ten ports with CaF_2 or MgF_2 windows are mounted at various positions to permit optical diagnostics of the active region.

The gases are mixed turbulently in this 300 liter chamber by means of fast injection through a perforated pipe running the length of the cavity ($\sim$ 2 meters). The mixing is observed to be good since several shots may be made with a single mixture. The fluorescence signals, discharge behavior, and lasing behavior are reproducible from shot to shot and fill to fill, with the exception of a slight change due to F_2 removal by the chamber walls. During operation the chamber is evacuated, then passivated by exposure to 5-10 torr of F_2 for several hours, then purged with N_2, and finally filled. After each run, it is again evacuated and the procedure repeated. The F_2 is not purified beyond the level stated by the supplier, i.e., 98% minimum purity. The argon, krypton, and xenon are also used as supplied and are specified to be greater than 99.99% pure in the case of krypton and xenon, and 99.999% in the case of the argon.

OPTICAL INSTRUMENTATION AND LAYOUT

The behavior of the excited state population of the dimer and trimer species is monitored by viewing the short axis (20 cm) of the active region by fast photodiodes through appropriate interference or color filters. All of the oscilloscope, cable and photodiode combinations have

better than a 5×10^{-9} second response. In order to ensure that radiation from KrF^* lasing near 2500 Å did not enter the longer wavelength detectors, plastic sheets with a cutoff near 3600 Å were also placed in some of the optical trains. Noise due to electrical pickup or X-ray signals is less than 1% of the optical emission signal for these monitors. Lasing was looked for by viewing the long axis of the active region through a hole in one of the resonator mirrors with similar detector-filter combinations. The laser cavity was formed by an unstable resonator having an equivalent loss of $\cong 2.5 \times 10^{-3}$ cm^{-1}, including mirror reflectivity losses.

The absorption measurements were made by transmitting the output from a He-Cd laser into the chamber, bringing the signal out and into the screen room after multiple reflections in the laser cavity. There it was focussed on the entrance slits of a 1 meter Jarrell-Ash spectrograph. Detection was accomplished by means of a high gain photomultiplier. The photomultiplier was gated on approximately 1 μs prior to the electron beam pulse by changing the potential of the first grid. The observed decay time of this pulsing circuitry was greater than 20 μs, so that during the 1 μs electron pulse, the detected laser light level was essentially flat in the absence of absorption. The photomultiplier, cable and oscilloscope combination have a response time of less than 10^{-7} seconds in the configuration utilized. A major difficulty with this apparatus is the high level of fluorescence produced by the active region. Very narrow slits and careful adjustment prior to each shot were necessary to reduce the detected fluorescence signal to a small fraction of that due to the laser. Electrical pickup and signal due to X-rays are less than $\sim$ 5% of the detected laser signal.

RESULTS

Lasing, as would be indicated by an enhancement of the signal from the transverse photodiode relative to that of fluorescence photodiode, was not observed on either transition.

The 4416 Å probe laser transmission during the pump pulse always indicated net absorption in the optical train. A representative set of traces are shown in Figure 3. In this particular case the optical cavity was lasing at 2485 Å; note how the Kr_2F^* signal closely follows that of the KrF^* signal, indicating that KrF^* is a direct predecessor of Kr_2F^*, or that the optical field is interfering with the formation of Kr_2F^*, or that the two species have a common precursor. Of particular interest is the observation that the absorption does not directly follow the fluorescence signal and appears to have a 200 ns afterglow. This leads to the conclusion that the absorption is not due to the radiating species.

A summary of the shots taken is shown in Table 1. The absorption value represents the peak during the pulse.

The absorptions are typically 10^{-3} cm^{-1} at this pump level and are remarkably constant with respect to the change from xenon to krypton as the added gas.

DISCUSSION

The observation of net absorption in these mixtures under conditions in which gains on the order of 10^{-3} cm^{-1} are expected[1] leads immediately to the question of the identity of the absorber(s) and the mechanisms controlling the level of absorption. The temporal behavior of the absorption during the excitation indicates that it is not due to absorption from its excited state or that of the associated diatomic species. The recent measurements of Zamir et al.[2] of three types of visible absorption in electron beam pumped rare gases are of interest. Those measurements showed (a) a bound-bound absorption from low-lying excited atomic states in the rare gases, (b) absorption attributed to molecular transitions

Table 1

Shot No.	Pumping[1] Rate (watts/cm^3)	Mixture (torr)	Peak Absorption g_o (cm^{-1})	Diatomic Fluorescence Signal (volts)	Triatomic Fluorescence Signal (volts)
9-11	1.2×10^5	1500:200:3.5 (Ar:Kr:F_2)	1.5×10^{-3}	4.4	15
9-12	1.2×10^5	1500:100:1.7 (Ar:Kr:F_2)	1.5×10^{-3}	4.8	15
9-18-2	10^5	2000:100:3.6 (Ar:Kr:F_2)	10^{-3}	3	15
9-15-1	1.2×10^5	1500:6.4:1.1 (Ar:Xe:F_2)	1.9×10^{-3}	5	20
9-15-2	1.2×10^5	1500:4.9:0.84 (Ar:Xe:F_2)	1.7×10^{-3}	5	--

[1]Energy input by electron beam except for Shot #9-18-2 for which an electron beam sustained discharge with an enhancement ratio of 3 was utilized.

from the two low-lying bound states in the dimers,[1,3] and (c) a broad, continuous absorption throughout the visible that has uncertain origin. Only the latter absorption is of primary interest for obtaining lasing on these new systems, since the others are of characteristic width of $\sim$ 10-100 Å. With such widths it should be possible to find a region under the broad fluorescence ($\cong$ 900 Å FWHM) that is not absorbing at a prohibitive level. However, the lumped cross sections (10^{-17} cm^2 per excitation) observed in the visible in their experiment are comparable to the absorptions observed in this experiment where the excited state density is approximately 10^{14} cm^{-3}. Other candidates for the absorbing species include the dimer ion species Kr_2^+ and Xe_2^+, which are anticipated to be the dominant positive ion species for these mixtures. The $A^2\Sigma_u^+ \rightarrow D^2\Sigma_g^+$ dissociative transition from the ground state of the homonuclear ions[3] should be intense and lie in the wavelength range of interest.[4]

Another possibility is an absorber associated with F_3^-. However, our data is not sufficient to resolve such questions. The main question of interest for the trimers as laser candidates is the scaling of the absorption to higher pressures. For systems such as Ar/I_2 and $Ar/Xe/F_2$ that lase on transitions near 3500 Å, the presence of absorption of this size has serious implications if it extends that far into the blue. Thus, the origin of the observed absorption is not only of interest as far as obtaining laser action on $ArXeF^*$ and Kr_2F^*, but also has a major bearing on the efficiency of XeF^* and I_2^* lasers.

CONCLUSIONS

Absorption has been observed in electron beam pumped mixtures at a single wavelength (4416 Å) which falls within a factor of 3 of the peak gain anticipated in Kr_2F^* and $ArXeF^*$. Further work should be directed toward conditions (higher total pressure) and wavelengths nearer line

center which are more promising. The identity of the absorbing mechanism is of interest not only for these lasers but for others involving the same types of gases. With regard to these visible laser candidates, the major question is whether or not the absorption processes are truly continuous. The experiments indicate that self-absorption is not the major contribution; hence, the present experiments are inconclusive with respect to the possibility of obtaining efficient output in the visible from such transitions.

ACKNOWLEDGEMENTS

Discussions with D. L. Huestis about the origin of the emissions and the nature of the absorptions are gratefully acknowledged.

REFERENCES

1. D. C. Lorents, R. M. Hill, D. L. Huestis, M. V. McCusker and H. H. Nakano, "Spectroscopy and Kinetics of the 248 and 410 nm Bands from Electron Beam Pumped Argon/Krypton/Fluorine Mixtures," Paper presented at the Summer Colloquium on Electronic Transition Lasers, Snowmass, Colorado, September 7-10, 1976.

2. E. Zamir, D. L. Huestis, D. C. Lorents and H. H. Nakano, "Visible Absorption by Electron-Beam Pumped Rare Gases", Paper presented at the Summer Colloquium on Electronic Transition Lasers, Snowmass, Colorado, September 7-10, 1976.

3. R. S. Mulliken, J. Chem. Phys. 52, 5170 (1970).

4. Private conversations with M. Krauss, National Bureau of Standards, Washington, D.C. and D. Huestis, SRI.

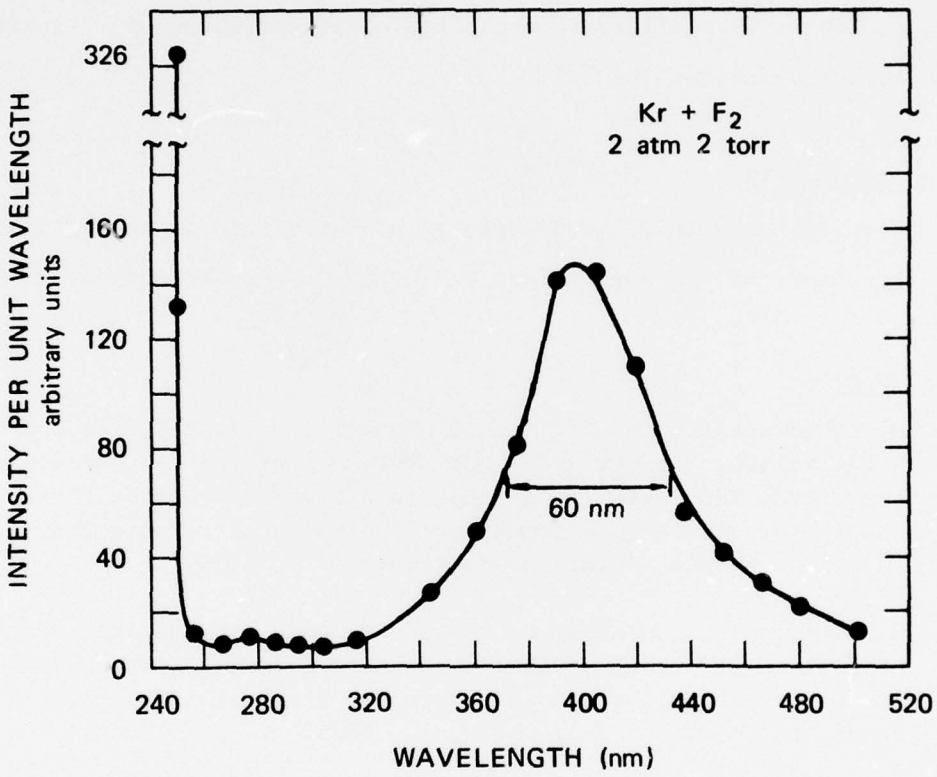
INTENSITY PER UNIT WAVELENGTH
arbitrary units
326
160
120
80
40
0
Kr + F2
2 atm 2 torr
60 nm
240
280
320
360
400
440
480
520
WAVELENGTH (nm)

SA-3190-113

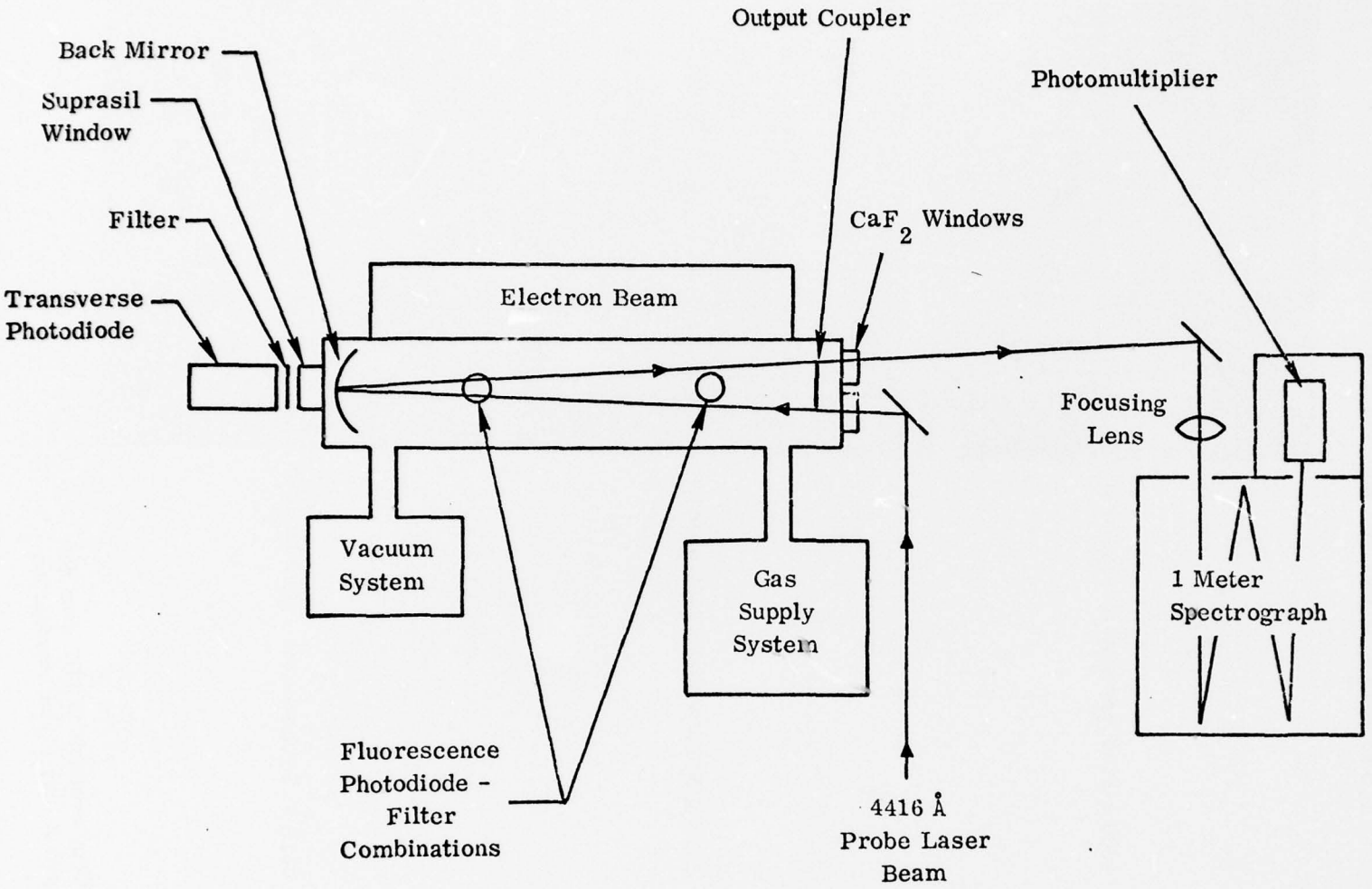

Figure 2. Experimental Schematic

Figure 3

ELECTRON BEAM DRIVEN Kr_2F GAIN MEASUREMENT

1.5 torr F_2 **100 torr Kr** 1500 torr Ar

4000 Å Fluorescence (200 ns/div)

2485 Å Fluorescence (200 ns/div)

4416 Å Probe Laser (500 ns/div)

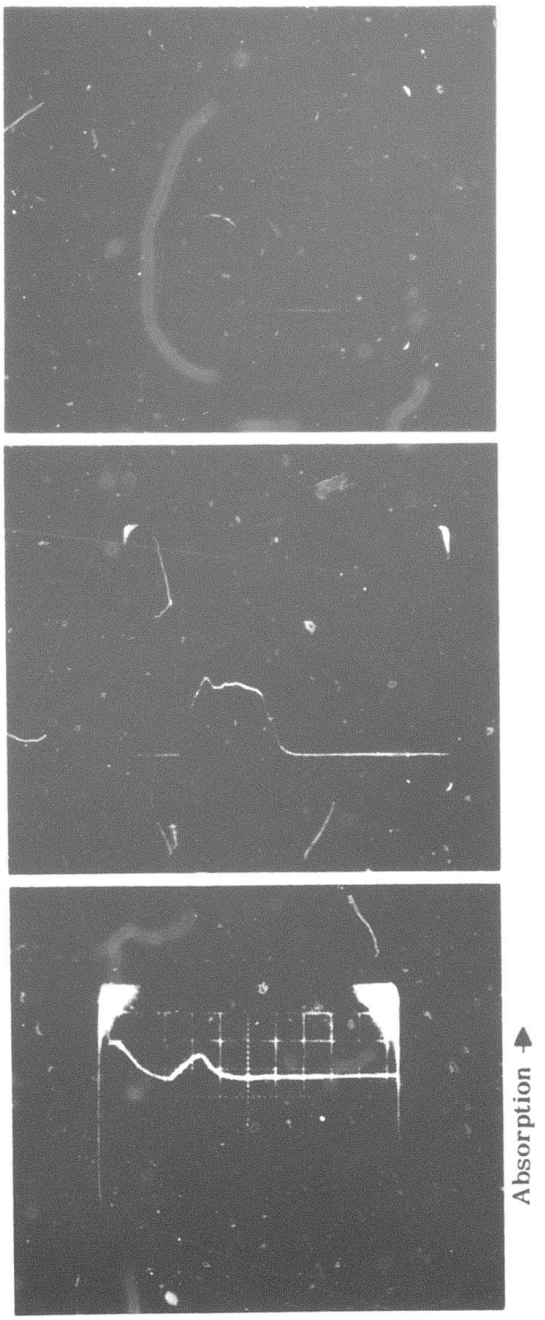

PART II: CHEMICALLY PUMPED SYSTEMS

1. INTRODUCTION

This report marks the completion of a four-year program, under Contracts DAAH01-73-C-0444 and DAAH01-74-C-0524, that has been devoted to the development of electronic transition (visible) chemical lasers. Efforts to date have been described in a number of technical reports [EEB74a, EEH74, EPP76] and publications [EEB74b, BLE74, EEP74, EEH75, LEE76, AE76, EBH76, EH76, EPE76]. Related work has been carried out at SRI under different sponsorship [EL76, LEB76a, LEB76b, LEB76c, LEB76d].

The objective of the work has been to find highly exothermic chemical reactions that deposit (or transfer) a substantial fraction of their excess energy into electronic states of the newly formed molecule or into a radical atom or molecule from one of the reactants. That such reactions occur was known from observations of visible chemiluminescence in low-pressure flames and afterglows. The requirement for a high branching ratio into an excited state is coupled with the requirement that the overall kinetics of the reaction be such that population inversions between electronic states sufficient for lasing can be generated and maintained.

We approached our objectives through a combination of experimental, analytical, and theoretical studies. Most of our experimental work involved reactions of metal atoms with oxidizers (oxygen- or halogen-atom donors). These involved cw diffusion flames with evaporation metal sources, both with metal in excess [EEH74, EPP76, EEB74b, BLE74, EEP74, EEH75, EPE76] and oxidizer in excess [EEB74a, EEH74, EPP76, EEB74b], diffusion flames with metal carbonyls and metal alkyls [EEB74a, BLE74], ternary flames that used alkali metal reactions to strip volatile metal polyhalides [LEB76a-d], and pulsed reactions that used thermal heating by a shock wave to dissociate volatile metal carbonyls or metal alkyls [EPP76]. Early efforts centered on quantifying the photon yields and

radiating states for a large number of such reactions. We also carried out direct lasing attempts on the Ba + N_2O and Sm + NF_3 reactions [EEH74]. Later, we made sensitive gain/absorption measurements by intracavity dye laser spectroscopy on Ba + N_2O, Ca + N_2O + CO, and Sr + N_2O + CO flames [EBH76]. Finally, we studied ground-state BaO population distributions by the laser-induced fluorescence technique [EH76, EL76].

Analytical studies included: extensive kinetic modeling calculations aimed at determining energy pathways by comparison with experimental results [EEH74]; a numerical solution for a spherical diffusion flame with variable temperature, finite convective velocities, and multiple reactions [AE76]; and numerical solutions of the vibrational relaxation equations that predict ground-state vibrational distributions, again for comparison with experimental data [EH76].

The results of these various studies have already been reported in detail as indicated by the references, or are now available in preprint form. In following sections, we briefly summarize those results and give an overview of visible chemical laser development.

2. SUMMARY OF RECENT WORK

Spherical Diffusion Flame Model

Preliminary results from a numerical solution of the spherical diffusion flame that incorporates multiple reaction kinetics, temperature variations in the flame, and convective velocity effects have been presented previously [EEH74(c)]. This work has now been refined and completed, and the results prepared for publication [AE76].

Vibrational Distribution Modeling

The vibrational distribution model and preliminary results have been reported previously [EEH74(c)]. Additional calculations have now been made for the Ba + N_2O reaction, and the results compared with the limited experimental data for this reaction [RWH76]. We have concluded from the comparison that the Ba + N_2O reaction primarily populates a state that is collisionally isolated from low vibrational levels of the ground state, and that the latter levels are populated primarily by radiative cascade. The reservoir states, which are probably the $a^3\Pi$ or $x^3\Sigma^+$ metastable electronic states, may be populated by collisional processes following the initial reaction. The work is described in a new preprint [EH76].

Laser-Induced Fluorescence Studies

We used a nitrogen-laser-pumped dye laser to optically pump $BaO(X^1\Sigma, v'')$ levels produced in Ba + N_2O and Ba + O_2 reactions, with detection of the fluorescence by a monochromator-gated photomultiplier-boxcar integrator system. Although product distributions from the Ba + O_2 reaction could be readily determined, we were unable to detect products from the Ba + N_2O reaction. The implications of this observation are discussed in the work on vibrational modeling described above.

Intracavity Dye Laser Spectroscopy

We extended our work on Ba + N_2O, described previously [EPP76], to include the BaO [$A^1\Sigma, v' = 1 \rightarrow X^1\Sigma, v'' = 7$] transition as 7904 Å. The transition was transparent at a sensitivity for absorption or gain of $\sim 10^{-4}$/cm. We also studied the arc bands of CaO and SrO from Ca(Sr) + N_2O + CO flames, which were considered laser candidates [BSH76]. We found absorptions on the green arc bands of CaO and the red arc bands of SrO. Our results are consistent with assignment of these bands to transitions between excited electronic states of the diatomic metal oxide. This work is described in a new preprint [EBH76].

3. CURRENT STATUS

Although the base of knowledge required for development of electronic transition chemical lasers has been advanced considerably in the last few years, we must emphasize that the level of understanding of the energy flow processes in exothermic reactions is still extremely elementary. While there have been no discoveries of basic physical limitations that preclude achievement of these lasers, it is by now obvious that the task will not be easily accomplished. In particular, the most promising ideas for near-term laser development have been tried, without apparent cause for optimism (a possible exception to this is the $H + NF_2 \rightarrow HF + NF(a^1\Delta)$ reaction under study at Aerospace Corporation [HC73]). It is our view that considerably more basic research is required before this major technological advancement will be achieved.

In our own studies, we have considered four classes of excitation reaction:

Reaction	Classification
(1) $A + BC \rightarrow AB^* + C$	Metathesis
(2) $AB^* + C \rightarrow AB + C^*$	Molecule → Atom Transfer
(3) $A + B + C \rightarrow AB^* + C$	Atom Association (Recombination)
(4) $ABC + D \rightarrow AB^* + CD$	Elimination

Most of our interest and attention has been on metathesis reactions with metal atoms, but we have had at least a small look at the other classes as well. We summarize what we have observed and what we think about each class as a basis for our above conclusion, as follows:

(1) Metathesis

- Our qualitative theoretical model [EEH74] predicts that reactions of all but the lightest atoms produce primarily vibrationally excited, ground-state molecules rather than

electronically excited molecules in the first step.* However, there is no experimental verification of this prediction, and recent analytical and experimental studies in alkaline earth + N_2O reactions appear to challenge it [EH76]. The energy flow in exothermic metathesis reactions is not established, even for the well-studied Ba + N_2O reaction. In particular, no currently proposed kinetic model predicts all of the experimental observations. It seems likely that the production of radiating states is much more complex than originally thought.

- Secondary reactions that interfere with the production of excited molecules are likely to be a serious problem, particularly when scaling the reaction rates to laser threshold values. For example, in metal-in-excess flames, our work on Ba + N_2O [EEH74, EPE76] and on ternary flames [LEB76] in heat-pipe-oven reactors shows that metal-atom quenching seriously reduces molecular photon yields. We think that this is primarily an energy-transfer process that should be rapid when the atom has energy states below those of the excited states of the molecule. (There is no evidence for resonant energy transfer in this case.) This postulate is supported by our observations of high populations of Ba^* in Ba + N_2O flames [EEH76, EBH76, EPE76]. Likewise, Felder, Gould, and Fontijn [FGF75] have found that O_2 and N_2O quench BaO^* emission with gas kinetic efficiency. This could be because of reactions such as $BaO^R + N_2O \rightarrow BaO_2 + N_2$. Since many of the candidate laser molecules are radicals (BaO, SmF, SnO, ScF), second-step reactions with the oxidizer may

*Some complex-forming reactions do yield excited atomic states, but in a statistical fashion. In the case of $K_2 + C\ell \rightarrow KCl + K^*$, the statistical weight of the 4P state is three times that of the 4S state, and one observes 50-75% production of excited atomic states.

be rapid and thus pose a serious quenching problem. Finally, quenching by product molecules could be important. Fontijn and Felder have observed such a process in Sn + N_2O reactions [F76]. Furthermore, the falloff of the Ba + N_2O photon yield at higher pressures in diffusion flames [EEP74, EEH75] could be due to quenching by products rather than by argon.

- There are some reasons to believe that rapidly initiated pulsed reactions in shock tubes or reactions carried out with high convective velocities, as in shock tunnels, would more likely achieve population inversions and gain. However, results at SRI [EPP76] and elsewhere [JSW74, C76] have not yet borne out that hope.

(2) Molecule-Atom Transfer

- We believe that the strong quenching of molecular emission by atoms is due to a V → E energy-transfer process, and that in general this process has large cross sections.
- For every case we have examined, the atomic state populations we could determine were not inverted. This applied to Ba^* populations in Ba + N_2O flames [EEH74, EPE76], and to alkali* populations in ternary flame systems [LEE76]. However, these were all CW flames; pulsed reactions may lead to different results.
- In our opinion, the prospects for V → E chemical lasers are very small. There is no evidence to suggest that V → E transfer is likely to produce a population inversion.

(3) Atom-Association Reactions

- It is well known that such reactions produce excited states in afterglows, flames, etc. However, it seems likely that the atomic concentrations required to make a chemical laser could only be achieved in a shock-tube expansion nozzle device.
- The spectroscopic and kinetic properties of most molecules are not known in sufficient detail to predict the prospects for success in such a shock tunnel scheme. For some of the few cases known (O + O + M, Cℓ + Cℓ + M, Br + Br + M), we have carried out a simple calculation that predicts gains less than 10^{-6}/cm for plausible atom concentrations [EPP76]. On the basis of this calculation, we do not consider this class of reactions sufficiently promising to warrant experimental studies.
- The predictions above are consistent with negative experimental results in other laboratories [VDK76, WBF76].

(4) Elimination Reactions

- Spin conservation rules should apply for light molecules in reactions of this class, so that high excited-state yields are plausible. By spin conservation, as well, one expects the excited products to have long radiative lifetimes.
- We studied some alkali + NF_3 reactions where stripping reactions could lead to NF^* production. However, we never detected any NF^* spectroscopically [LEE76] and concluded that NF^* + alkali reactions were also probably rapid. In contrast, work at UCSB on aluminum + NF_3 did yield weak NF emission [R76].
- The H + NF_2 system being studied at Aerospace Corporation [HC73] deserves more work in view of the reported high yields

of $NF(a^1\Delta)$ in the reaction. However, the gain of $NF(a^1\Delta \rightarrow X^3\Sigma^-)$ is extremely low because of the long radiative lifetime, and selective transfer of the excitation to another state which then becomes the upper laser level may be difficult.

4. CONCLUSIONS

It is our conclusion that achievement of a visible chemical laser in the near future is possible but unlikely. Furthermore, development of a practical device as opposed to a laboratory tool will be particularly difficult because of the problems inherent in generating and handling metal atoms and metal oxides or metal halides as required in most of the candidate systems now under study. Thus, ARPA should be aware that the time scale for chemical laser development is considerably longer than for electron-beam or discharge-pumped systems.

The data base for understanding of chemiluminescent reactions has been greatly increased during this research, and several important new diagnostic methods for studying these reactions have recently been developed. While we cannot claim to understand any one reaction system, it seems that the necessary tools and much of the required information are rapidly being assembled. We believe that it is worthwhile to continue the basic research aspects of this program with the goal of advancing our understanding of exothermic reaction dynamics and, ultimately of achieving a visible chemical laser.

REFERENCES
Part II

AE76 C. M. Ablow and D. J. Eckstrom, "Numerical Solutions of the Spherical Diffusion Flame with Application to Chemiluminescence Studies," (to be published).

BLE74 G. Black, M. Luria, D. J. Eckstrom, S. A. Edelstein, and S. W. Benson, J. Chem. Phys. 60, 3709 (1974).

BSH76 D. J. Benard, W. D. Slafer, and J. Hecht, Third Summer Colloquium on Electronic Transition Lasers, Snowmass-in-Aspen, Colorado (September 1976); submitted to J. Chem. Phys.

C76 T. A. Cool, Cornell University (private communication).

EBH76 D. J. Eckstrom, J. R. Barker, J. G. Hawley, and J. P. Reilly, "Intracavity Dye Laser Spectroscopy Studies of the Ba + N_2O, Ca + N_2O + CO, and Sr + N_2O + CO Reactions," (to be published).

EEB74a D. J. Eckstrom, S. A. Edelstein, S. W. Benson, G. Black, and M. Luria, Technical Report RK-CR-73-6, Contract DAAH01-73-C-0444.

EEB74b D. J. Eckstrom, S. A. Edelstein, and S. W. Benson, J. Chem. Phys. 60, 2930 (1974).

EEH74 D. J. Eckstrom, S. A. Edelstein, D. L. Huestis, B. E. Perry, and S. W. Benson, (a) Semiannual Technical Report No. 1, August 1974; (b) Semiannual Technical Report No. 2, April 1975; (c) Semiannual Technical Report No. 3, September 1975, Contract DAAH01-74-C-0524.

EEH75 D. J. Eckstrom, S. A. Edelstein, D. L. Huestis, B. E. Perry, and S. W. Benson, J. Chem. Phys. 63, 3828 (1975).

EEP74 S. A. Edelstein, D. J. Eckstrom, B. E. Perry, and S. W. Benson, J. Chem. Phys. 61, 4932 (1974).

EH76 D. J. Eckstrom and D. L. Huestis, "Analytical Modeling of Vibrational Distributions of BaO($X^1\Sigma$) in the Ba + N_2O Reaction and Comparison with Experiment," (to be published).

EL76 D. J. Eckstrom and M. Lev-On, Final Technical Report, Contract AT(04-3)-115, Project Agreement No. 98, October 1976.

EPE76 D. J. Eckstrom, B. E. Perry, and S. A. Edelstein, "Heat-Pipe-Oven-Reactor Studies. IV. BaO* and Ba* Emission from the Ba + N_2O Reaction as a Function of Ba Concentration," (to be published).

EPP76 D. J. Eckstrom, S. G. Prakash, B. E. Perry, and S. W. Benson, Semiannual Technical Report No. 4B, Contract DAAH01-74-C-0524, May 1976.

F76 W. Felder, AeroChem Corporation (private communication).

FGF75 W. Felder, R. K. Gould, and A. Fontijn, AeroChem TP-325, July 1975.

HC73 J. M. Herbelin and N. Cohen, Chem. Phys. Lett. 20, 605 (1973); D. J. Spencer, J. M. Herbelin, and M. A. Kwok, Third Summer Colloquium on Electronic Transition Lasers, Snowmass, CO, September 1976.

JSW74 S. E. Johnson, P. B. Scott, and G. Watson, J. Chem. Phys. 61, 2834 (1974).

LEB76a M. Luria, D. J. Eckstrom, and S. W. Benson, AFWL-TR-75-194, Final Technical Report, Contract F29601-74-C-0071, March 1976.

LEB76b M. Luria, D. J. Eckstrom, and S. W. Benson, J. Chem. Phys. 64, 3103 (1976).

LEB76c M. Luria, D. J. Eckstrom, and S. W. Benson, J. Chem. Phys. 64, 1595 (1976).

LEB76d M. Luria, D. J. Eckstrom, and S. W. Benson, J. Chem. Phys. 65, 1581 (1976).

LEE76 M. Luria, D. J. Eckstrom, S. A. Edelstein, B. E. Perry, and S. W. Benson, J. Chem. Phys. 64, 2247 (1976).

R76 S. Rosenwaks, J. Chem. Phys. 65, 3668 (1976).

RWH76 M. A. Revelli, B. G. Wicke, and D. O. Harris, Chem. Phys. Lett. 39, 454 (1976); J. Chem. Phys. (to be published).

VDK76 A. Y. Volkov, A. I. Dyomin, E. M. Kudryavtsev, and N. N. Sobolev, in Electronic Transition Lasers, edited by J. I. Steinfeld, MIT Press, 1976.

WBF76 J. Wilson, J. Bouesc, B. Fontaine, and B. Forestier, in Electronic Transition Lasers, edited by J. I. Steinfeld, MIT Press, 1976.